New Jersey Institute of Technology
Digital Commons @ NJIT

Theses | Theses and Dissertations

Fall 1994

Use of multiple transmitters for 3-D non-intrusive particle tracking

Jitesh H. Agrawal
New Jersey Institute of Technology

Follow this and additional works at: https://digitalcommons.njit.edu/theses

 Part of the Manufacturing Commons

Recommended Citation
Agrawal, Jitesh H., "Use of multiple transmitters for 3-D non-intrusive particle tracking" (1994). *Theses*. 1163.
https://digitalcommons.njit.edu/theses/1163

This Thesis is brought to you for free and open access by the Theses and Dissertations at Digital Commons @ NJIT. It has been accepted for inclusion in Theses by an authorized administrator of Digital Commons @ NJIT. For more information, please contact digitalcommons@njit.edu.

Copyright Warning & Restrictions

The copyright law of the United States (Title 17, United States Code) governs the making of photocopies or other reproductions of copyrighted material.

Under certain conditions specified in the law, libraries and archives are authorized to furnish a photocopy or other reproduction. One of these specified conditions is that the photocopy or reproduction is not to be "used for any purpose other than private study, scholarship, or research." If a, user makes a request for, or later uses, a photocopy or reproduction for purposes in excess of "fair use" that user may be liable for copyright infringement,

This institution reserves the right to refuse to accept a copying order if, in its judgment, fulfillment of the order would involve violation of copyright law.

Please Note: The author retains the copyright while the New Jersey Institute of Technology reserves the right to distribute this thesis or dissertation

Printing note: If you do not wish to print this page, then select "Pages from: first page # to: last page #" on the print dialog screen

NJIT New Jersey's Science & Technology University

The Van Houten library has removed some of the personal information and all signatures from the approval page and biographical sketches of theses and dissertations in order to protect the identity of NJIT graduates and faculty.

ABSTRACT

USE OF MULTIPLE TRANSMITTERS FOR 3-D NON-INTRUSIVE PARTICLE TRACKING

by
JITESH AGRAWAL

A method for non-intrusive tracking of a particle in 3-dimensional space, based on processing of signals emitted from a transmitter embedded in the particle, is being developed. This method uses a mathematical model, which predicts the induced signal in receivers present in the vicinity of flowing particle, and supporting numerical techniques. Specific application aspects related to improving the accuracy of this method are presented.

The focus here is the development of flexible software capable of processing information coming from multiple transmitters with known distinct spatial orientation. Implementation aspects of modified existing empirical corrections for improving model-reality agreement, and new techniques for selecting quality information to overcome stray discontinuities in position and improving the accuracy of results are discussed. Future work to foolproof the system under varying applications is suggested.

USE OF MULTIPLE TRANSMITTERS FOR 3-D NON-INTRUSIVE PARTICLE TRACKING

by
Jitesh H Agrawal

A Thesis
Submitted to the Faculty of
New Jersey Institute of Technology
in Partial Fulfillment of the Requirement for the Degree of
Master of Science in Manufacturing Systems Engineering

Manufacturing Engineering Division

January 1995

APPROVAL PAGE

USE OF MULTIPLE TRANSMITTERS FOR 3-D NON-INTRUSIVE PARTICLE TRACKING

Jitesh H Agrawal

Dr. Rajesh N. Dave, Thesis Advisor — Date
Associate Professor of Mechanical Engineering,
New Jersey Institute of Technology

Dr. Anthony D. Rosato, Committee Member — Date
Associate Professor of Mechanical Engineering,
New Jersey Institute of Technology

Dr. Bruce G. Bukiet, Committee Member — Date
Assistant Professor of Mathematics,
New Jersey Institute of Technology

Dr. Ian S. Fischer, Committee Member — Date
Associate Professor of Mechanical Engineering,
New Jersey Institute of Technology

BIOGRAPHICAL SKETCH

Author: Jitesh H. Agrawal

Degree: Master of Science in Manufacturing Systems Engineering

Date: January 1995

Undergraduate and Graduate Education

- Master of Science in Manufacturing Systems Engineering,
  New Jersey Institute of Technology
  Newark, New Jersey, 1995

- Bachelor of Science in Mechanical Engineering,
  Maharaja Sayajirao University
  Baroda, India, 1992

Major: Manufacturing Systems Engineering

This thesis is dedicated to
my family
and my friends

ACKNOWLEDGMENT

I express my sincerest thanks to Dr. Rajesh N Dave for his ingenious contributions throughout this work. His constant counsel and advice to me has been peerless.

I express my thankfulness Dr. Anthony Rosato, Dr. Bruce Bukiet and Dr. Ian Fischer for their guidance.

I acknowledge the contributions of all my seniors on this project. I thank Jerry Volcy, Anthony Troiano and Prashant Patel to help me accomplish this work.

I am grateful to the U. S. Department of Energy for funding this project.

TABLE OF CONTENTS

TABLE OF CONTENTS
(Continued)

TABLE OF CONTENTS
(Continued)

LIST OF TABLES

LIST OF FIGURES

LIST OF FIGURES

(Continued)

LIST OF FIGURES

(Continued)

CHAPTER 1

INTRODUCTION

1.1 Study of Bulk Solids Flow

Bulk solids composed of different sized solid particles are handled extensively in industry. Most of this is done by automatic material handling devices. The design of such handling devices are sub-optimal as the nature of bulk particle flow is largely unknown. The ability to characterize this flow would result in improved design and better equipment and performance hence would result in huge savings.

Research in field of particle flow, primarily concentrated to numerical simulations and theoretical investigations, has now rapidly advanced to practical experiments. Flexible, cheap and easy to implement experimental methods for studying bulk solids flow are yet being developed. Existing methods for this stud can be largely classified as either intrusive or non-intrusive. Intrusive techniques are inherently inaccurate as they disturb the flow needs to be studied experimentally. Non-intrusive methods are often not accurate enough, costly and some times pose health hazards. This is particularly true for methods based on X-ray radiation and Radio-Isotope/Photon Counting. Dave, Ashok and Bukiet [2], while proposing a new technique which is simple and effective, have provided a background on existing techniques with their relative advantages and disadvantages.

The new technique based on the principle of electromagnetic induction, using one or more transmitters and six or more receiving antennae, aims to overcome shortcomings of existing methods. A single particle, containing the transmitters, associated electronics and batteries, is tracked in a flow by measuring the voltage induced in the array of receiving antennae using a signal processing algorithm together with a theoretical model. Volcy [15] has shown the practical feasibility of this technique and also provides a study of implementation issues and limitations using a single transmitter. The focus of the

current study is to improve and perfect this technique through the use of multiple transmitters.

1.2 Proposed Tracking System

1.2.1 Principle of Electro-Magnetic Induction

The principle of electro-magnetic induction states that a current flowing in a closed circuit wound around a high permeability material creates a magnetic field around it. The strength of this magnetic field changes with the current. The resultant magnetic field induces a voltage in any closed loop present in the vicinity of the magnetic field. Thus the changing current in any closed loop wound around a high permeability material produces a magnetic field of varying strength to form a transmitting source. This transmitter induces a voltage in nearby conducting receivers. The receivers are referred to as *antennae*, while the high permeability material of the transmitter is called the *core*.

1.2.2 Principle of Reciprocity

Through the principle of reciprocity, the changing current and the induced voltage for electro-magnetic induction can be interchanged (Van Valkenburg [14]). Hypothetically, a current flowing in an antenna will induce an equivalent voltage in the loop of a transmitting source.

1.2.3 Non-Intrusive Particle Tracking System

Based on the principle of electro-magnetic induction and perfect reciprocity, the voltage induced in transmitting coil can theoretically be computed if the physical position and orientation of the transmitting coil is known with respect to the antenna. This computation is a multivariate complex non-linear function referred to as the "Forward Model". Using the Forward Model and numerical techniques, the position and orientation of the transmitter can be computed if the induced voltages are known. This computation, now on

referred to as the "Backward Algorithm", is essentially the heart of the "Non-Intrusive Particle Tracking System".

1.3 Development of System with Single Transmitter

The Forward Model was developed by Parasar [9], incorporating several factors, i.e., antenna geometry, transmitter position and orientation, and conductance of the medium. Ashok [1] developed the Backward Algorithm using the forward model and numerical solution techniques to predict the position and orientation of the particle. Through simulations, the practical feasibility of such a technique was shown (Volcy [15]), and the system was developed on a model chute instrumented with antenna, using a sphere with single transmitter embedded in it. This sphere is referred to as *tracer particle*. For practical experiments, issues concerning systematic errors were addressed.

1.4 Statement of Problem

The main objective of this thesis is to extend the existing system to accurately monitor the tracer particle trajectory using multiple transmitters. The major task is to develop tracking system software so that it is flexible in handling one, two or three transmitters. The other objectives include, construction of a spherical particle packaged with multiple transmitters, modification of the data acquisition system for increased speed and improvement of the Backward Algorithm through development of newer techniques to consistently achieve results within acceptable levels of accuracy.

1.5 Outline of Remaining Chapters

Chapter Two covers code development for multiple transmitters. Initial results with the use of multiple transmitters are presented. A new approach to data acquisition and construction of the miniature particle packaged with multiple transmitters is also discussed. Chapter Three considers model-reality deviations of voltages, and presents a

scheme to address systematic noise present in induced signals. Chapter Four addresses some of the numerical convergence issues and discusses an algorithm modification permitting the selection of only those signals which are deemed to produce better results. Chapter Five focuses on the very important issue of making the tracking system independent of initial values of system variables. This enables the particle tracking system to be easily used in a variety of flow conditions in different chutes. Chapter Six summarizes the progress on the development of the system, draws conclusions based on current results and outlines directions for future work.

CHAPTER 2

DEVELOPMENTS FOR USE OF MULTIPLE TRANSMITTERS

The transition from the use of a single transmitter for particle tracking to multiple transmitters is accomplished through developments in both, hardware and software. In this chapter, these developments are discussed.

2.1. Particle Tracking using Single Transmitter

2.1.1 Forward Model

The particle tracking technique is based on Parasar's [9] "Forward Model" and supporting numerical techniques. For sake of convenience only the final formulae of the forward model are presented below and the details can be found in Dave [3]:

$$\vec{B} = \sum_{k=1}^{4}\left[\left(\frac{\mu I_i}{4\pi R_k}\right)\left(\cos\varphi_{k1} - \cos\varphi_{k2}\right)\right]\hat{\theta}_k \tag{2.1}$$

and

$$V = -N\omega\left(\vec{A}\cdot\vec{B}\right)$$

$$\therefore\ V = -N\omega(A_x B_x\cos\alpha + A_y B_y\cos\beta + A_z B_z\cos\gamma) \tag{2.2}$$

Where,

$\vec{B}$ is the resultant magnetic flux density

μ is the permeability of the transmission medium, (air)

I_i is the current in transmitter i (i = 1, 2, 3)

R_k, $\cos\varphi_k$, $\hat{\theta}_k$ are the parameters that describe the relative position and orientation of the transmitter with respect to the receiving antenna.

$x, y, z,$ are position coordinates of the transmitter in the antenna coordinate system (explanation in next paragraph)

α, β and γ are the direction cosines of transmitter axis in the antenna coordinate system

R, φ, $\hat{\Theta}$ are functions of x, y, z, α, β and γ and the geometry of the receiver. (See, Dave [3])

ω is 2π times the frequency of oscillation

A is the area vector of the transmitter

V is the voltage induced in the receiver,

From the intermediate formulae in Dave [3], it is noted that $\vec{B}$ can be computed by using only the position variables x, y, z of the particle. Here x, y, z are position variables of the particle in antenna reference (right-handed) coordinate system. As seen in Figure 2.1, the origin of this reference system is in the center of the antenna plane, the longer side of the antenna being the X-axis, while the Z-axis is out of the plane of the antenna. We develop a convention by denoting the Z-axis as the axis of the antenna. For case of multiple antennae, each will have a reference coordinate system attached to its center, and the forward model then requires x, y, z values for each of them.

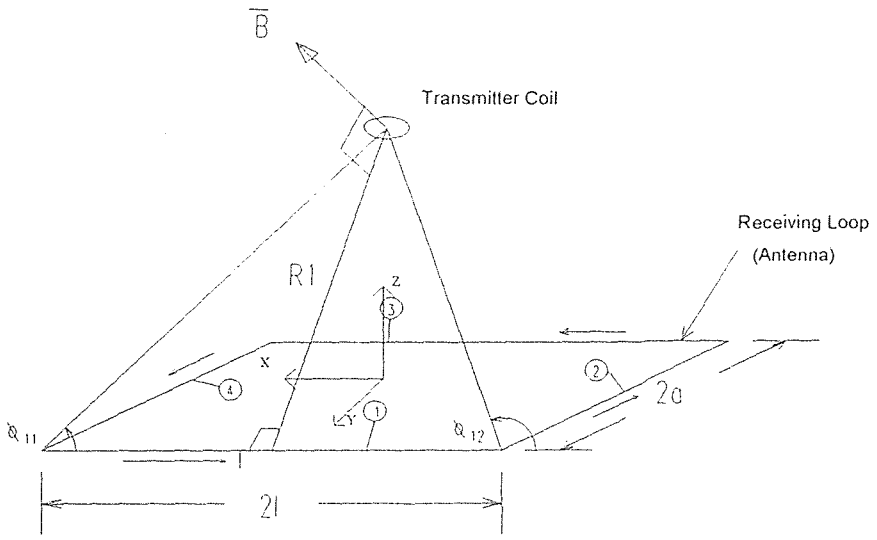

Figure 2.1 Transmitting Coil and Receiving Antenna

2.1.2 Orthogonality Effect

Figure 2.2 shows the disadvantage of using a single transmitter for a specific orientation.

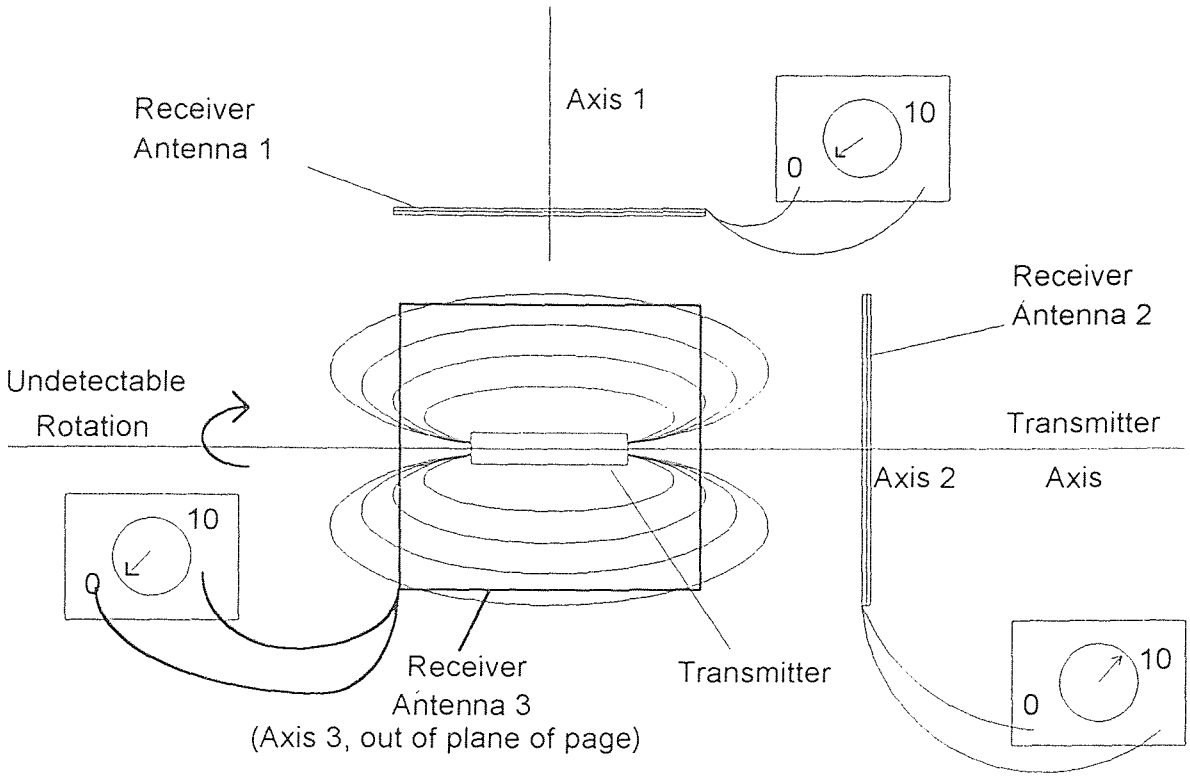

Figure 2.2 Orthogonality Effect

Here, three mutually orthogonal antennae (Antenna 1, Antenna 2 and Antenna 3) are shown. The convention followed for transmitter being perpendicular or parallel to antenna always refers to the angle between the transmitter axis and the antenna axis. Since the transmitter axis is parallel to the axis of antenna 2, almost null voltage is induced in the other two antennae (1 and 3). As a result, the ratio of the induced signal to noise is small. Since the axes of antenna 1 and 3 are orthogonal to the transmitter axis, a motion of the transmitter along axis 1 or 3 produces a very small variation in induced signals. Hence it is difficult to accurately predict the position of transmitter along the direction of axes of antenna 1 and 3. Poor results due to this type of orientation are referred to as

orthogonality effects. In Figure 2.2, if the transmitter rotates about its own axis, voltage readings in all three antennae do not change. Such a rotation of transmitter, and hence of the particle within which it is embedded, remains undetected by software when only one transmitter is used.

The detection of a null signal in any antenna is very dependent on having an orthogonal orientation, and even a slight deviation from orthogonality results in occurrence of a tangible signal. This sensitivity, due to the dot product term in equation [2.2], is very useful while manually orienting the transmitter to obtain orthogonal positioning. Since signal to noise ratio always declines as the transmitter nears the orthogonal position, the orthogonal orientation is not conducive to effective particle tracking. Experiments in lab are conducted in a model chute mounted with antennae as shown in Figure 2.3. The dotted rectangles in the figure represent the antennae, as mounted with respect to chute origin(marked as Global Origin (0, 0, 0)). The numbers in brackets show the sequencing of antennae, while X_1, X_2, Y_1, Z_1 etc. are the antennae names(as per the chute axes on which they are mounted).

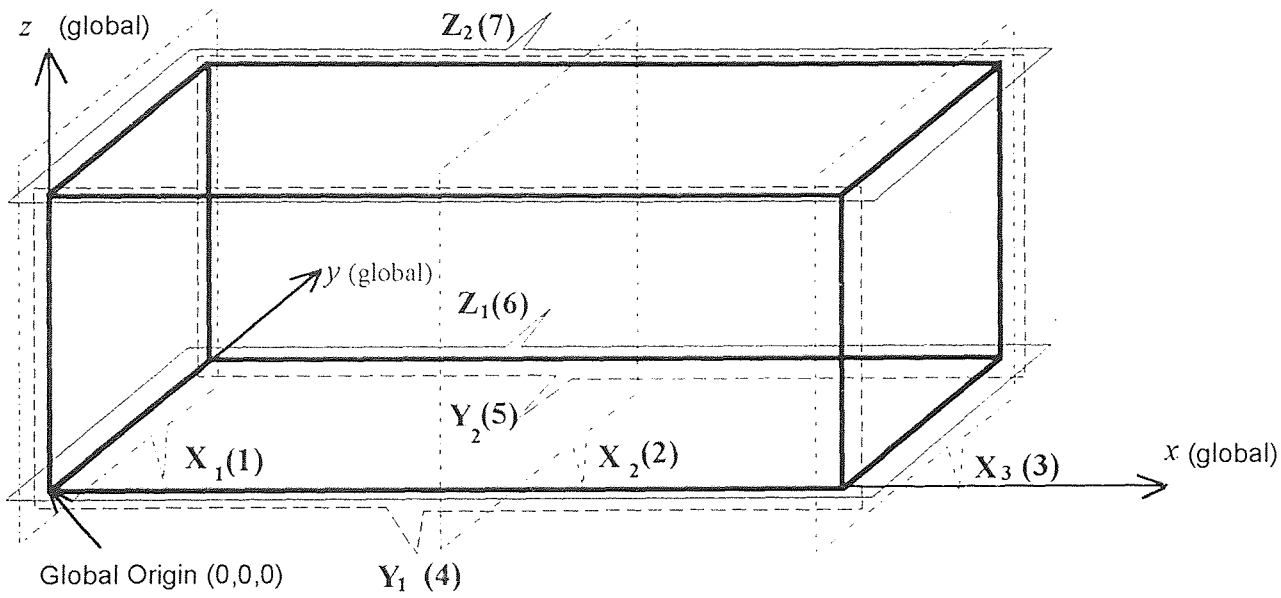

Figure 2.3 Chute for Experiments in Lab.

2.1.3 Limitations of a One Transmitter System

For a one transmitter tracer particle, orthogonality or near orthogonality situation can occur frequently along its trajectory. Consequently, large deviations in predicted trajectory results are immediately observed. Intuitively, it appears that increasing the number of mounted antennae in slant orientations would help overcome the orthogonality effect. However, experimentation with slant antennae mounted along the chute have not shown marked improvements in the results(Volcy [15]). This may be due to the reason that a single transmitter can induce high signals only in one direction and the two vectors perpendicular to this direction always have poor signals. The application of other correction and solution improvement schemes to increase agreement of model-reality voltages have not shown remarkable and consistent improvements either(Volcy [15]). Figures B.1 through B.6 in Appendix[B] show a typical set of results obtained using a single transmitter tracer particle. Based on Volcy's [15] research and experimental results, the use of multiple transmitters is necessary to obtain results within acceptable levels of accuracy. As suggested by Figure 2.2 three transmitters having their cores mutually orthogonal would be the ideal configuration.

2.2 Hardware Development

The use of multiple transmitters for particle tracking calls for the modification of the existing system on both hardware and software levels. For hardware, severe limitations exist since building a tracking particle of 1" diameter sphere packaged with three transmitters is not a trivial task. Also, more transmitters would require measurements of many signals, and for a given particle speed, a faster data acquisition system is required.

2.2.1 Construction of Three - Transmitter Assembly

Each transmitter needs driver circuitry and a source of power. For transition from one to three transmitters, essentially triple the amount of space is required to package the

components. However, the size of the sphere is still limited to a maximum of 1" diameter. Hence to make such a tracer particle, the complete task can be broken into three sub tasks: (i) arranging the three transmitters such that the field developed due to each of them is mutually orthogonal; (ii) providing a circuitry chip and/or a printed circuit board for each transmitter; and (iii) connecting all three transmitters to a power source.

2.2.1.1 Perfect 3 - Transmitter Assembly

A three transmitter orthogonal core is shaped like a jack. The envelop of a jack occupies significant space, and the internal space in the octants cannot be effectively used for circuits as the components are mounted on a flat printed circuit board. As a solution, a cross core is machined to act as core of two transmitters, and the third transmitter coil is wound around these two using flat ferrite of the first two transmitters as core material. Using the power from a single battery of higher voltage just makes it possible to contain all components in a 1" diameter sphere. The actual building of 3 transmitter package is described in detail in Troiano [13]. In practical construction, there are many complexities, such as ensuring the windings are perfectly orthogonal, that the core for any one transmitter does not contribute to the field of other, etc. Figure 2.4 shows the construction of a three transmitter assembly from the initial cross core to the final packaging in the sphere. Figure 2.5 shows how the space within the sphere is occupied by the batteries and the three transmitter assembly.

2.2.1.2 Actual Three - Transmitter Assembly

The construction of a perfect three transmitter assembly requires precision machining. Three transmitter assembly constructed in lab has some imperfections. Of these imperfections, the deviation in orthogonality of three cores and hence, the deviation in the developed fields is of particular concern. As seen in equation [2.2], the forward model requires the orientation of the transmitter with respect to a given antenna for voltage

computation. Therefore it is important to determine the actual orientation of all three transmitters after they have been packaged in the sphere. As two transmitters are wound around the arms of a ferrite cross, their deviation from perfect orthogonal position is negligible. But as the third transmitter is wound around the cross, it has a greater chance of being slightly skewed. This amount of skew has to be determined in order to use the forward model correctly.

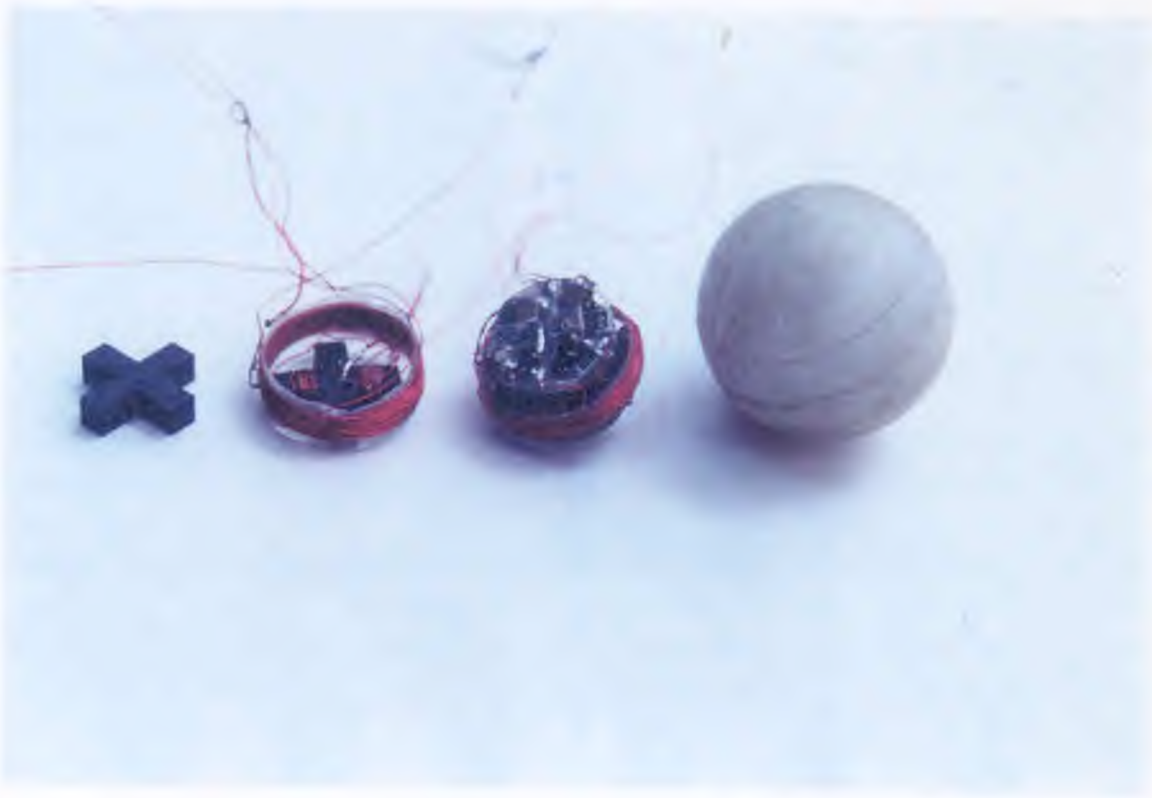

Figure 2.4 Exploded View of 3 Transmitter Assembly

The next imperfection of three transmitter package is the weight imbalance. The packaged sphere has a heavy side due to unequal weight distribution around its centroid. Technically this does not affect the particle tracking system, but could pose a problem when experimental results are compared with simulation results.

computation. Therefore it is important to determine the actual orientation of all three transmitters after they have been packaged in the sphere. As two transmitters are wound around the arms of a ferrite cross, their deviation from perfect orthogonal position is negligible. But as the third transmitter is wound around the cross, it has a greater chance of being slightly skewed. This amount of skew has to be determined in order to use the forward model correctly.

Figure 2.4 Exploded View of 3 Transmitter Assembly

The next imperfection of three transmitter package is the weight imbalance. The packaged sphere has a heavy side due to unequal weight distribution around its centroid. Technically this does not affect the particle tracking system, but could pose a problem when experimental results are compared with simulation results.

2.2.2 Data Acquisition

Volcy [15] has described in detail the data acquisition system for a single transmitter system. A brief description is presented below for data acquisition system for use of multiple transmitter system.

2.2.2.1 Need for Better Data Acquisition System

Signals picked up by an antenna are filtered through demodulator boards and fed to a pin on the data acquisition card and then stored on a personal computer. A channel is defined as the flow path of a signal from a transmitter (emitting at a given frequency) to the equivalent signal (stored as counts) on the hard disk of PC. The signal path is: receiving antenna $\rightarrow$ demodulator boards $\rightarrow$ input pin on data acquisition card. Thus one demodulating board and a corresponding input pin on the data acquisition card is required for each transmitter-antenna pair. Usual data acquisition cards on PC have up to 32 pins allowing use of 32 channels. If more than 32 channels are to be read, an external multiplexer is used. The use of an external multiplexer still requires construction of demodulator boards for each channel. Since each demodulator board has its own amplification gain and other characteristics, higher number of boards lead to a variety of problems. For a single transmitter, using only a few antennae on a small chute, this approach works fine. The use of 3 transmitters requires tripling the number of demodulator boards and requires a data acquisition card with a considerably higher number of input pins. Even then, the limitation imposed by number of input pins on data acquisition card remains. Hence a better method of data acquisition needs to be developed for the use of multiple transmitters.

2.2.2.2 New Data Acquisition System

Figure 2.6 shows a schematic of the faster data acquisition developed by Troiano [12] and Volcy [16]. The left-dashed block, labeled "antenna system", shows sixteen antennae

which receive signals from the tracer particle. Up to sixteen antennae can be read through such a setup. Numbers 1 to 7 correspond to antennae as shown in Figure 2.3. The middle dashed block labeled "antenna multiplexing and detection" has three subparts: (i) multiplexer, (ii) clock circuitry and (iii) demodulator boards. This data acquisition system uses a multiplexer to sequentially select each antenna to be read. The clock generates pulses which are fed to the counter and a variable duty clock. The counter controls switching of multiplexer between antennae. Every time an antenna is switched by the multiplexer, receiving circuitry on demodulator boards require 25 to 30 μs to stabilize.

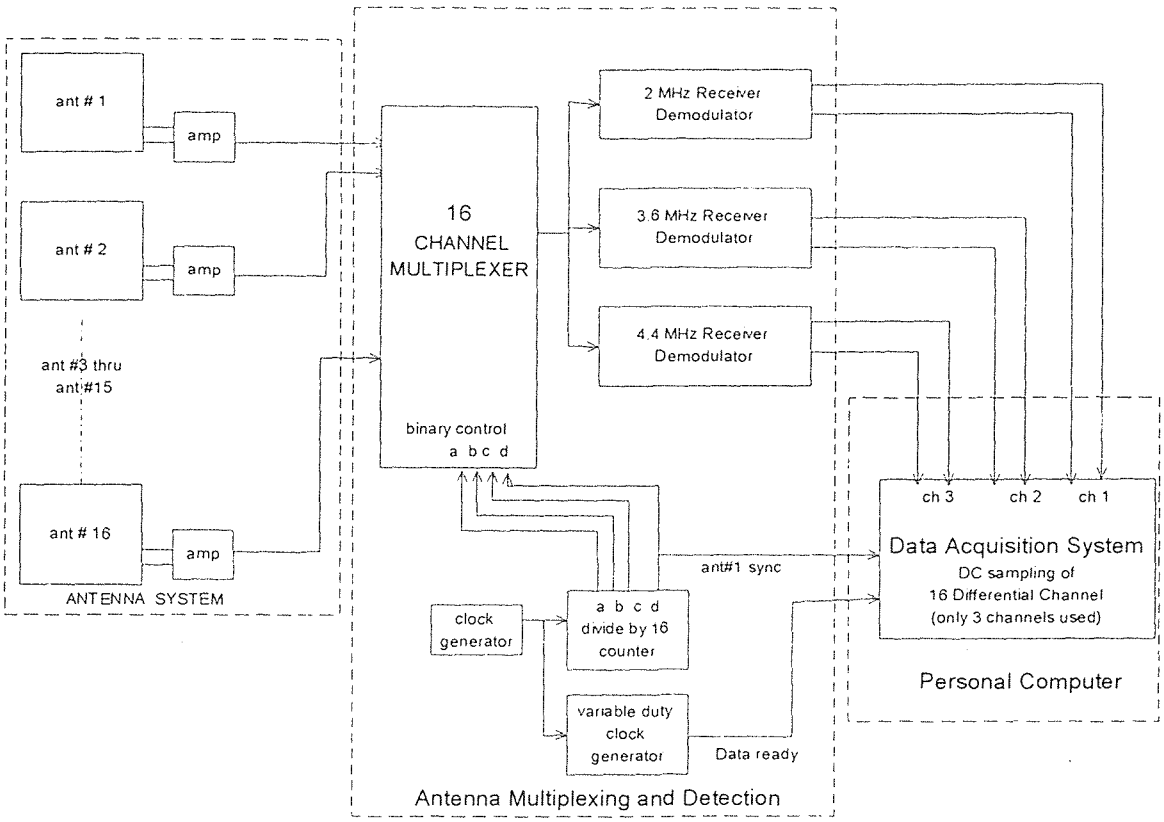

Figure 2.6 New Data Acquisition System

Data should not be collected during this transient response time. At a given time, only one antenna is connected to all three demodulator boards, built for each of the 3 frequencies.

While the signal induced in antenna may be positive or negative, only its magnitude is output from the demodulator board. This signal goes to the input pin the of the data acquisition card on the PC. After a delay for transient response of boards, a data ready signal is sent to PC through variable duty clock. This triggers the scanning cycle for scanning sixteen antennae at 2.0, 3.65 and 4.4 MHz frequency in succession. The time of sampling each frequency within the scan is controlled internally by the data acquisition program parameters. A fourth channel called a synchronization pulse is also scanned. Every time antenna 1 is connected to the multiplexer to be read, this pulse goes from a low value to a high value. This ensures synchronization of multiplexer switching with internal data storage on PC.

A double buffering technique is used to increase the speed of data acquisition. Data in binary form is stored at a very fast rate in virtual memory of PC during data acquisition. Later on it is transferred in ASCII format to hard disk.

With this new approach to data acquisition, up to 520 sets/second of data are obtained on a 66 MHz Pentium machine and up to 208 sets/second are obtained on a 25 MHz 486 PC. Each set comprises of all three frequency readings of all sixteen antennae.

The multiplexing technique used here can be layered to increase the number of antennae scanned. In the current setup, a scan cycle reads sixteen (or a multiple of 16) antennae in every cycle. This results in a loss of time if the number of antennae mounted on the experimental chute is different. It is possible to alter the number of antennae read in a scan cycle by changing data acquisition board configuration and including some extra circuitry. This change configures the hardware to be good for a particular constant number of antennae. By doing so, the gain in speed of data acquisition is not large enough to compromise the flexibility of using a varying number of antennae. Hence we continue to use current set-up of data acquisition at loss of some speed in data acquisition.

As mentioned before we scan only the magnitude of the signal and not the sign. Due to this, the phase information is lost, as phase a shift of 180^{o} in signals because of

angular rotation of transmitter by 180^{o} gives same magnitude of signal. This loss of information is a major disadvantage.

Packaging of the three transmitters in tracer particle and development of faster data acquisition system is a major achievement for improving the particle tracking system. However, the tracking software for new setup must be developed in order to handle multiple transmitters. This is the next major task described in remainder of this chapter.

2.3 Software Development

2.3.1 Transformation Matrix

As discussed in Section 2.1.1, computing voltages using the forward model requires the position and orientation of the transmitter in the antenna coordinate system. This orientation is found from combining four matrices as follows :

$$ {}^{a_j}T_{tp_i} = {}^{a_j}T_g \cdot {}^{g}T_s \cdot {}^{s}T_{tp_i} \qquad (2.3) $$

where,

j : 1, ... n, the number of antennae

i : 1 .... m, the number of transmitters

${}^{a_j}T_{tp_i}$: *Transmitter 'i'* in perfect alignment with sphere's axis as referenced by *Antenna 'j'*

${}^{a_j}T_g$: The *Global* (Chute) coordinate system as referenced by *Antenna 'j'*

${}^{g}T_s$: *Sphere* coordinates system as referenced by the *Global* coordinate system. Elements of this matrix *Continuously Change*

${}^{s}T_{tp_i}$: *Transmitter 'i'* in perfect alignment with sphere's axis as referenced by the *Sphere*

2.3.1.1 Final Matrix

Matrix ${}^{a_j}T_{tp_i}$ is the one required for use with the forward model. It shows how transmitter i (i = 1, 2, 3; for three transmitters) is positioned and oriented in the coordinate system of

antenna j (j = 1, 2, 3; ..... m; the number of antennae). Thus it is used to find the values of x, y, z, α, β and γ in equation [2.2]. This matrix is a product of matrices which transform the transmitter axis from the transmitter coordinate system to antenna j's coordinate system. As will be explained in section 2.3.1.4, the 3rd column of this matrix is of major importance.

2.3.1.2 Antenna - Chute Matrix

Matrix ${}^{a_j}T_g$ is the global coordinate system referenced to antenna *"j's"* coordinate system. The global coordinate system is the same as the chute coordinate system and the terms global and chute coordinate system are used interchangeably. In Figure 2.3, the physical location of each antenna with respect to the chute is shown. The coordinate system attached to the chute is denoted by X, Y and Z. As the location and the size of each antenna in the chute is known, this transformation matrix can be easily computed. Known values of position and orientation variables in the global system after this transformation will yield the value of the variables in the antenna coordinate system. For example in Figure 2.3, point (0, 0, 0) belonging to the global system will be point (-10, -10, 0) for antenna 1 and point (-20, -10, 0) for antenna 4. Construction of this transformation matrix is a matter of simple translation and rotation. Since the chute is stationary and the antennae are fixed on it, elements of this matrix remain constant for a given chute-antenna configuration.

2.3.1.3 Chute - Sphere Matrix

Matrix ${}^{g}T_s$ is the sphere coordinate system referenced to global coordinate system. Tracking of the particle means tracking the sphere coordinate system. Six variables are required to track this system, three for position and three for orientation.

In a Cartesian system, the first three variables are position of the tracer particle, x, y, and z, in the chute space. For orientation, there is no conventionally unique physical

meaning for the three variables. These three variables have different physical connotations depending upon the application or angular motion constraints. Goldstein [6] and Paul [10] have discussed commonly used conventions. Usually these three variables represent three rotations. Each convention is different from the other as it follows a particular sequence of rotations about the three coordinate axes, and considers either the original stationary coordinate system or the new moving coordinate system.

Aim is to clearly establish a meaning of these three variables so that the orientation of the sphere can be defined. Among commonly available options, the Roll-Pitch-Yaw (RPY) representation is selected. For this representation, any orientation can be defined by three successive rotations about the stationary chute coordinate system. The first rotation about the stationary X-axis, referred to as 'Roll' (ψ), is followed by the second rotation about stationary the Y-axis referred to as 'Pitch' (θ). The final rotation is about the stationary Z-axis called as 'Yaw' (φ). Hence matrix ${}^{g}T_{s}$ is formed from the multiplication of three matrices, i.e. Rot[X, ψ], Rot[Y, θ] and Rot[Z, φ]. It transforms known values of variables in sphere coordinate system to corresponding values of variables in global coordinate system. As the sphere coordinate system is the moving tracer particle in our case, the elements of this matrix *continuously change*. Figure 2.7, in which the subscript 'g' refers to the global coordinate system, shows how (ψ, θ, φ) can define a unique orientation in space. It is an example for Roll (ψ= 45^{O}), Pitch (θ = 30^{O}) and Yaw (φ= 45^{O}) of the transmitter axis with respect to the global coordinate system (X_g, Y_g, Z_g). The calculation of ${}^{g}T_{s}$ as the multiplication of these three sequential rotations, Rot[X, ψ], Rot[Y, θ]and Rot[Z, φ] is shown in Appendix[A].

It can be observed that for a given orientation in space, these three variables do not have a unique value. That is, more than one set of rotations(ψ, θ, φ) can produce the same spatial orientation. This fact is true for all the schemes representing the orientation of the transmitter axis. A simplistic example of such a case is that the orientation of a particle initially aligned with Z axis seen in Figure 2.7 can be defined as [0, -90, 0] or [180, 90, 0].

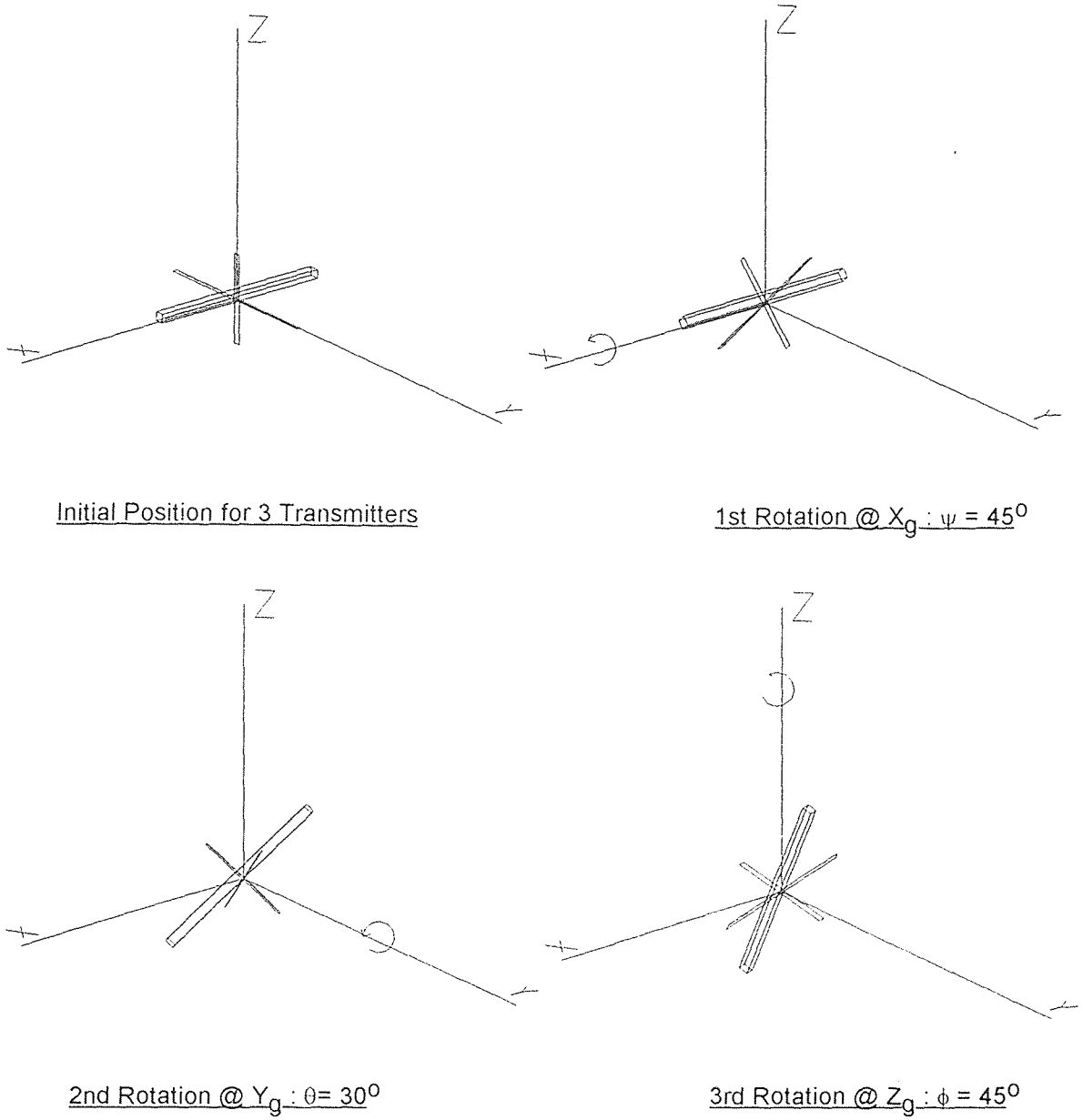

Figure 2.7 Physical Meaning of ψ, θ and ϕ

Thus tracking the particle involves finding correct values of six variables, three for position *x, y, z* and three for orientation ψ, θ, and ϕ. These six unknowns are represented in array as X = [*x, y, z,* ψ, θ, ϕ]. Throughout the remaining presentation, the notation X[] will refer to six unknown variables (*x, y, z,* ψ, θ, ϕ).

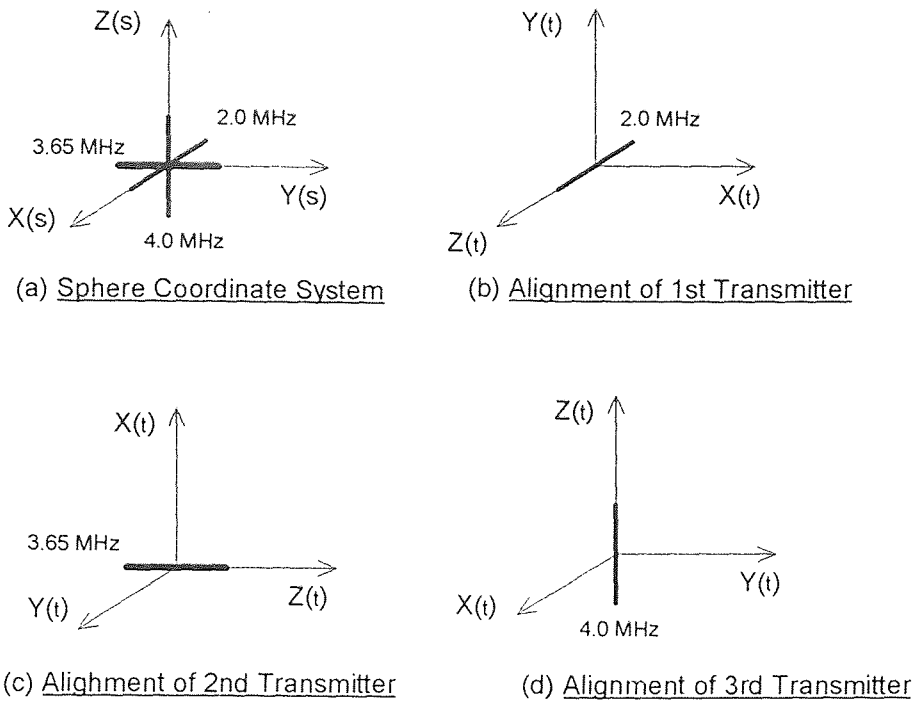

Figure 2.8 Arrangement of 3 Transmitters in the Sphere Coordinate System (X_S, Y_S, Z_S)

2.3.1.4 Sphere - Transmitter Matrix

Matrix ${}^{s}T_{tp_i}$ gives the *'i'* th transmitter location referenced to the sphere coordinate system. Since the three transmitters are orthogonal, each transmitter axis is considered to be aligned along a major axis of the sphere coordinate system as shown in Figure 2.8. The 2.0 MHz transmitter is along the X-axis of the sphere, the 3.65 MHz transmitter is along the Y-axis and the 4.4 MHz transmitter is along the Z-axis. The sphere origin is coincident with the intersection point of the three transmitters. The coordinate system of the *i*'th transmitter is oriented such that its axis of symmetry is along the Z axis and the center of the transmitter is at the origin (see Figure 2.8 a, b, c, d). This is just an arbitrary selection and based on this, the 3rd column of matrix ${}^{a_i}T_{tp_i}$ gives the direction cosines $\cos\alpha$, $\cos\beta$ and $\cos\gamma$ as required by equation [2.2]. As each transmitter is firmly packed in the sphere, there is no relative motion between the transmitter and the sphere coordinate systems. Hence the elements of this transformation matrix remain constant as the particle moves.

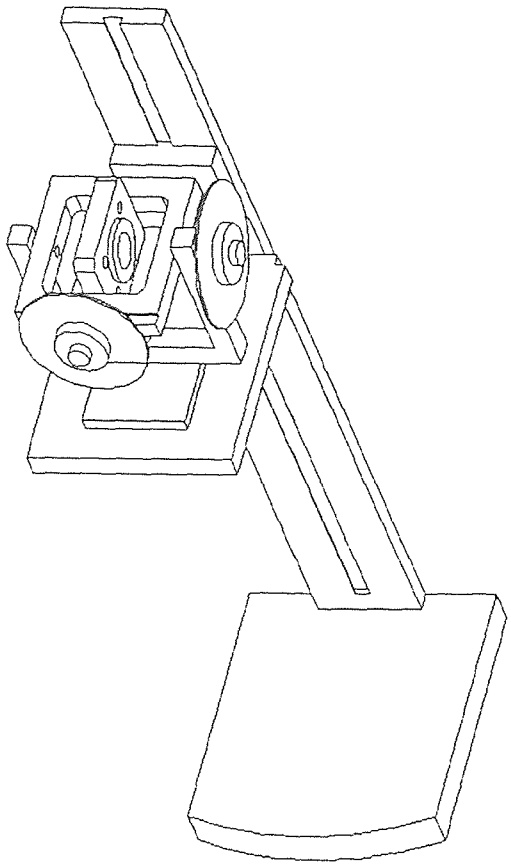

Figure 2.9 Fixture used in Laboratory Experiments

2.3.2 Corrected Transformation Matrix

As discussed in Section 2.2.1.2, the actual packaging of three transmitters in the sphere results in a deviation from perfect orthogonality of the transmitting cores. To find the trajectory of the tracer particle, the forward model given by equation [2.2] is used. The accuracy of the results largely depends upon the agreement between the measured voltage and the predicted voltages. Here, predicted voltage refers to that computed by the forward model, assuming that the actual position and orientation of the transmitter at which the measured voltage is obtained is known. Hence it is very important to determine the correct

orientation of the transmitter as precisely as possible to effectively use the forward model. Figure 2.2 shows that the signal is almost null when transmitter axis is orthogonal to antenna axis. This null is value very sensitive to the deviation from orthogonality. Based on this sensitivity, it is easy to find out how much deviation in transmitter orientation from that shown in Figure 2.8, is present in the packaged sphere. The sphere coordinate system shown in Figure 2.8 is considered to be centered in the flexible jig shown in Figure 2.9. The jig has 3 degrees of freedom mounted on a base support. The jig permits adjustments values of ψ, θ, and ϕ. while the base support allows changes of x, y and z when conducting experiments. Hence controlled trajectory experiments can be conducted in the lab. To keep the explanation generic, we continue to refer to this setup as the sphere coordinate system.

For orientation correction, the transmitter is placed parallel to one antenna so that the signal induced in the other two antennae perpendicular to it is expected to be null. However in reality this is not the case since the three transmitters are not perfectly orthogonal to each other. The presence of significant signal is detected instead of expected null. By rotating the transmitter assembly marginally about one or more axes using the jig, and following the RPY convention, it is possible to reduce the signal detected to almost null. By recording these angles, the actual orientation of transmitters in the packaged assembly is found. Thus an extra transformation matrix ${}^{tp_i}T_{ta_i}$, called a correction matrix is appended to equation [2.3]. Hence equation [2.3] in new form becomes:

$$ {}^{a_j}T_{ta_i} = {}^{a_j}T_g \cdot {}^{g}T_s \cdot {}^{s}T_{tp_i} \cdot {}^{tp_i}T_{ta_i} \qquad (2.4) $$

where

${}^{tp_i}T_{ta_i}$: Transformation for *transmitter 'i'* in *actual position* (after being packaged) as referenced with respect to its *perfect position*

Due to inconsistencies in the orthogonality of the transmitter cores from fabrication, each transmitter must be aligned individually. For the transmitter assembly used in lab experiments these corrections are found as follows.

The 2 MHz transmitter is already aligned along X-axis of the sphere as shown in Figure 2.8. The transmitter assembly is oriented in the chute so that the X-axis of the sphere is aligned with the global X-axis. The transmitter assembly is then positioned anywhere along the 'Z' axis of the antenna coordinate system. In lab, we positioned the 2.0 MHz transmitter on Z axis of antenna number 2. Antennae 1 and 2 as seen in Figure 2.3, are mounted along the global X axis.. For this orientation and position, signals in antenna number 4, 5, 6 and 7 are expected to be null. In reality this not the case because of imperfect transmitter assembly. Therefore the sphere is rotated (which in turn also rotates the 2 MHz transmitter) following the RPY convention to get the best possible null in antenna 4, 5, 6 and 7. A rotation of $+4^{o}$ about the global Y-axis followed by a rotation of -8^{o} about the global Z-axis produces the desired null for 2 MHz transmitter. The axes of these two rotations is different in the global, the sphere and the 2 MHz transmitter coordinate systems. Figure 2.10 shows the relative arrangement of these three coordinate systems. Hence a rotation about the Y-axis in the global coordinate system, is a rotation about the transmitter X-axis and a rotation about the Z-axis in the global coordinate system is a rotation about the transmitter Y-axis.

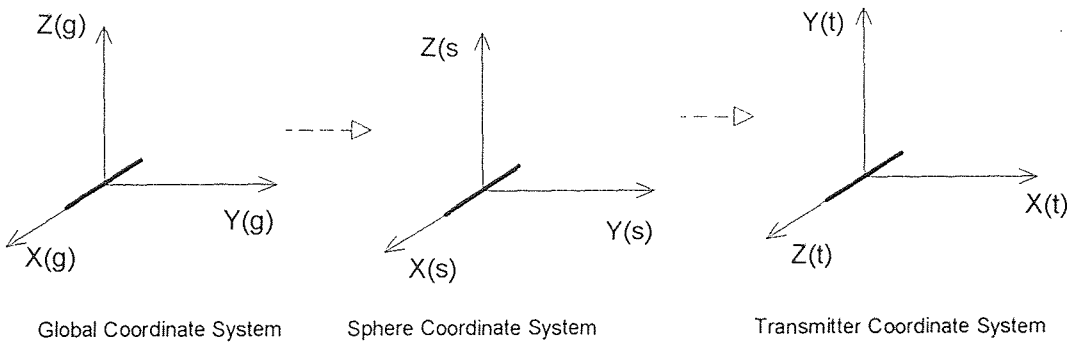

Figure 2.10 Axis of Rotations for Orientation Correction in Different Coordinate Systems

The two rotations measured for getting null signal have taken the transmitter from the actual imperfect orientation (no null observed) to a "perfect" orientation (null observed). The matrix, ${}^{tp_i}T_{ta_i}$, is then reverse of this. The two rotations described here in the global coordinate system, must be specified in the transmitter coordinate system in order to find the correction matrix ${}^{tp_i}T_{ta_i}$. Apparently, the matrix ${}^{tp_i}T_{ta_i}$ can be easily obtained by two rotations about the corresponding axes in the transmitter coordinate system, in reverse order and with opposite signs. Thus ${}^{tp_i}T_{ta_i}$ should be composed of 2 rotations, and for the 2.0 MHz transmitter : a rotation of $+8^{o}$ about the transmitter Y-axis, followed by a rotation of -4^{o} about the transmitter X-axis. As depicted in Figure 2.11, the transmitter coordinate system rotates, that is, after the 1st rotation, the transmitter X-axis is along the dashed line marked as "undesired X rotation axis". The second rotation must be about the original transmitter X-axis as shown in Figure 2.8 (or solid line showing the transmitter X-axis in Figure 2.11b). Hence this straight forward reversal of sequence and angles does not work to find correct ${}^{tp_i}T_{ta_i}$.

To obtain the required correction matrix we consider the transmitter coordinate system as the base system. If all subsequent transforms (which may be either rotations/translations) are post multiplied to the base system matrix, then each transformation will be with respect to the stationary base system. While the details of such transformations are presented in Paul [10], the required correction matrix for the 2 MHz transmitter is obtained by a rotation of -4^{o} about X-axis followed by a rotation of $+8^{o}$ about Y-axis. The required correction rotations to align the transmitter from perfect orientation to actual orientation, are depicted in Figure 2.11. Numerical calculations for computing correction matrix for all three transmitters are given in Appendix[A].

The correction angles producing a null for the 3.65 MHz transmitter are $+4^{o}$ about X_g followed by -10^{o} about Z_g. For 4.4 MHz transmitter, a rotation of $+4^{o}$ about X_g is needed. It is noted that the readings for the 2.0 MHz and 3.65 MHz transmitters are nearly equal since they are wound around the same orthogonal cross shaped ferrite core. Part of

angular deviations come while mounting the transmitter assembly centrally in the jig of Figure 2.9. Since the correction angles are unequal for the 3 transmitters, the jig position (x, y, z, 0, 0, 0) with reference to which the correction angles are measured, is NOT independent of rotation of 180^{o} about any major axis. Hence initial orientation of jig (0, 0, 0) (at which the correction angles are measured) always needs to be consistently maintained for all the experiments.

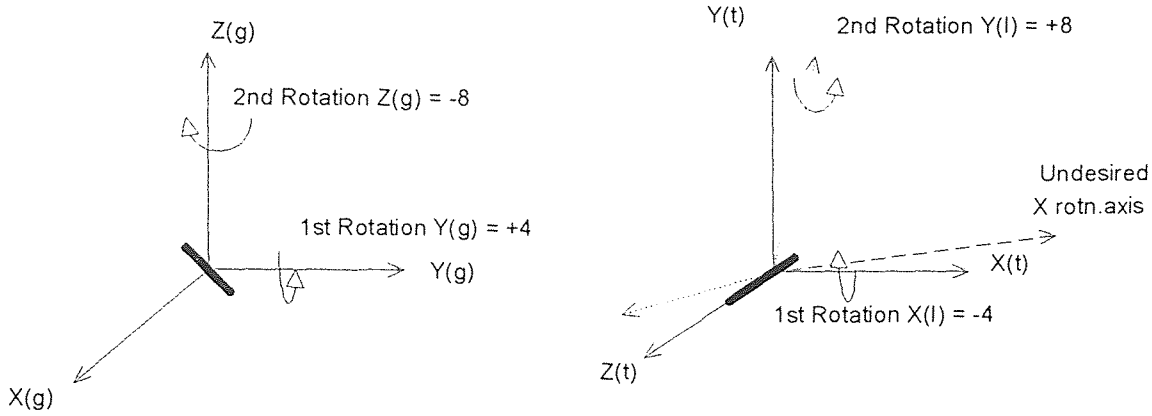

Figure 2.11 Sequence of Rotations for Orientation Correction

Once the correction matrix ${}^{tp_i}T_{ta_i}$ is known, matrix ${}^{a_j}T_{ta_i}$ is computed using equation [2.4] for all three transmitters. By using the matrix ${}^{a_j}T_{ta_i}$ and the forward model, the backward model is constructed to accomplish particle tracking.

2.4 Backward Algorithm

Figure 2.12 shows a flow chart for backward algorithm developed so far. Computing the solution is essentially a two step process; the first step as shown above the dotted line is called the calibration and the second step shown below the dotted line is the numerical solution step.

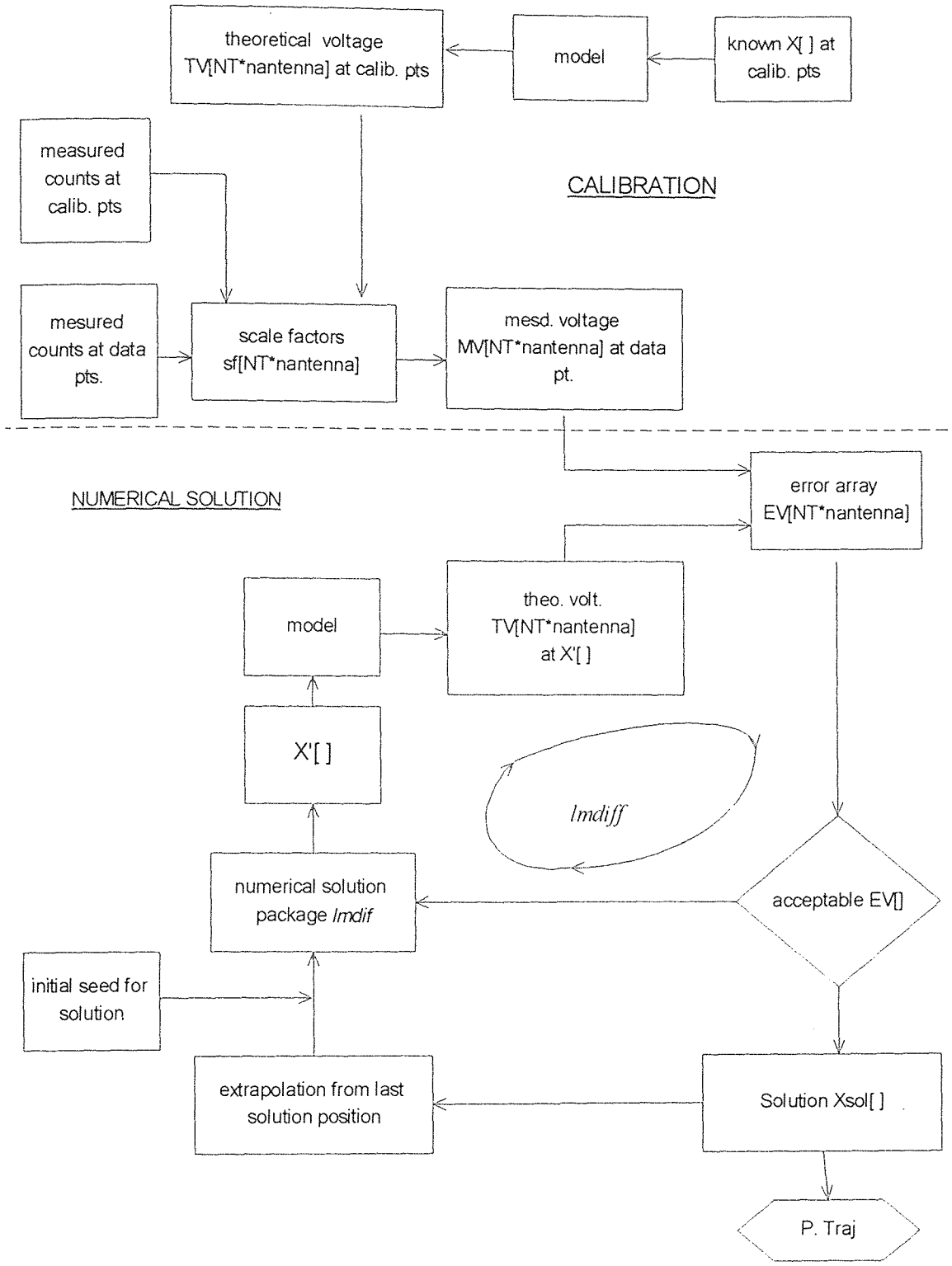

Figure 2.12 Flow Chart of Backward Algorithm

2.4.1 Calibration

The forward model equation is given in units of volts, while the actual measured signals coming from data acquisition are in arbitrary unit of "counts". Therefore the "counts" need to be scaled down to the actual voltage in unit of volts. The ratio of model voltage to the measured voltage (at same X[]) gives the scaling factor for converting counts to voltages, a process called calibration.

2.4.2 Numerical Solution Technique

2.4.2.1 Numerical Function

The numerical solution involves solving for the six variable parameters in X[] by minimizing the residual R defined as:

$$R = \frac{1}{2}\sum_{i=1}^{m} r_i(x)^2 \qquad (2.5)$$

where :

$r_i = (V_{model} - V_{mesd})$

V_{model} is voltage computed at X[] by forward model and

$V_{measured}$ is voltage scanned by data acquisition system at X_{actual}[].

To minimize equation [2.5], we use the *lmdiff* routine from MINPACK which is Moré's [8] implementation of the Levenberg-Marquardt [7] algorithm. Here we solve an over determined system of *m* equations (m = NT x nantenna) to solve for six variables X[].

We examine the role of the numerical technique in the backward algorithm. The lower left box in Figure 2.12 marked as initial seed, refers to the "initial guess" X[] required for solution by *lmdiff*, the numerical solution package. The "initial guess" X[] is needed as input to use the voltage model for the first time. This "initial guess" is referred to as initial seed for the rest of the presentation. This seed X[] defines the variables

determining ${}^{g}T_{s}$ matrix which in turn defines the ${}^{a_j}T_{ta_i}$ matrix. Based on seed X[], each transmitter's position and orientation is determined in the antenna coordinate system. Using the forward model, a theoretical voltage array of number of the transmitters times number of antennae referred to as TV[NT x nantenna] is calculated. A similar measured voltage array MV[NT x nantenna] of scaled down counts after calibration is available from the data acquisition system. We define an error array EV[NT x nantenna] as the absolute difference between the theoretical and measured voltages. The magnitude of this error voltage array is,

$$\|EV\| = \sum_{i=1}^{m} fabs(V_{model} - V_{mesd}) \tag{2.6}$$

If ||EV|| is zero, it means that seed X[] is the solution we seek because the measured voltage is exactly that produced with the transmitter placed at the seed X[]. However the magnitude of the error voltage ||EV|| is usually non zero since the model and the data acquisition system are not perfect. Hence a non zero level of error in voltage $\|EV_{accept}\|$ is allowed.

To compute the solution X[], *lmdiff* (as shown in the circular loop in Figure 2.12) iteratively changes X[] to reduce the magnitude of EV[] until it falls within the acceptable range. In Figure 2.12, seed X[] is required only while solving for the first data point. The second data point is seeded in the vicinity of the solution for first data point. From the third point onwards, the seed is provided by linear extrapolation of the previous two data point solutions.

At present, the magnitude of error voltage ||EV|| includes all [NT x nantenna] elements of EV[]. While some of these elements have a low signal to noise ratio, some other elements represent a case where the transmitter is so far from the antenna that

measured voltage is essentially noise. These elements can adversely affect the convergence of *lmdiff* and should be disregarded if possible.

2.4.2.2 Perturbations

The solution to which *lmdiff* converges is dependent on $X_{seed}[]$, the linear extrapolation of the previous two points. Linear extrapolation inherently assumes the speed of the tracer particle and change in magnitude of the six variables from one data point to next is constant. The nature of the forward model, physical meaning of (ψ, θ ϕ) and noise in the data acquisition system together make convergence by lmdiff to the correct solution, $X_{sol}[]$, at every data point unlikely. (Subscript "sol" refers to the exact solution for X[]). This is because the global minimum of equation [2.5] ($X_{truesol}[]$), often has other local minima with acceptable $||EV_{accept}||$ near $X_{sol}[]$.(The subscript "truesol" refers to X[] at the point at which the model voltages give the best fit to the measured voltages). In order to always converge to $X_{truesol}[]$, we use perturbation techniques.

The perturbation technique we apply, involves providing '*k*' initial guesses of position $X_{seed}[]$. These are stored in two dimensional array $X_{seed}[k][]$. Thus in *k* cycles, $X_{seed}[k][]$ provided within distance '*r*' of the extrapolated points, converges to *k* solutions stored in the two dimensional solution array $X_{sol}[k][]$ and the corresponding array $||EV[k]||$. Then row of $X_{sol}[]$ yielding the lowest value of $||EV[k]||$ gives the best solution $X_{sol}[]$ from all converged solutions $X_{sol}[k][]$. Usually $X_{sol}[]$ found by this method is $X_{truesol}[]$. Perturbation thus involves use of two parameters, *k* and *r*. In our current application, it appears that the value of *k* equals six is optimal. The parameter *r* referred to as radius of perturbation, is a function of tracer particle speed and data acquisition rate.

While generating $X_{seed}[k][]$ for perturbations only position variables *x*, *y* and *z* are randomly distributed within linear radius *r*. In some of our experiments, the orientation variables ψ, θ, and ϕ are also randomly perturbed with angular radius *r1*. Thus *r1* is a angular measurement.

The perturbation technique improves considerably the robustness of the algorithm and helps to prevent the solution from straying. The perturbation method is represented by the circular loop in the flow chart and is shown only once for the sake of simplicity. In the actual code, the loop is executed k times.

2.4.2.3 Initial Seed

Volcy[15] has studied the sensitivity of the solution to the 1st data point, to initial seed X[]. Getting $X_{seed}[]$ fairly accurate for the first data point has been crucial for effective use of the particle tracking technique. In the current stage where a single tracer particle is manipulated using a calibrated jig for experiments, it is relatively easy to obtain an accurate $X_{seed}[]$. However, for free flow experiments where the packaged sphere is rolling down the chute with many other similar spheres, getting an accurate initial seed X[] is a difficult task. To use the particle tracking system in varying chute configurations with steady particle flow, the software needs to be independent of the initial seed $X_{seed}[]$ at the first data point.

2.5 Initial Experiments With Multiple Transmitters

Once the solution algorithm was setup for use with multiple transmitters and a 3 transmitter sphere was ready, initial experiments were conducted to observe improvements in results using multiple transmitters against a single transmitter. Calibration for each antenna transmitter pair was done using only one data point with the transmitter pointing into the antenna and being 10 inches away from it. This method of calibration has empirically produced scaling factors resulting in good solutions.

The primary goal of the particle tracking system is to locate the position of the tracer particle accurately. Hence, a scheme for measuring deviation in location has been established. As all experiments are performed using controlled trajectories, actual X[] at all data points is known. This enables us to compute the position difference as

$$P_{dev} = \sqrt{\left(x_a - x_p\right)^2 + \left(y_a - y_p\right)^2 + \left(z_a - z_p\right)^2}$$

where *'a'* refers to the actual value and *'p'* refers to the predicted value

P_{dev} is one way of measuring the accuracy of particle tracking and is used here to observe the efficacy of various improvements in the backward algorithm presented in the following chapters.

Figures B.7 through B.12 in Appendix[B] show a set of results for the same trajectory shown in Figures B.1 through B.6. Overall results look much better than one transmitter results for the same run. However, a glitch in the X plot (at X ≅ 18.5") clearly demonstrates the need for further investigation. The magnitude to this glitch increases (in the X plot), as the transmitter assembly approaches the plane of antenna 2. This kind of increase in deviation is seen in most of the runs suggesting the presence of some kind of systematic error. Various solution improvement techniques have been tried for the one transmitter case yielding marginal improvements in the results. In the next chapter we discuss the modified and improved implementation of the 27 point empirical correction scheme as proposed by Dave [3] to address model-reality discrepancies in voltage.

CHAPTER 3

REDUCING SYSTEMATIC ERRORS

3.1 Sources of Systematic Errors

The signals coming from the data acquisition system inherently have noise due to imperfections in the transmitters, the data acquisition system, variations in background noise etc. Noise can be dealt with if the source from which it emanates is studied. Volcy [15] has identified and classified systematic and random noise and suggested ways to reduce its adverse effect on the solution. Here we further investigate two aspects of that study namely; antenna coupling and a 27 point empirical correction as applied to multiple transmitters.

3.2 Antenna Coupling

Antenna coupling is the change in magnitude of the induced signal for a given antenna in relation to the magnitude of induced signals in antennae surrounding it. This is because the principle of electro-magnetic induction acts between any two wires belonging to two different antennae. Coupling thus distorts the magnitude of the signal induced in an antenna due to a single transmitter. As the forward model does not provide for this kind of signal distortion; the solution reached can be inaccurate. Theoretically, it may be possible to model the phenomenon of antenna coupling; but an easier and more practical approach is adopted here.

Signal distortion due to antenna coupling is higher in leads of antennae and when any one of four antenna wires run parallel and near each other in the chute. The lead is the portion of the wire joining the antenna ends to the distant demodulator boards. To reduce antenna coupling due to parallel sides in chute; antennae were repositioned so that no two wires of any two antennae are within 1/2" of each other. This showed a marginal but

distinct improvement in the results. The bulk of the antenna coupling occurs in the leads as leads from all antennae usually run parallel and near each other. To prevent coupling in leads, they can be shortened by placing receiver boards right at the base of antenna near the chute. In the lab, a similar approach is adopted by bringing the experimental chute and the receiver boards closer. Improvements in results were immediately observed. This approach however is impractical for many practical applications. A better approach, as suggested by Troiano [12], is to build isolating circuits and place them at the base of antennae. The isolating circuits marked as 'amp' in Figure 2.7 are placed at the antennae ends. Isolating circuits prevent the flow of self generated currents developed in leads due to inter wire capacitance and thus reduce noise in signals being measured. The antenna coupling problem which increased noise generation has been satisfactorily addressed in this manner.

3.3 27 - Points Correction for Multiple Transmitters

As discussed in Section 2.4.1, the scaling factor calculated for each antenna transmitter pair is assumed to be constant throughout the chute space. However when actual calibrations are taken at different points in the chute, scaling factors vary significantly. The variation can be attributed to many causes. Two very significant reasons are:-

(1) The Forward Model is based on the principle of reciprocity. The assumption of reciprocity does not hold well when the distance between the transmitting coil and receiving antenna is low. Thus when the sphere(transmitters) approaches the plane of the antenna, agreement between the model and reality decreases. As a result, a constant scaling factor taken at one point in space cannot be used to scale exactly the reading of data acquired in the entire experimental space.

(2) The scaling factor is a function of the characteristic response of various electrical components in the data acquisition system, especially those mounted on the

demodulator boards. This response of the data acquisition system varies with time and with the magnitude of signals induced in the antennae.

As the trajectory of the tracer particle is unknown, the effect of varying scaling factors (at the many different points through which the trajectory passes) on the predicted results is unknown. The non-linear behavior of the scaling factor can be incorporated in the backward algorithm, if the non-linear behavior is understood.

3.3.1 Model - Reality Voltage Plots

The adverse influence of using a single calibration point for the whole chute can be studied by observing trends in the voltage plots. The following voltage plots are used for comparison of measured voltages (obtained after calibration of counts) and the model voltage computed along the same trajectory. The scaling factor for every antenna is influenced by many factors. Hence, comparing measured voltage after calibration, takes in account the influence of antenna and data acquisition system. Scaling reduces measured voltage to very small numbers and hence the plots presented below are scaled up by a factor of 10^6 to get a reasonable Y axis scale. The trend analysis presented below is for an antenna of size 20" x 20".

Figure 3.1 shows a voltage comparison of the model vs. reality when the transmitter axis and antenna axis are parallel and the transmitter is approaching plane of antenna. This transmitter orientation results in maximum signal induction. The X axis represents the distance of the transmitter from the plane of the antenna. At the start of the plot, the transmitter is 10" away from the plane of the antenna. The distance is decreased by 1/2" at every subsequent data point to give a decreasing series marked on the X axis of the plot. As *calibration is done 10" away from plane of the antenna for all runs*, the predicted and measured voltage curves coincide at that point. After that, the rise in theoretical voltage is steeper than in measured voltage. At distance = 0 on X axis of the

plot, the difference in voltages is almost 8% of the maximum reading, a very big number which can degrade results. On the same scale $||EV_{sol}||$ (Section 2.4.2.1) for a good solution is in the range of 150 - 200 using all 21 elements of EV[] (7 antenna x 3 transmitters) for the convergence process. For trend analysis plots in Figures 3.1 to 3.3, a single element contributes an error of magnitude of over 100, clearly preventing convergence by *lmdiff* to an accurate solution.

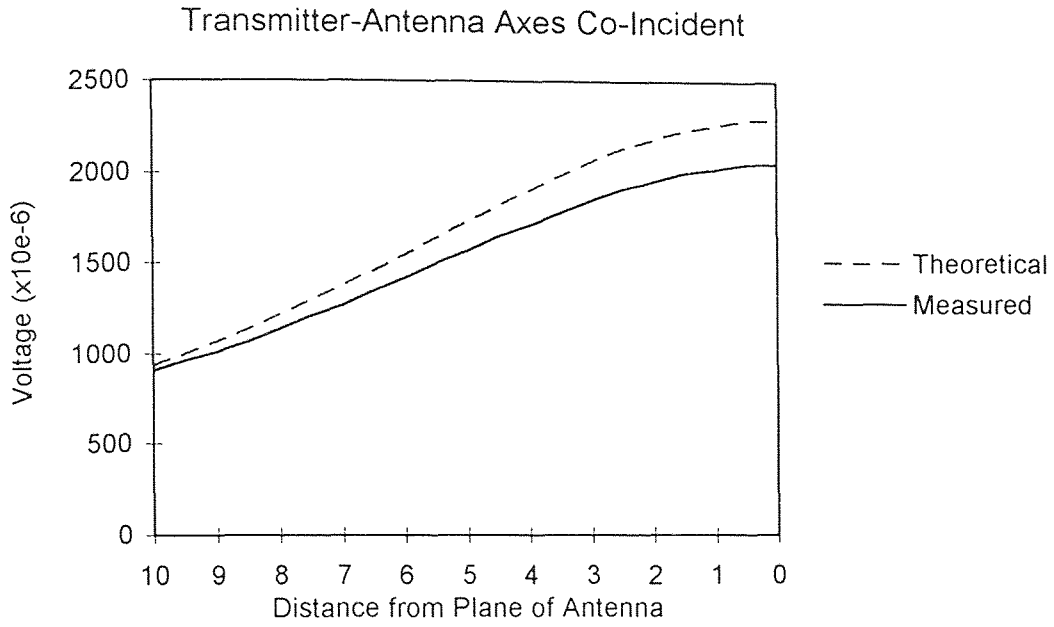

Figure 3.1 Model-Reality Voltage Comparison With Axes Coincident

Figure 3.2 is similar to Figure 3.1 with transmitter axis and antenna axis parallel but offset by 7 inches. The disagreement in model and reality curves is higher both in terms of percentage (approx. 15%) and absolute value of $||EV_{sol}||$. During the actual experiments when the transmitter and antenna are positioned in this manner; the signal induced disagrees with the model and throws the solution completely off.

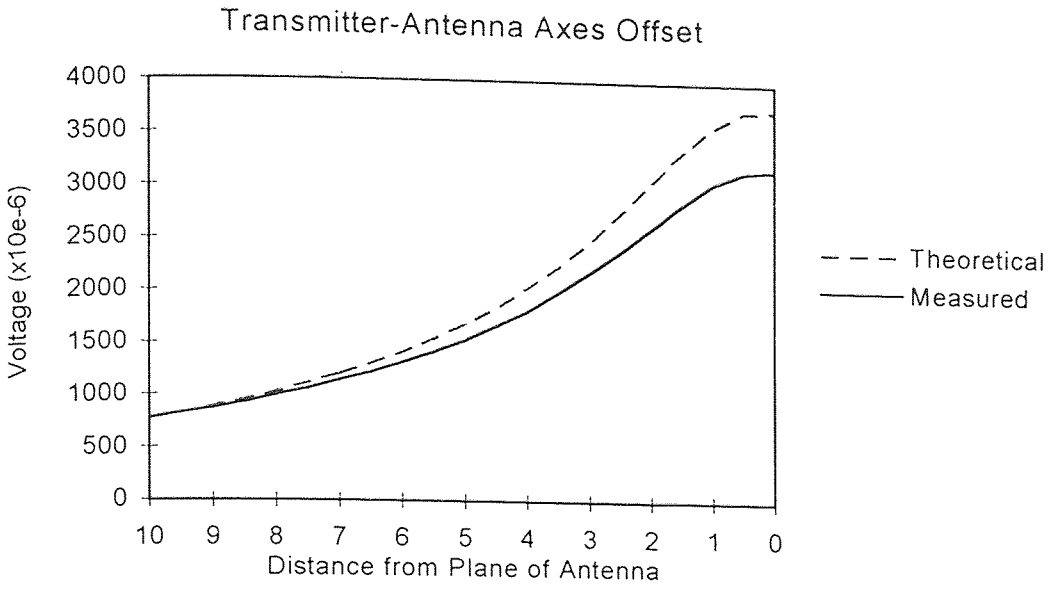

Figure 3.2 Model-Reality Voltage Comparison With Axes Offset

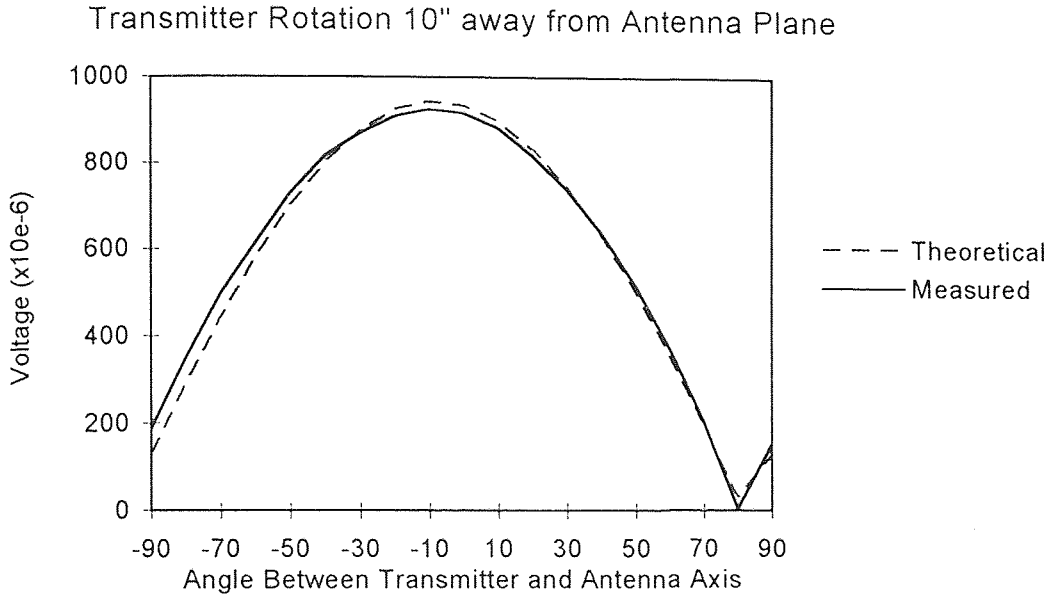

Figure 3.3 Model-Reality Voltage Comparison With Transmitter Rotation 10" Away From Antenna Plane

Figure 3.3 shows model-reality match when the transmitter is rotated around the global Z axis. In the antenna system, this is a rotation such that the transmitter and antenna axis are initially orthogonal, gradually get parallel and coincident and become orthogonal

ıgain as the transmitter completes a rotation of 180 degrees. Here, the transmitter is ɔlaced 10" away from the antenna. The discrepancy between the model and reality is ıotably low, as the present point is also the calibration point. Thus, it can be inferred that *'he model-reality disagreement is not severe with rotation of transmitter at the :alibration point.*

In this plot, the X axis (marked in degrees), is the angle between the transmitter axis and the antenna axis. The two curves match at an angle of approximately 10^{o} and the plot is asymmetrical about its peak even though X axis angles are labeled from -90^{o} to 90^{o}. This is because we are able to measure the angle between the sphere coordinate (packaged transmitter and not the actual transmitter axis as marked in Figure 3.3) axis and the antenna axis. The actual transmitter axis is offset from sphere coordinate axis by $+8^{o}$ for the current transmitter as discussed in Section 2.3.2.

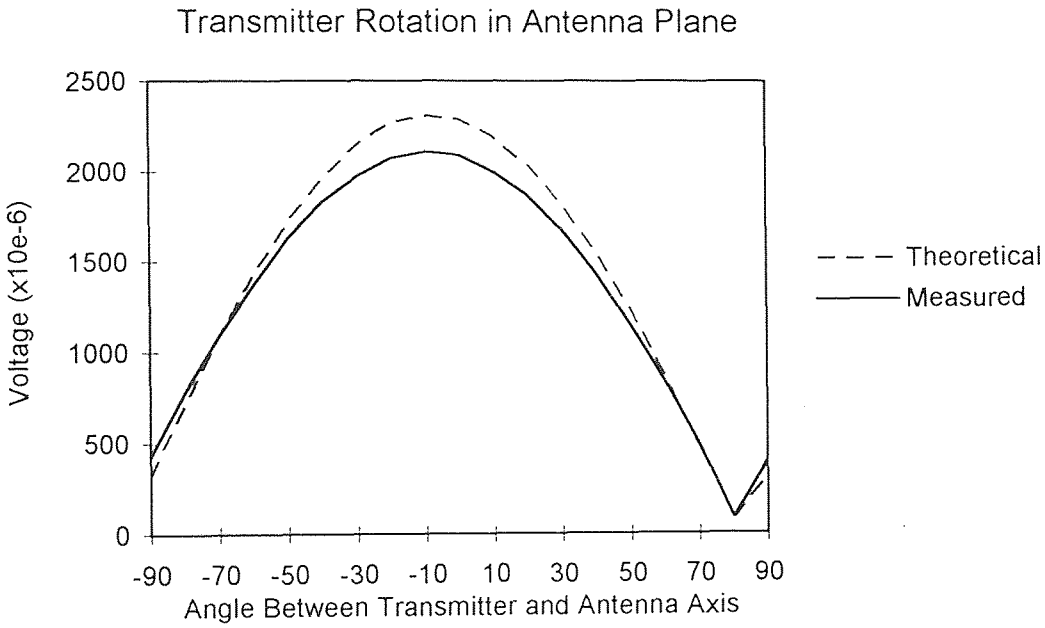

Figure 3.4 Model-Reality Voltage Comparison With Transmitter Rotation In Antenna Plane

Figure 3.4 shows a comparison similar to Figure 3.3. Here the transmitter is placed right in the plane of antenna. The disagreement between model and reality is relatively large. Looking at the Y-axis scale in the plots, it is big enough to throw the solution off.

In Figures 3.1 through 3.4 we clearly see that the disagreement between the model and reality is systematic. As the transmitter comes nearer to the antenna plane the difference increases. This is because the assumption of reciprocity in the derivation of the forward model becomes invalid when the transmitting source and receiving loops are close. The systematic noise seen in the plots needs to be accounted for in the inverse solution technique in order to improve the accuracy of the results.

In Figures 3.2 and 3.4, if calibration is done in the plane of the antenna, then the two curves would have matched at the last point. This shifts the disagreement to lower values of signals. This renders the lower signals with a very poor signal to noise ratio and thus is not conducive to a good solution. For randomly varying trajectories in chute space, a higher number of data points are obtained away from the plane of the antenna and hence calibration is taken at 10" away from it. Also for Y and Z antennae, the particle never crosses the plane of the antennae, as they are mounted outside the chute. Thus, using a single calibration point in the plane of the antenna is not a reasonable solution to this problem.

3.3.2 Mathematical Function for 27-Point Correction

Based on the systematic deviation observed between model and reality voltage plots, some kind of mathematical correction to the model is required. The computation of this mathematical model is discussed here.

In the case of Figure 3.2, if, for example, the calibration is taken at both points, 10 inches away and 0 inches away from the plane of the antenna, then two respective values of scaling factors, *s.f 1* and *s.f 2* are obtained. As we move towards the antenna, let a correction factor *c.f = fn(sf1, sf2)* be used to modify the model voltage so that the

discrepancy between the model and reality gets minimized. In this case the function would yield values of correction factors as $c.f = 1$ at 10" away and , $c.f = sf2/sf1$ at distance of 0", as the measured voltage has been scaled down by multiplying counts with $s.f.1$. Such a function would ensure good agreement in voltage curves for straight line trajectories similar to that of Figure 3.1. The concept of 27 points is based exactly along these lines. It is an extension of the specific straight line trajectory discussed here to generic 3-D trajectories. The 27 points are 27 nodes in one octant of the antenna coordinate system. Scaling factors are obtained at each of these nodes. Volcy [15] has lucidly explained the distribution of nodes in the antenna system, physical steps of acquiring 27 scaling factors and initial functions for computing correction factors. For ease of reference, a modified representation of the 27 node distribution in the antenna coordinate system is presented in Figure 3.5.

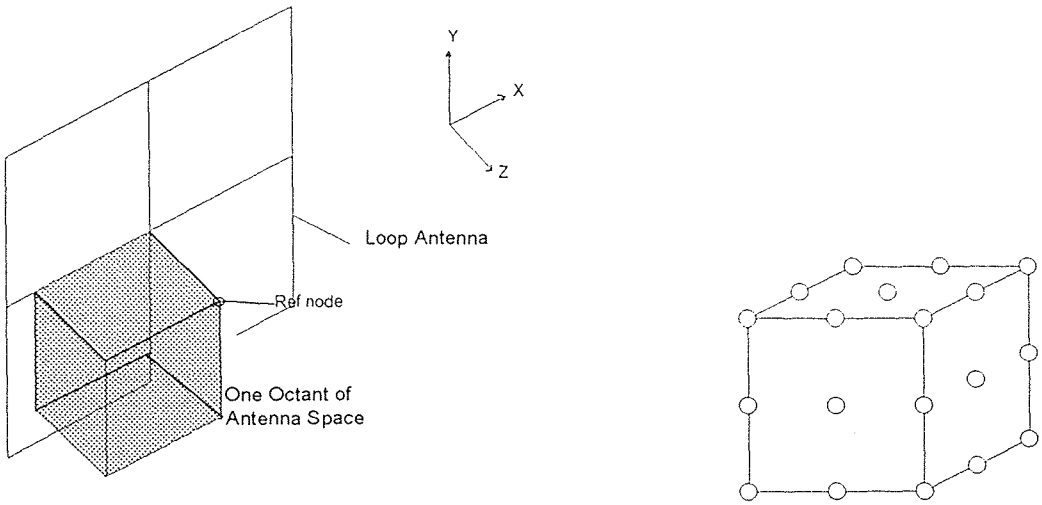

Figure 3.5 27 Node Distribution in One Octant of Antenna Space

Once the 27 scaling factors are obtained; they can be referenced with any one node to get a map of all ratios, $c.f._x = s.f._x/s.f._r$ where $s.f._r$ is the scaling factor at the reference node and $s.f._x$ are scaling factor at all other nodes, $x = 1$ *through* 27, except for $x = 18$,

which for our case is the reference node. Reference node, as shown in Figure 3.5, is the one at which the counts are calibrated for regular experiments.

Thus each correction factor signifies how much the model voltage should be multiplied by to get a corrected model voltage value for better agreement with reality. During the course of a trajectory, if a data point lies on one of the nodes the *c.f.* the corresponding correction factor $c.f_X$ value for the node is readily used to modify the model voltage. When the data point is not on one of the nodes a good method to compute the value of correction factor needs to be developed. The function to compute this correction factor has to minimize the deviation seen in Figures 3.1 through 3.4. Due to the very high non-linearity in computation of voltage it is difficult to represent this deviation as a function. After testing few alternative methods to build such a function, a Finite Element Method's, shape factors type weight distribution function to compute the correction factor is adopted (see below).

The correction factor for point (x, y, z) in the antenna coordinate system is computed using the cube immediately surrounding the current point. This cube has its vertices on eight nodes defined by two nodes along each of the three axes. Of two nodes along X axis between which x lies, the node closer to the antenna system origin is node termed as x_1 and the node away from the antenna system origin is termed x_2. Nodes y_1, y_2, z_1 and z_2 are defined following the same convention. Variables x_W, y_W and z_W representing weights for current point along X, Y, and Z axis in antenna system respectively are then defined as defined as:

$$x_w = \left\| \frac{x - x_1}{x_2 - x_1} \right\| \quad y_w = \left\| \frac{y - y_1}{y_2 - y_1} \right\| \quad z_w = \left\| \frac{z - z_1}{z_2 - z_1} \right\|$$

Once x_W, y_W and z_W are calculated, the correction factor is computed as:

$$
\begin{aligned}
c.f._{(x,y,z)} = \; & c.f.(x_1, y_1, z_1) * (1 - x_w) * (1 - y_w) * (1 - z_w) \\
+ \; & c.f.(x_2, y_1, z_1) * x_w * (1 - y_w) * (1 - z_w) \\
+ \; & c.f.(x_1, y_2, z_1) * (1 - x_w) * y_w * (1 - z_w) \\
+ \; & c.f.(x_2, y_2, z_1) * x_w * y_w * (1 - z_w) \\
+ \; & c.f.(x_1, y_1, z_2) * (1 - x_w) * (1 - y_w) * z_w \\
+ \; & c.f.(x_2, y_1, z_2) * x_w * (1 - y_w) * z_w \\
+ \; & c.f.(x_1, y_2, z_2) * (1 - x_w) * y_w * z_w \\
+ \; & c.f.(x_2, y_2, z_2) * x_w * y_w * z_w
\end{aligned}
$$

Correction factors calculated in this manner provide a good model-reality voltage match and hence this formula is currently being used in the particle tracking code.

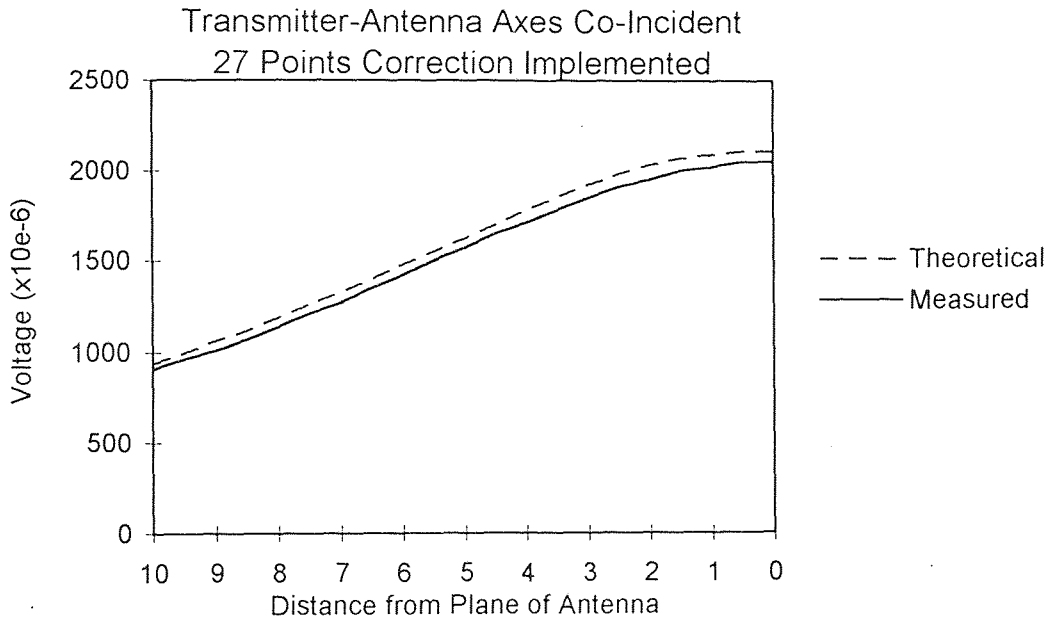

Figure 3.6 Model-Reality Voltage Comparison After 27 Point Correction With Axes Coincident

3.3.3 Model Reality Voltage Plots After Implementing 27 Points Correction

Knowing *c.f.(x,y,z)*, the voltage model is multiplied by a correction factor at every point to get empirically corrected voltages. Figure 3.6 through 3.9 represent Figures 3.1 through 3.4 after the implementation of the 27 points correction scheme in the backward algorithm. The agreement in measured and model voltages shows significant improvement. Thus implementation of such a scheme is expected to improve the accuracy of predicted results significantly and consistently

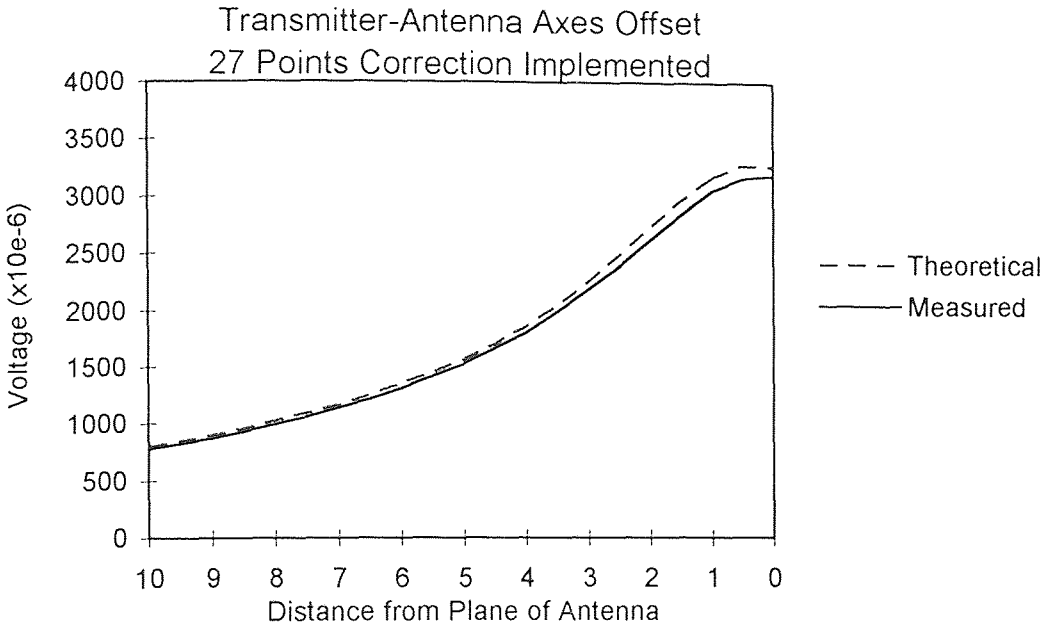

Figure 3.7 Model-Reality Voltage Comparison After 27 Points Correction With Axes Offset

3.3.4 Improvements To 27 Points Correction

Although the 27 point correction scheme is expected to improve the results, several other improvements may be needed in the future for the following reasons:

(1) The 27 point scheme assumes perfect symmetry of the mapping when the octant in which they are taken is mirrored in the antenna coordinate system. Theoretically this is valid but practically it is not exactly true.

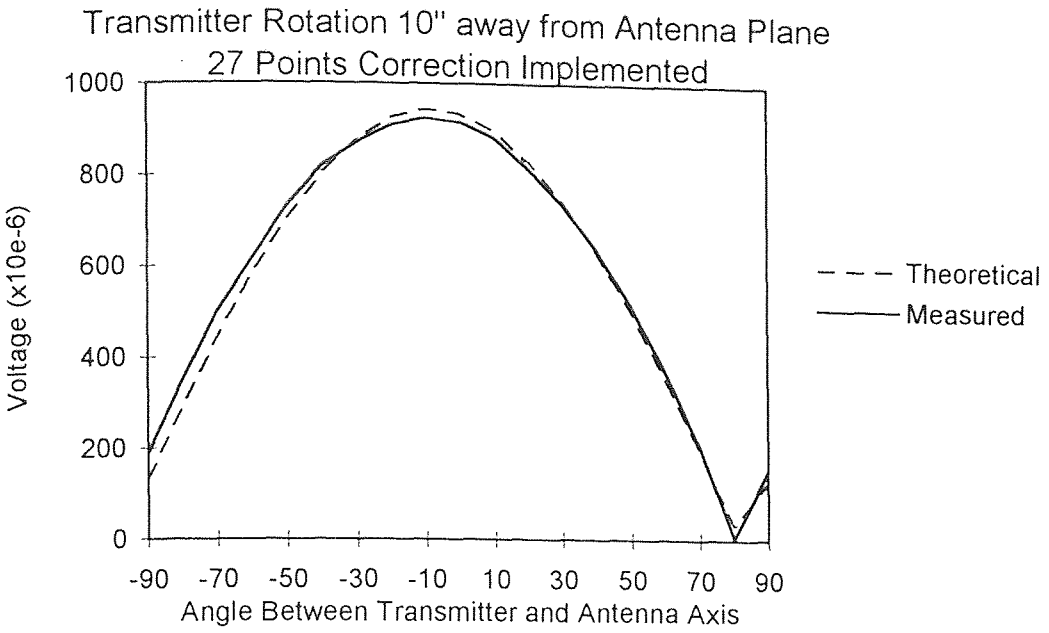

Figure 3.8 Model-Reality Voltage Comparison After 27 Point Correction Transmitter Rotation Away 10" From Antenna Plane

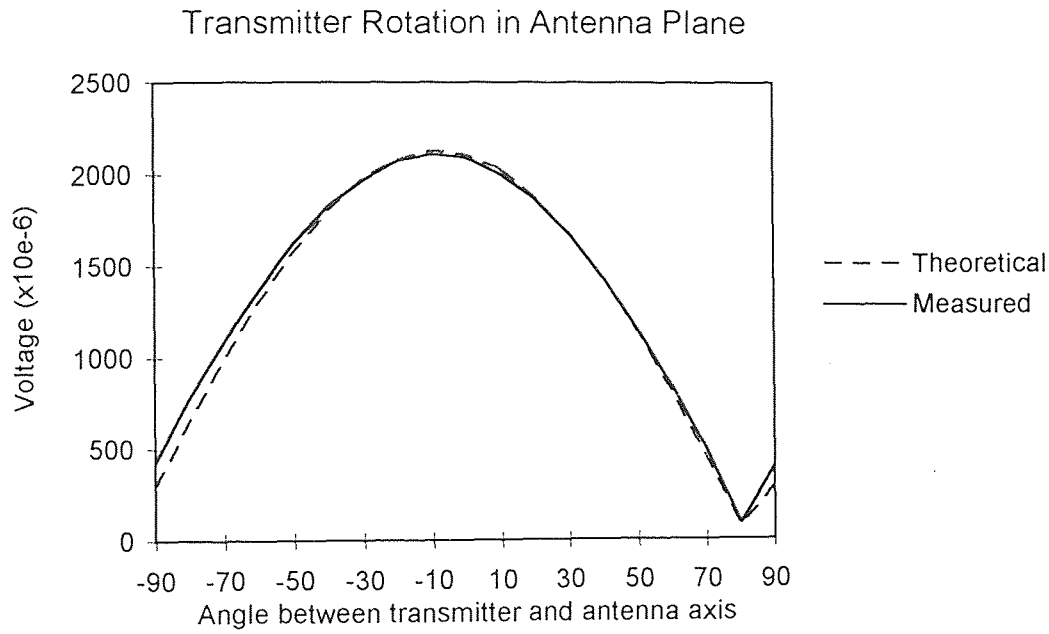

Figure 3.9 Model-Reality Voltage Comparison After 27 Points Correction Transmitter Rotation In Antenna Plane

(2) The 27 point map is implemented only for a single transmitter as against use of three transmitters.

(3) When the chute is very large, 27 nodes may not be enough to model the non-linearity of scaling factors. In such cases a higher number of nodes may be required and the interpolation function will have to be modified accordingly.

3.4 Practical Issues for Implementing the 27 point correction

Since the voltage readings at the 27 points have to be taken for every new setup of chute and antenna configuration, the following points are worth noting:

(1) The correction map based on only one antenna is assumed to hold true for all antennae with the same aspect ratio. Hence, one correction map has to be constructed for every antenna with a different aspect ratio.

(2) The correction map is based on the reference node with respect to which all correction factor ratios $c.f._X$ *(x = 1 through 27)* are computed. For the 27 point empirical correction to be valid, the regular calibration point for all experiments in lab has to be taken at the same reference node.

(3) Theoretically, the correction map should remain independent of the transmitter. In practice this is not the case. The difference in correction factor ratios at the nodes is observed to be very small and hence is neglected for the current 3 transmitter assembly. Use of a single 27 point map for three transmitters for all possible three transmitter assemblies has yet to be tested for robustness.

(4) Since the same map is used for all three transmitters; data acquisition counts obtained at 27 nodes should be in the orientation where *transmitter axis and antenna axis are parallel* and NOT the packaged transmitter assembly axis (sphere coordinate system) and antenna axis. This is done using a minor adjustment of the three transmitter assembly mounted on the jig. Hence when computing the model voltage, the final matrix ${}^{tp_i}T_{ta_i}$ should be ignored and only ${}^{a_j}T_{tp_i}$ as given by equation[2.3](Section

2.3.1.1) should be used for callibration at node points. It is particularly important to do so as after assembly, the magnitude of angular deviation for all 3 transmitters is different.

(5) The extent of octants which determine node positions should be carefully chosen keeping the antenna size, inter-antenna spacing and antenna configuration in mind. It is pointless to take nodes at antenna edges as they are beyond the chute boundaries and the tracer particle does not reach there. Also the nodes on or very near the edge represent a special case from a reciprocity point of view and can render the correction map incorrect. As observed in Figure 3.5, the octant for the 27 point implementation does not extend to the edge of the antenna.

The results discussed at the end of chapter two have been reprocessed after implementation of the 27 points correction scheme to get results as presented in Figures B.13 to B.18 of appendix[B]. The steadily increasing glitch seen in the X plot before has almost disappeared. Maximum and mean deviation numbers have come noticeably down to reflect improvements through 27-point correction scheme. The maximum deviation in X still is at a point where the trajectory crosses the plane of antenna number 2. Since 27 points take care of most of model-reality discrepancy problems, the glitch seen in Figure B.13 appears to be a problem related to the convergence of numerical solution. Chapter 4 proposes a scheme to prevent erroneous solutions due to the convergence problems.

CHAPTER 4

SELECTION OF QUALITY INFORMATION

The availability of a three transmitter tracking sphere has increased the amount of information available for use in the backward solution. The numerical solution approach and hence the converged position, hinges on a single number; magnitude of the error voltage array EV[] which is $||EV_{sol}||$. As noted in Section 2.4.2.1, not all the elements of EV[] are equally important for convergence. This chapter addresses some convergence issues and proposes an idea for using only important information elements for the backward algorithm.

4.1 Solution Convergence Problem

The perturbation approach as discussed in Section 2.4.2.2 usually works fine for the present set-up of seven antennae resulting in [7 * 3 = 21]elements of EV[]. However there are cases where the correct solution does not have minimum $||EV_{sol}||$ and hence the selected converged solution selected is not optimal. The acceptance of such a non-optimal solution is called 'Multiple Solutions'; since the error at the correct solution has a higher ||EV[]|| value. Since such a multiple solution is based on the $||EV_{sol}||$ value alone and the error is mainly in position, we refer to it more specifically as a 'position multiple solution'. For use of 1 transmitter, many position multiple solutions occur but with 3 transmitters they are less frequent. Such convergence problems usually arise due to equal weighing of all elements of EV[]. Figures C.1 through C.6 in appendix[C] show a particular set of results. The deviation in these results is high even after implementing the 27 points correction scheme, suggesting that there is a convergence problem.

For any given position and orientation of the transmitter in the chute; there are some "Quality Information Elements" among all elements of measured voltage MV[].

"Quality Information Elements" are those elements of measured voltage MV[] which have a high signal to noise ratio. In the code they are detected in following way.

Measured voltage elements representing more parallelism (less than $\pm 45^{o}$ angle) between transmitter and antenna axis, have higher signals and better signal to noise ratios. The term "more parallel" is subjective implying that as the angle between transmitter and antenna axis increases the signal to noise ratio becomes less favorable to converging to a good solution. Similarly, elements of measured voltage MV[] where the distance between the plane of antenna and transmitter is lower have higher readings. The term "lower" is again subjective implying that as distance between the antenna and transmitter increases, the induced signal becomes less favorable to convergence to a good solution.

Thus, the elements representing a small distance or small angle between the transmitter and antenna axes are termed as "Quality Information Elements". Such elements play a dominant role in the solution process. Even a marginal difference in position and orientation in trial X[] by *lmdiff* from the actual position and orientation $X_{actual}[]$ produces a large value of EV[] for these elements. Giving high weight to such readings reduces the possibility of converging to a multiple solution. Thus every antenna has an "active region" within which their readings have a large significance in terms of converging to the correct solution. Beyond this region the readings cease to contribute positively to the solution convergence process.

4.2 Detecting Quality Information Elements

For any position and orientation of transmitter assembly in chute space, there are six antennae immediately surrounding it. These antennae have a higher signal induced (better quality information). Also each transmitter is "more parallel" to one or two axes of chute giving better information in antennae along these axes. Theoretically, for numerical solution, at least six elements of MV[] are required. Empirically it is found that around 15 to 18 elements of EV[] are of primary importance to the solution. Most of the other

elements of EV[] can be attributed either to low signal to noise ratio (higher orthogonality) or higher distance. These less significant elements tend to assume low level EV[] values irrespective of trial X[] and do not contribute to the convergence of solution. As a result, many times a solution with minimum $||EV_{SOl}[k]||$ (where k is number of perturbations) is not a true solution but a case of 'position multiple solution'. Intuitively for a higher number of antennae, the number of key elements remains the same and the chances of multiple solutions are higher.

4.3 Quality Information Selection

The parallelism between a transmitter and antenna can be determined in the code. Matrix ${}^{a_j}T_{ta_i}$ gives direction cosines of transmitter axis with respect to antenna axis. Looking at values of direction cosines, a cutoff value of orientation can be determined below which the element is not to be considered for the backward solution. The convention is to consider the transmitter axis as the Z axis of the transmitter coordinate system and the antenna axis as Z axis of the antenna coordinate system. As we look for higher parallelism between the transmitter axis and the antenna axis, the cutoff value is based on last element of the 3 x 3, matrix ${}^{a_j}T_{ta_i}$. Being a cosine function, if this number is lower than a particular value, we ignore the corresponding element for computing the solution.

The transmitter position (x, y, z) with respect to each antenna coordinate system is also available in the code. Based on the z value we can determine the distance cutoff for a given element computation of solution.

The particle tracking code is modified to select "Quality Information Elements" for the convergence process. At every data point reading, measured voltage MV[] is processed considering all elements of EV[] to reach a solution $X_{SOl}[]$. This solution $X_{SOl}[]$ is evaluated in terms of the transmitter axis orientation and the distance from the antenna, and the low quality information elements ignored. The solution is reprocessed only with key elements contributing to convergence. If the original solution was a case of multiple

solution, the new solution will be different and usually is a correct one. The Quality Information Selection approach in the form of a flow chart is shown in Figure 4.1. Quality Information Selection is thus a solution improvement scheme based on the three parameters described in next three subsections.

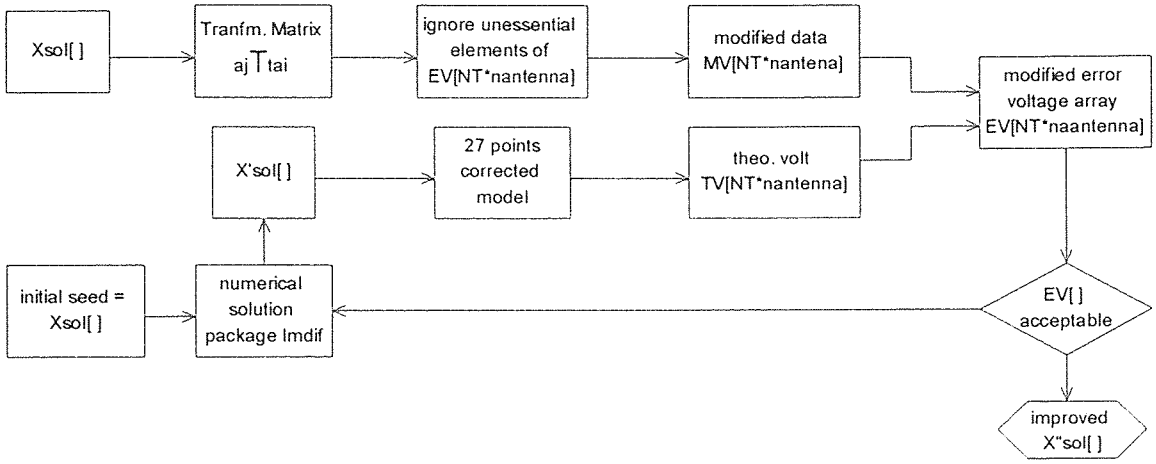

Figure 4.1 Quality Information Selection

4.3.1 Cut Off Distance

The distance from the plane of the antenna to the transmitter is given by the local 'z' value. This 'z' value is available from the position(x, y, z) of the transmitter in the antenna coordinate system. When 'z' is higher than a particular value, the signal induced in antenna is insensitive to the position and orientation of the transmitter. Empirically this particular value is found to be approximately 1.5 times the diagonal length. Hence the distance cut-off is set at ±1.5 times the length of antenna diagonal. For lower values of 'z', approximately less than 0.5 times the diagonal length, it is advisable not to neglect elements based on poor orientation for reasons explained in Section 4.3.3 below.

4.3.2 Cut Off Orientation

The transmitter orientation in the antenna coordinate system is available in the code. Usually the antenna configuration is such that the antennae are mounted along the major axes of the chute system and are mutually orthogonal. Hence if any transmitter orientation is bad for one antenna, it is favorable for an adjacent antenna which is perpendicular to it. Thus, the cutoff value of orientation should be set at 0.707 which corresponds to a 45^{o} angle between the transmitter and the antenna axis.

In the worst scenario, the transmitter would be so oriented, that it is equiangle to three mutually perpendicular antennae. Direction cosine values of the transmitter axis and the antenna axis for all three antennae in this case are 0.577, 0.577, 0.577. Hence if the cutoff acceptance value is fixed at 0.577; then information is used from each transmitter (of the three transmitter assembly) by at least one of the three mutually orthogonal antennae. At present the cutoff value set in the code is 0.577. Higher values of cutoff, for ignoring elements in the convergence process can be used since the probability of an equiangle orientation is low.

4.3.3 Minimum Information Elements

As discussed earlier, about 18 elements should be used to drive the solution using quality information. For the lab experiments, information elements between 18-21 have consistently given good results. The important point here is that if "quality" elements are neglected, the possibility of rejecting a bad solution due to high EV[] values in these elements is also reduced. In other words, a bad solution which is previously not selected because of high values of EV[] in "quality" elements may now be accepted. Thus the situation can occur where we accept a bad solution while trying to prevent a multiple solution. This is especially the case when the minimum number of elements is very low. It is always better to ignore all possible elements first based on distance and then based on orientation. This ensures that really poor signal to noise ratio elements are all discarded.

4.4 Effectiveness of Quality Information Selection Scheme

The results presented in appendix[B] using the 27 point correction have very high accuracy. To improve accuracy further calls for detailed investigation of many possible causes. Results for the same trajectory after implementation of the 'Quality Information Selection' scheme are presented in Figures B.19 through B.24 of appendix[B]. As expected, the improvements are not very significant. This is primarily due to two reasons. First, the accuracy after 27 points scheme itself is so high that further improvement is difficult. Second, current setup of chute-antennae configuration uses only 21 elements in EV[]. With around 18 elements required by the numerical solution approach, neglecting 3 elements doesn't change much. Quality Information Selection has shown improvements where 27 point implementation itself is not enough for accurate results as seen in Figures C.1 through C.6 in appendix[C]. Figures C.7 through C.12 in appendix[C] represent the same run after implementation of Quality Information Selection to realize marked improvements in results.

For chutes with a higher number of antennae, it is expected that Quality Information Selection will show further marked improvements in results. Results in Figures B.19 through B.24 of appendix[B] using Quality Information Selection highlights an interesting fact. In plots for angles there are three points where the match is very poor. These kind of stray mismatches in angles, are also seen without implementation of Quality Information Selection for many runs. This is investigated and explained in chapter 5.

CHAPTER 5

COMPUTATION OF INITIAL SEED

As seen in Figure 2.12, the particle tracking system converges to a correct solution using numerical techniques under the assumption that X[] is available at the first data point. For free flow experiments this assumption does not hold. In such experiments, to maintain continuous steady flow, the tracer particle is introduced along with other particles flowing at a high speed. In such circumstances, it becomes very difficult to determine X[] for the particle at first data point. Typically the position $X_p[x, y, z]$ at this point can be roughly approximated; but the orientation $X_o[\psi, \theta, \phi]$ is totally undetermined. For practical applications of the particle tracking system, the problem of the initial seed X[] has to be overcome. This chapter focuses on a method to make the particle tracking system independent of X[] at first data point.

5.1 Approaches to Initial Seed

An obvious approach to get an initial seed X[] would be to randomly try many perturbations (Section 2.4.2.2) and pick the best amongst different converged solutions. This approach is a brute force, exhaustive search type method with success totally dependent upon how good the initial seed X[] is. The main reason why such an approach has not worked so far is that the position elements of $X_p[x, y, z]$ and orientation elements of $X_o[\psi, \theta, \phi]$ are what we call inter compensatory. In other words, if a transmitter is very close to any antenna; with transmitter axis almost orthogonal, the signal computed by the model would be low. Similarly. a low signal also will be computed if the distance between the antenna and transmitter is high almost independent of the orientation. Thus X_p and X_o variables tend to mask each other's effect on voltage computation. An approach where the number of variables are fewer than six [viz.: $x, y, z, \psi, \theta, \phi$] would be more amenable to a

random guessing technique. Hopefully these fewer variables should not be inter compensatory for computing voltage.

5.2 Two Step Solution

As mentioned above, orientation and position elements of X[] do not work in tandem during the solution procedure. For the three transmitter assembly, it is possible to solve for the position elements independent of the orientation elements (Dave[4]). We utilize this to find the required initial seed X[] in two steps. In the first step we solve for position elements $X_p[x, y, z]$ only. Once the position variables are known; in the second step, the initial $X_{seed}[]$ is obtained by solving for both position and orientation. In second step more emphasis is placed on solving for orientation.

5.2 1 Solving for Position Independent of Orientation

The Forward Model computes voltage as a dot product of the magnetic field $\vec{B}$ and the area of transmitter $\vec{A}$. While a complete derivation of the forward model can be found in Dave[3], equation [2.1] and [2.2] appearing in chapter 2 are reproduced below :

$$\vec{B} = \sum_{k=1}^{4}\left[\left(\frac{\mu I_i}{4\pi R_k}\right)\left(\cos\varphi_{k1} - \cos\varphi_{k2}\right)\right]\hat{\Theta}_k \tag{5.1}$$

and

$$V = -N\omega\left(\vec{A}\cdot\vec{B}\right) \tag{5.2}$$

$\vec{B}$ is defined by variables $\hat{\Theta}$ and φ. $\hat{\Theta}$ and φ are functions of the transmitter position $X[x_l, y_l, z_l]$ in the local antenna coordinate system as seen in the model derivation. Thus $\hat{\Theta}$ and φ here are different from the similar terms appearing in system variables $[x, y, z, \psi, \theta, \phi]$. In equation[5.1], except for I_i, all elements for finding $\vec{B}$ are constant for a given transmitter. Voltage V is the dot product of the magnetic flux density $\vec{B}$ and the area $\vec{A}$ of

the transmitter coil. Taking a dot product of the normalized voltages with the transmitter area gives the components of magnetic flux $\vec{B}$ along three mutually perpendicular transmitter axes as explained towards end of Section 5.2.2. Summation of squares of these components gives the magnitude of $\vec{B}$ which is independent of the orientation as long as the area vectors of the transmitters are mutually orthogonal.

5.2.2 Derivation for 2 Step Solution

Expressing all parameters of equation[5.1] which are related only to the position as $\bar{f}(x,y,z)$, the equation can be rewritten as,

$$\bar{B}_j = I_j \cdot \bar{f}(x_l, y_l, z_l) \tag{5.3}$$

where I_j, the current in transmitter j is given as, $I_j = I_{0j} \cdot \sin(\omega_j \cdot t)$
and $j = 1 \ldots$ NT; number of transmitters
Equation [5.2] defines voltage as;

$$V_j = -\frac{\partial}{\partial t}(\bar{B}_j \bullet \bar{A}_j)$$

where : $\vec{A}_j = \|A\| \cdot \hat{A}$; $\hat{A}$ being the area vector of the transmitter coil.
Separating scalar terms out of the dot product;

$$V_j = (-\omega_j \cdot I_j \cdot \|A_j\|) \cdot (\bar{f}(x,y,z) \bullet \hat{A})$$

If we define normalized voltage v_j as;

$$v_j = \frac{V_j}{-\omega_j \cdot I_j \cdot \|A_j\|} = (\bar{f}(x,y,z) \bullet \hat{A}), \quad j = 1, 2, 3 \tag{5.4}$$

we get,

$$v_1 = \bar{f}(x,y,z) \bullet \hat{A}_1, \quad v_2 = \bar{f}(x,y,z) \bullet \hat{A}_2 \text{ and } v_3 = \bar{f}(x,y,z) \bullet \hat{A}_3$$

As $\hat{A}_1$, $\hat{A}_2$, $\hat{A}_3$ are orthogonal, v_1 is the component of $\bar{f}(x,y,z)$ along $\hat{A}_1$, v_2 is the component of $\bar{f}(x,y,z)$ along $\hat{A}_2$ and v_3 is the component of $\bar{f}(x,y,z)$ along $\hat{A}_3$.

Therefore, by taking the square root of sum of squares, we obtain the magnitude of $\bar{f}(x,y,z)$.

$$\sqrt{v_1^2 + v_2^2 + v_3^2} \quad = \quad \left\| \bar{f}(x,y,z) \right\|$$

Thus the magnitude $\left\| \bar{f}(x,y,z) \right\|$ is independent of the orientation of the transmitter in the chute coordinate system.

5.2.3 Implementing the 2 Step Solution

During calibration, as discussed in Section 2.4.1, the model voltage is computed using equation [5.2]. After substituting for $\bar{B}$ from equation[5.1] in equation [5.2], constant terms like μ, N, ω_j, I_j, $\|A_j\|$ etc. can be grouped together in a generic constant k. k contains all the terms appearing in the denominator of equation [5.4]. For three transmitters we have three constants k_1, k_2 and k_3.Normalization of voltages as required by equation [5.4] can be performed directly using a single value of $k = k_1 = k_2 = k_3$ in the computation of model voltage during calibration. Thus, the scaling factor scales down as well as normalizes the measured voltages. In this approach, the single value of k may be any of k_1, k_2 or k_3. Figure 5.1 shows a sample of $\left\| \bar{f}(x,y,z) \right\|$ scaled up by a factor of six. X[] values at all data points of Figure 5.1 are given in Table 5.1. The magnitude of $\left\| \bar{f}(x,y,z) \right\|$, which basically is a measure of combined magnetic field due to all three transmitters is referred to as "Square Root of Normalized Sum Squared Voltages". The plot in Figure 5.1 serves as a practical proof of the derivation shown in Section 5.2.2. The marginal non-constancy observed in it is mainly attributed to deviation from perfect mutual orthogonality of three transmitters. Based on the fact that $\left\| \bar{f}(x,y,z) \right\|$ is independent of transmitter orientation, a code was developed which solves only for the three position variables $X_p[x, y, z]$ using all [NT x nantenna] elements of measured voltage.

To solve for position variables $X_p[x, y, z]$ in the first step, many perturbations with a large radius of perturbation, are carried out. Since the two step approach has to be

adopted only for 1st data point, the number of perturbations can be very large without significantly increasing total processing time. The first step algorithm and numerical techniques being same as regular solution algorithm, initial seed $X_p[x, y, z]$ is still needed. For the majority of experimental chutes $X_p[x, y, z]$ can be easily approximated within ±12" along X, Y and Z direction of chute coordinate system. This approximate seed $X_p[x, y, z]$ is provided to the code and the radius of perturbation is kept at 12" to 15". Solutions after executing the first step with initial seed $X_p[x, y, z]$ given up to 18" away from known actual $X_p[x, y, z]$ have converged to within 1" of the actual $X_p[x, y, z]$.

Table 5.1 X[] Values for Finding Sum Squared of Normalized Voltages

Point #	X	Y	Z	ψ	θ	ϕ
1	10	10	10	0	0	0
2	10	10	10	0	0	330
3	10	10	10	0	0	300
4	10	10	10	0	0	270
5	10	10	10	0	30	270
6	10	10	10	0	60	270
7	10	10	10	0	90	270
8	10	10	10	30	90	270
9	10	10	10	60	90	270
10	10	10	10	90	90	270
11	10	10	10	30	30	330
12	10	10	10	45	45	315
13	10	10	10	60	60	300

In the second, the usual approach for solution is used with large perturbations for angular elements. Position variables in the second step are perturbed within a very small

radius for fine tuning of the solution. Table 5.2 shows a set of results for finding initial guess using the two step approach. While most results are fairly accurate, the last four are noticeably off in the orientation, calling for further investigation. It is noted here that three of these four sets are the same as those for which angle plots presented at the end of chapter 4 were totally off.

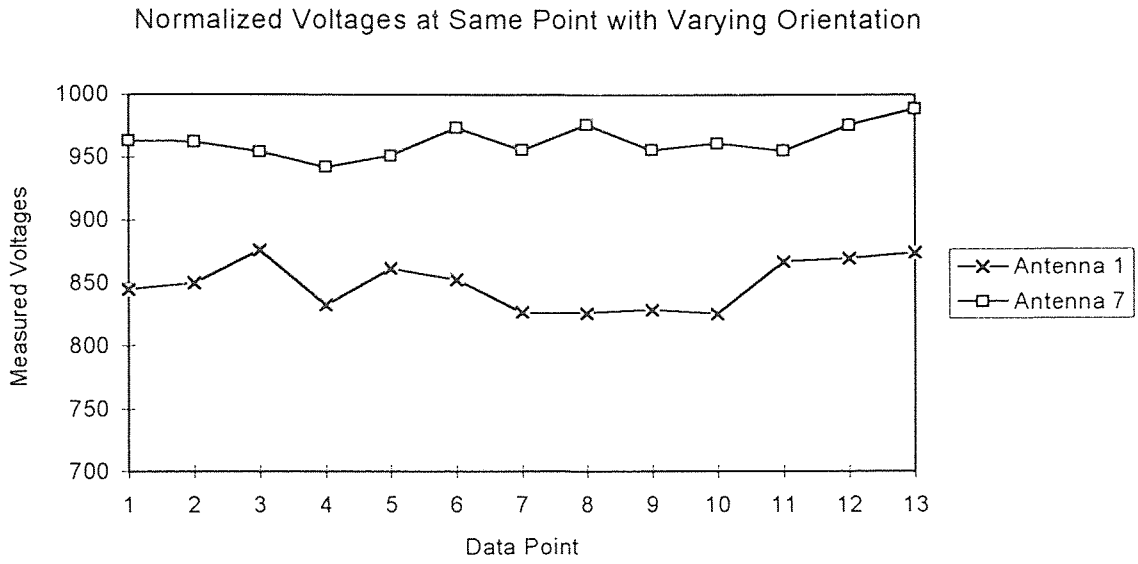

Figure 5.1 Sample of Square Root of Normalized Sum Squared Voltages

Table 5.2 Results for 2 Step Solution Approach

pnt #	Actual Position						Converged Position					
	X	Y	Z	ψ	θ	ϕ	X	Y	Z	ψ	θ	ϕ
1	8.0	3.7	6.9	20	345	30	8.1	4.0	7.0	19	349	31
2	11.4	5.6	7.8	60	345	30	11.4	5.7	7.6	57	344	32
3	16.5	8.4	9.3	120	345	30	16.3	8.5	9.2	116	342	32
4	18.3	9.4	9.8	140	345	30	18.1	9.4	9.7	134	340	29
5	21.7	11.3	10.8	180	345	30	20.8	11.8	10.7	177	341	31
6	23.4	12.2	11.3	200	345	30	22.9	12.5	11.1	200	341	31
7	6.3	2.8	6.4	0	345	30	6.1	3.2	6.5	174	193	211
8	12.3	6.0	8.1	70	345	30	12.1	6.1	7.9	247	196	213
9	14.0	7.0	8.6	90	345	30	13.8	6.7	8.2	267	197	212
10	14.8	7.5	8.8	100	345	30	15.3	7.8	8.9	260	16	208

5.3 Orientation Multiple Solution

Section 4.1 discusses a case of 'position multiple solution'. Position multiple solution is off both in position and orientation, mainly due to the minimum $||EV_{sol}||$ condition for solution selection. Solutions 7 through 10 seen in Table 5.2 match fairly well for position elements but are apparently totally off in orientation.

The Forward model predicts the theoretical voltage based on the direction cosines of transmitter axis in antenna coordinate system. These direction cosine values, given by the third column of ${}^{a_j}T_{ta_j}$, are function of elements of matrix ${}^{g}T_{s}$ as all remaining matrices have constant elements. Thus, the direction cosines are functions of $\psi, \theta,$ and ϕ which determine ${}^{g}T_{s}$. A given set of direction cosine values does not correspond to a unique set of $X_O[\psi, \theta, \phi]$. In other words two different sets of numbers $X_{actual}[\psi, \theta, \phi]$ and $X_{different}[\psi, \theta, \phi]$ can result in almost equal direction cosines values and hence almost equal theoretical voltage TV[NT x nantenna] computed by the forward model. Thus error voltage EV[] computed using values of same MV[] and almost equal TV[] will again be a case of minimum $||EV_{sol}||$ (Section 2.4.2.1). Thus the solution selected, $X_{different}[\psi, \theta, \phi]$ is off in orientation. Tables 5.3a through 5.3d show ${}^{g}T_{s}$ matrices (with $\psi, \theta,$ and ϕ values), corresponding to the actual and converged solutions 7 through 10 shown in Table 5.2. As elements in both matrices are almost equal, this kind of multiple solution is called "orientation multiple solution". In "orientation multiple solution", position is correct and angles are incorrect yet have the same direction cosines as the correct solution most to the time.

Table 5.3a Global-Sphere Matrix Elements - Solution 7 of table 5.2

Matrix at Actual X[] Values			Matrix at Converged X[] Values		
(6.3, 2.8, 6.4, 0, 345, 30)			(6.1, 3.2, 6.5, 174, 193, 211)		
0.8365	-0.500	-0.224	0.8301	-0.496	-0.251
0.4829	0.8660	-0.129	0.5077	0.8610	-0.027
0.2588	0.0000	0.9659	0.2303	-0.104	0.9674

Table 5.3b Global-Sphere Matrix Elements - Solution 8 of table 5.2

Matrix at Actual X[] Values			Matrix at Converged X[] Values		
(12.3, 6.0, 8.1, 70, 345, 30)			(12.1, 6.1, 7.9, 247, 196, 213)		
0.8365	-0.381	0.3931	0.8025	-0.429	0.4139
0.4829	0.1745	-0.858	0.5284	0.1900	-0.827
0.2588	0.9076	0.3303	0.2727	0.8828	0.3795

Table 5.3c Global-Sphere Matrix Elements - Solution 9 of table 5.2

Matrix at Actual X[] Values			Matrix at Converged X[] Values		
(14.0, 7.0, 8.6, 90, 345, 30)			(13.8, 6.7, 8.2, 267, 197, 212)		
0.8365	-0.224	0.5000	0.8015	-0.282	0.5270
0.4829	-0.129	-0.866	0.5148	-0.122	-0.848
0.2588	0.9659	0.0000	0.3042	0.9514	0.0473

Table 5.3d Global-Sphere Matrix Elements - Solution 10 of table 5.2

Matrix at Actual X[] Values			Matrix at Converged X[] Values		
(14.8, 7.5, 8.8, 100, 345, 30)			(15.3, 7.8, 8.9, 260, 16, 208)		
0.8365	-0.133	0.5313	-0.850	0.1618	0.5003
0.4829	-0.277	-0.830	-0.448	0.2748	-0.850
0.2588	0.9512	-0.167	-0.275	-0.947	-0.161

One of the objectives of the particle tracking system is to compute linear and angular velocities of flowing particles. Since the errors in the position $X_p[x, y, z]$ values are small even in the case of "Orientation Multiple Solution", linear velocities can be computed with little error. Angular velocities are computed based on the values of matrix elements and not directly on the orientation angles ψ, θ and ϕ. Since these elements are usually correct, they would allow for computation of correct angular velocities. However, the matrix elements may be in error for some of the 'orientation multiple solution' cases and hence corresponding angular velocities may be incorrect. These incorrect values can be spotted easily in the plot of angular velocity as a discontinuity. Though remedial measures can be taken heuristically for such incorrect values, it would be better to develop a proven add on algorithm to prevent convergence to 'orientation multiple solution'.

CHAPTER 6

SUMMARY OF PROGRESS AND CONCLUSIONS

Implementation issues related to the use of multiple transmitters for particle tracking in 3 dimensions have been discussed in the preceding chapters. Such a system relies on constructing a miniature transmitter assembly and using a theoretical model for voltage prediction.

Through the results presented so far, the feasibility of this system has been established. Figures C-13 through C-19 in appendix [C] show a final set of results for a double-sine-curve trajectory. The results are very accurate and mean deviation in distance is less than 1" throughout the course of the trajectory. As the tracer particle to be used for experiments is of 1" diameter the mean deviation in distance is within 1 particle diameter. This chapter outlines the summary of progress for the task of transition from a single transmitter to multiple transmitters in order to achieve such accurate results consistently. Directions for future work and conclusions about the progress of the project so far are also presented.

6.1 Summary of Progress

Work by Volcy [15] describes use of a single transmitter for predicting particle trajectory. Results so obtained were good but inconsistent. Based on the effect of orthogonality, use of multiple transmitters was recommended. In the present work, issues related to the use of multiple transmitters were addressed.

A flat ferrite cross acting as a core for a two transmitter coil was obtained. Winding the third transmitter around it, using a thin printed circuit board for electrical components and using smaller batteries for the power source enabled the packaging of three transmitters in a 1" sphere.

The speed to data acquisition system was increaded to desired level by modifying it to switch antennae by an externally driven multiplexer. This decreased the required number of demodulator boards and pins on the data acquisition card. The experimental data is first stored in virtual memory of the PC and is later on transferred to the hard disk.

A systematic approach to determine the position and orientation of three different transmitters by use of six variables in the chute coordinate system was established. The method takes into account the imperfections in the assembly of the multiple transmitter apparatus. The software was developed accordingly to handle the multiple transmitters.

Methods to improve the accuracy of the tracking system were investigated. In order to improve the model-reality agreement of voltages and rectify other inconsistencies in the data acquisition system a 27 point correction scheme as relates to three transmitters was implemented. Within the software, a method to select Quality Information Elements was established. Based on the chute configuration and users' discretion, three deciding factors, number of measured voltage elements, distance from the plane of the antenna and cutoff orientation are provided for use in improving the solution.

The particle tracking system requires an initial seed X[] for all flow experiments. This can be a problem for different chutes. To address this, a new solution scheme to solve for six variables in two steps was introduced. This solution scheme solves for position variables in the first step and uses them to solve for all six variables in the second step. This new solution scheme is used to obtain the initial seed X[] required by the particle tracking system. Thus a major hurdle for effectively and easily using the particle tracking system on all kinds of chute shapes and sizes has been overcome.

6.2 Future Work

Considerable work needs to be done to perfect the particle tracking system so that it can be readily used for all applications. Presented below is a brief outline of immediate tasks for further developing the particle tracking system.

1) Particle Packaging : The smaller the size of the particle within which three transmitters can be packaged, the better it is from an experimental point of view. The possibility of constructing smaller tracer particles needs to be investigated. Of immediate concern is the imbalance of the sphere due to unequal weight distribution around its center. This tends to bias the trajectory of the tracer particle as it travels within the flow.

2) Data Acquisition : For conducting experiments in the lab on a chute with steady particle flow, more than 16 antennae will be used. Present data acquisition is capable of monitoring up to 16 antennae only. To develop a data acquisition system which can monitor a higher number of antennae, the external multiplexing technique used in the current approach can be cascaded. Thus, an additional multiplexer can be used to select from a series of external multiplexers, each of which controls the connection of a particular group antennae to the data acquisition system. Though a bit complicated to develop, such a scheme would increase the number of antennae scanned exponentially.

   A simpler approach based on the above principle is to use two sequential multiplexers and a single trigger signal to switch between the two multiplexers. Triggering is to be so done that the data acquisition system cyclically proceeds to scan the first antenna connected to the second multiplexer after scanning the last antenna connected to the first multiplexer. This system is relatively easy to construct but has not yet been developed and rigorously tested.

   Better equipment or alternative methods of data storage such as storing the data on magnetic tape etc. may also increase the speed of data acquisition. Though not an immediate requirement, for flows having higher particle speeds; a faster data acquisition system may be needed.

3) Software : Further development of software is subdivided into three parts

3.1) Orientation multiple solution cases for three transmitters continue to exist. A method needs to be developed to prevent such problems.

3.2) Data acquired at a very fast rate has fluctuations in the readings from one data point to another when averaging the data over two points. Preprocessing of the data may be required before using the software for predicting the trajectory of the tracer particle.

3.3) Results obtained for the particle tracking system will be used for comparing experimental and theoretical linear and angular velocities of the tracer particle. The software in its present form does not record the timing parameters (which are required for computing velocities). It could be enhanced to compute such velocities automatically. This requires the data acquisition system to keep track of time.

4) Practical application aspects :

4.1) The accuracy of the system is dependent upon the quality of information generated. This information is related to the transmitter position in the antenna coordinate system. Hence the configuration of antenna around the chute determines the quality of the information. Antenna configuration around the actual chute should be carefully studied and optimized.

4.2) Antenna coupling is predominant when antennae wires run parallel and close to each other. Hence it is very important to mount antennae such that no two wires are within 1" of each other.

4.3) As the transmitter gets closer to the edge of the antenna, the signal induced becomes unusually large. It is difficult to account for this large reading through the scaling factor function in the 27 point correction scheme. Hence, the extreme nodes in the 27 points scheme are chosen to be away from the edge of the antenna. This requires mounting of antennae further away from the chute

boundary so that such unusual readings are pre-empted and the 27 points correction scheme can be used effectively.

4.4) Different antennae having different aspect ratios are believed to help in preventing multiple solutions. This would require obtaining more 27 point maps, a very tedious task. For an antennae system with only two different aspect ratios, symmetry of antenna arrangement should be avoided. Symmetry of antennae configuration from one section of the chute to the next is conducive to multiple solutions and should be avoided.

6.3 Conclusions

A Particle Tracking System based on the use of multiple transmitters has been developed successfully. The Backward Algorithm and data acquisition system have been tested through experiments in the lab. Through the results presented, it can be concluded that a system based on the 'Principle of Electromagnetic Induction' can be used effectively for particle tracking.

Further investigations along the directions outlined in 'Future Work' will make the system more robust. Accomplishing some of these goals will improve the accuracy of system under test condit

APPENDIX A

COMPUTATION OF TRANSFORMATION MATRICES

This appendix relates to transformation matrices discussed in article[2.3]. In the first part, construction of matrix ${}^{g}T_{s}$ is presented. In the second part numerical values for correction matrix for each transmitter are calculated.

Part I

Global to sphere matrix ${}^{g}T_{s}$ is comprised of three sequential rotations of ψ, θ and ϕ about the chute X, Y and Z axes repectively. Since the subsequent rotations are in the stationary coordinate system, the corresponding matrices are pre-multiplied. The unknown vector X[x, y, z, ψ, θ, ϕ] is hence defined as :

$$\mathrm{X}(x,y,z,\psi,\theta,\phi) \equiv {}^{g}T_{s}(x,y,z,\psi,\theta,\phi)$$

$$
{}^{g}T_{s} = \begin{bmatrix} 1 & 0 & 0 & x \\ 0 & 1 & 0 & y \\ 0 & 0 & 1 & z \\ 0 & 0 & 0 & 1 \end{bmatrix}
\begin{bmatrix} \cos\phi & -\sin\phi & 0 & 0 \\ \sin\phi & \cos\phi & 0 & 0 \\ 0 & 0 & 1 & 0 \\ 0 & 0 & 0 & 1 \end{bmatrix}
\begin{bmatrix} \cos\theta & 0 & \sin\theta & 0 \\ 0 & 1 & 0 & 0 \\ -\sin\theta & 0 & \cos\theta & 0 \\ 0 & 0 & 0 & 1 \end{bmatrix}
\begin{bmatrix} 1 & 0 & 0 & 0 \\ 0 & \cos\psi & -\sin\psi & 0 \\ 0 & \sin\psi & \cos\psi & 0 \\ 0 & 0 & 0 & 1 \end{bmatrix}
$$

$$
{}^{g}T_{s} = \begin{bmatrix} \cos\phi\cos\theta & \cos\phi\sin\theta\sin\psi - \sin\phi\cos\psi & \cos\phi\sin\theta\cos\psi + \sin\phi\sin\psi & x \\ \sin\phi\cos\theta & \sin\phi\sin\theta\sin\psi + \cos\phi\cos\psi & \sin\phi\sin\theta\cos\psi - \cos\phi\sin\psi & y \\ -\sin\theta & \cos\theta\sin\psi & \cos\theta\cos\psi & z \\ 0 & 0 & 0 & 1 \end{bmatrix}
$$

In the code for ease of handling the 4x4 matrix is broken in two matrices. One matrix of 3x3 for orientations and other 3x1 for position. We can do this as the projection elements

in the 4x4 matrix are always zero and scaling is always unity. Therefore the above matrix is equivalent to following two matrices :

$$ {}^{g}T_{s} = \begin{bmatrix} \cos\phi\cos\theta & \cos\phi\sin\theta\sin\psi - \sin\phi\cos\psi & \cos\phi\sin\theta\cos\psi + \sin\phi\sin\psi \\ \sin\phi\cos\theta & \sin\phi\sin\theta\sin\psi + \cos\phi\cos\psi & \sin\phi\sin\theta\cos\psi - \cos\phi\sin\psi \\ -\sin\theta & \cos\theta\sin\psi & \cos\theta\cos\psi \end{bmatrix} \text{ and } \begin{bmatrix} x \\ y \\ z \end{bmatrix} $$

In part II, since we are dealing with only orientation corrections, the 3x3 matrices are shown.

Part II

As the correction matrix ${}^{tp_i}T_{ta_i}$ and sphere to transmitter matrix ${}^{s}T_{tp_i}$ in equation [2.4] are both constant, they are grouped together as ${}^{s}T_{ta_i}$. After finding the values of elements in following manner ${}^{s}T_{ta_i}$ is hardcoded in the software :

For 1st transmitter :

The correction angles are +4° @ X_g and -8° @ Yg. As discussed in article [2.3.2] the direction of angles is reversed :

$$ {}^{s}T_{ta_{2.0}} = {}^{s}T_{tp_{2.0}} .\text{Rot}(x, -4).\text{Rot}(y, +8) $$

$$ {}^{s}T_{ta_{2.0}} = \begin{bmatrix} 0 & 0 & 1 \\ 1 & 0 & 0 \\ 0 & 1 & 0 \end{bmatrix} \begin{bmatrix} 1 & 0 & 0 \\ 0 & \cos\psi & -\sin\psi \\ 0 & \sin\psi & \cos\psi \end{bmatrix} \begin{bmatrix} \cos\theta & 0 & \sin\theta \\ 0 & 1 & 0 \\ -\sin\theta & 0 & \cos\theta \end{bmatrix} $$

substituting ψ = -4° and θ = +8° in above equation we get

$$ {}^{s}T_{ta_{2.0}} = \begin{bmatrix} -0.139 & -0.07 & 0.988 \\ 0.990 & 0.00 & 0.139 \\ -0.01 & 0.998 & 0.069 \end{bmatrix} $$

For 2nd transmitter :

The correction angles are +4° @ X_g and -10° @ Yg. As discussed in article [2.3.2] the direction of angles is reversed :

$$ {}^{s}T_{ta_{3.65}} = {}^{s}T_{tp_{3.65}} .\text{Rot}(x, -4).\text{Rot}(y, +10) $$

$$ {}^{s}T_{ta_{3.65}} = \begin{bmatrix} 0 & 1 & 0 \\ 0 & 0 & 1 \\ 1 & 0 & 0 \end{bmatrix} \begin{bmatrix} 1 & 0 & 0 \\ 0 & \cos\psi & -\sin\psi \\ 0 & \sin\psi & \cos\psi \end{bmatrix} \begin{bmatrix} \cos\theta & 0 & \sin\theta \\ 0 & 1 & 0 \\ -\sin\theta & 0 & \cos\theta \end{bmatrix} $$

substituting ψ = -4° and θ = +10° in above equation we get

$$ {}^{s}T_{ta_{3.65}} = \begin{bmatrix} 0.00 & 0.985 & -0.174 \\ 0.07 & 0.173 & 0.982 \\ 0.998 & -0.012 & -0.069 \end{bmatrix} $$

For 3rd transmitter :

The correction angle is -4° @ X_g . As discussed in article [2.3.2] the direction of angles is reversed :

$$ {}^{s}T_{ta_{4.4}} = {}^{s}T_{tp_{4.4}} .\text{Rot}(x, +4) $$

$$ {}^{s}T_{ta_{4.4}} = \begin{bmatrix} 1 & 0 & 0 \\ 0 & 1 & 0 \\ 0 & 0 & 1 \end{bmatrix} \begin{bmatrix} 1 & 0 & 0 \\ 0 & \cos\psi & -\sin\psi \\ 0 & \sin\psi & \cos\psi \end{bmatrix} $$

substituting $\psi = +4^{o}$ in above equation we get

$$ {}^{s}T_{ta_{4.4}} = \begin{bmatrix} 1.00 & 0.00 & 0.00 \\ 0.00 & 0.998 & 0.07 \\ 0.00 & -0.07 & 0.998 \end{bmatrix} $$

APPENDIX B

POSITION AND ORIENTATION PLOTS I

Trajectory for all plots presented below as related to chute in Figure 2.3 is as follows:

Start Point : X = 6.25", Y = 2.75" and Z = 6.375"

End Point : X = 24.25", Y = 12.675" and Z = 11.5"

Increment : 1" along the trajectory, Psi increases by 10^{o} along subsequent data points.

Based on direction of trajectory values of X[] become:

Start Point : X[] = [6.25, 2.75, 6.375, 0^{o}, 345^{o}, 30^{o}]

End Pont : X[] = [24.25, 12.675, 11.5, 220^{o}, 345^{o}, 30^{o}]

Note : Figure B.3 for "Z" Plot of 1-Transmitter has a higher deviation as compared to corresponding plots for 3-Transmitter, and 3-T with other improvements techniques. Hence Figure B.3 has a different scale than other "Z" plots presented in this appendix.

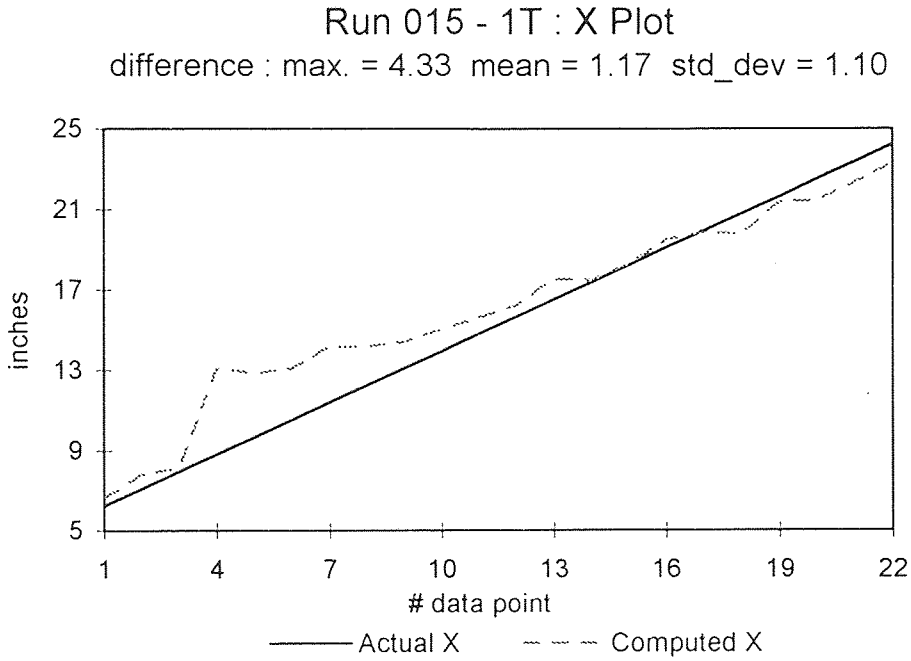

Figure B.1 Run015 : X Plot using 1 Transmitter

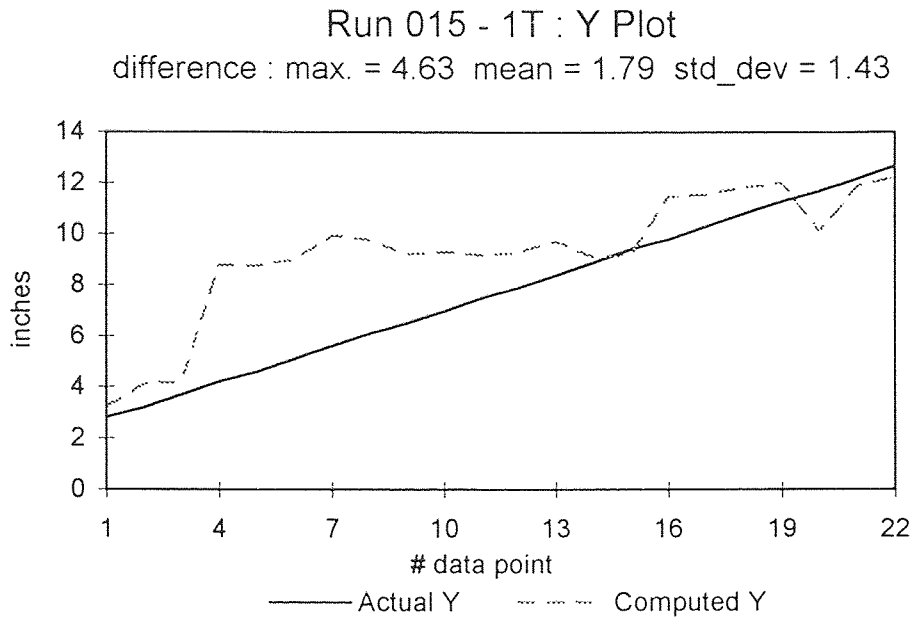

Figure B.2 Run015 : Y Plot using 1 Transmitter

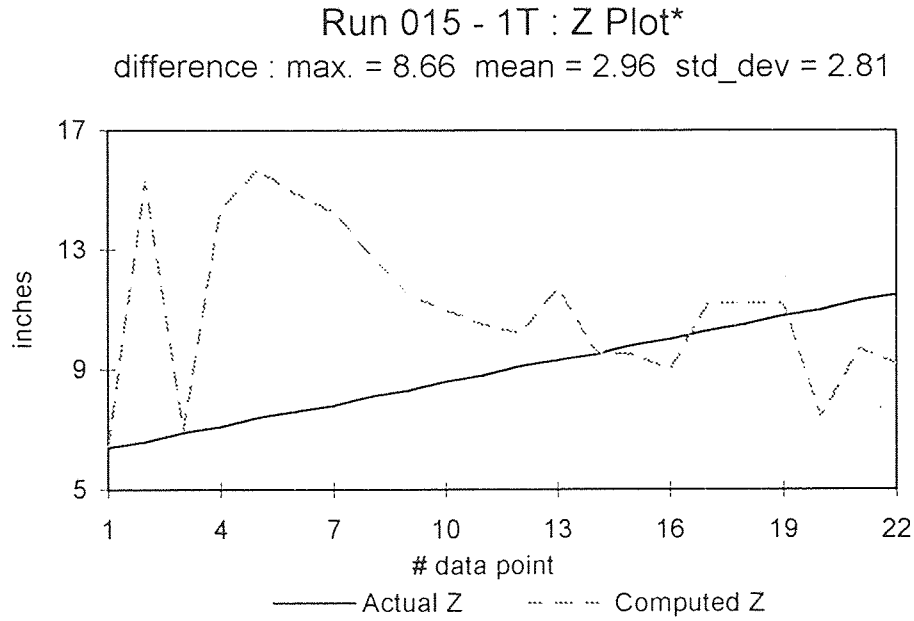

(* : This chart is on different scale than other "Z" Charts)

Figure B.3 Run015 : Z Plot using 1 Transmitter

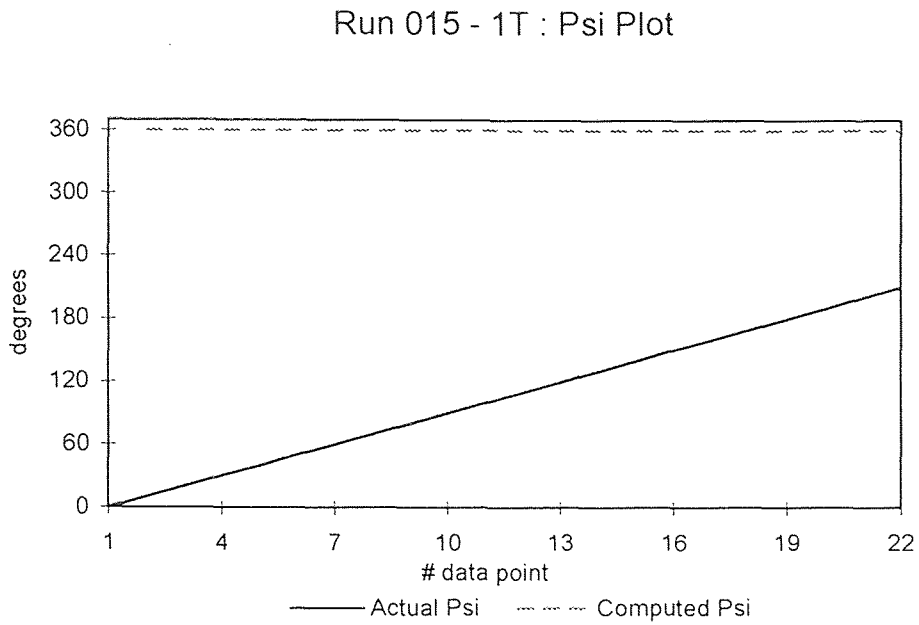

Figure B.4 Run015 : Psi Plot using 1 Transmitter

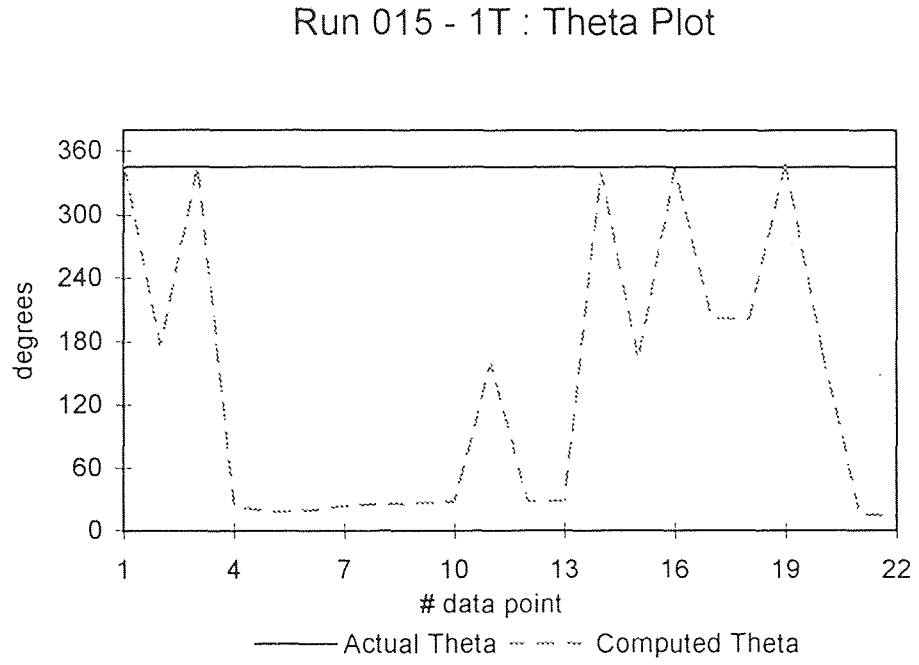

Figure B.5 Run015 : Theta Plot using 1 Transmitter

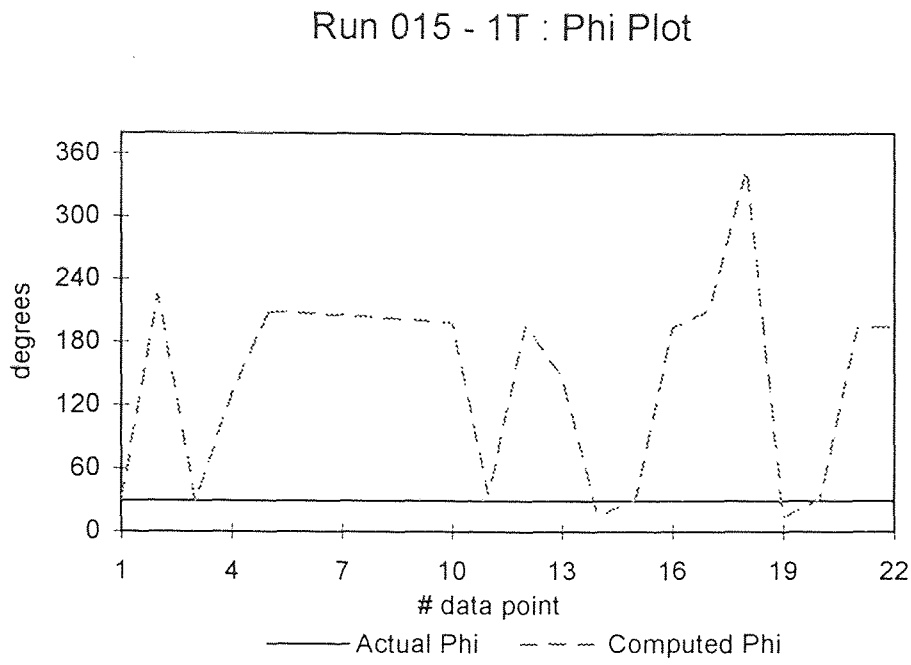

Figure B.6 Run015 : Phi Plot using 1 Transmitter

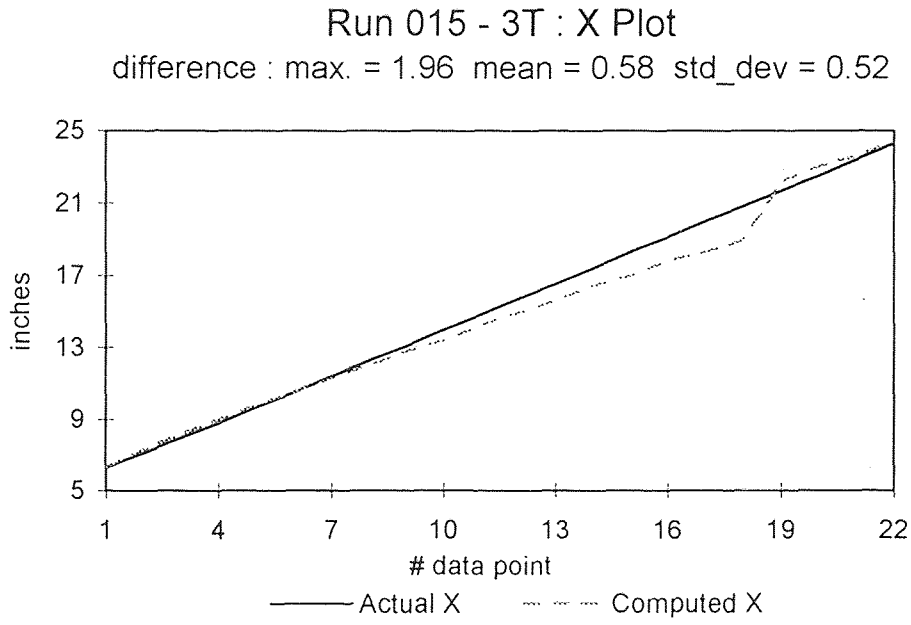

Figure B.7 Run015 : X Plot using 3 Transmitters

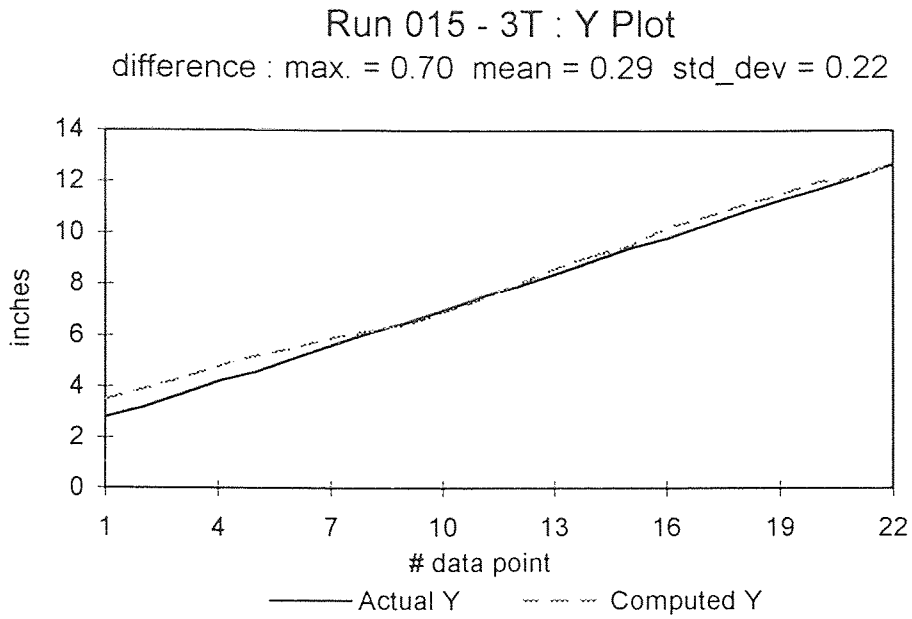

Figure B.8 Run015 : Y Plot using 3 Transmitters

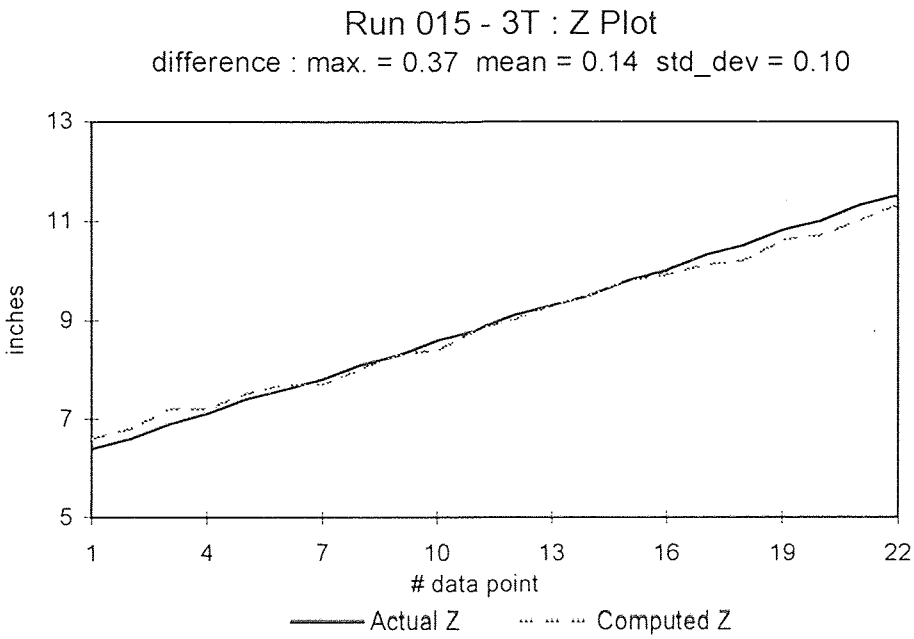

Figure B.9 Run015 : Z Plot using 3 Transmitters

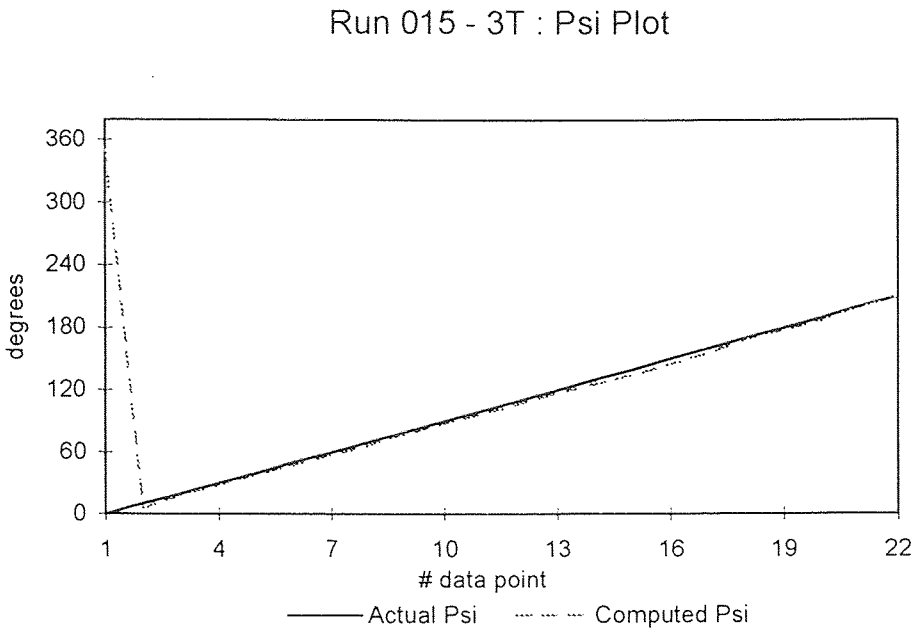

Figure B.10 Run015 : Psi Plot using 3 Transmitters

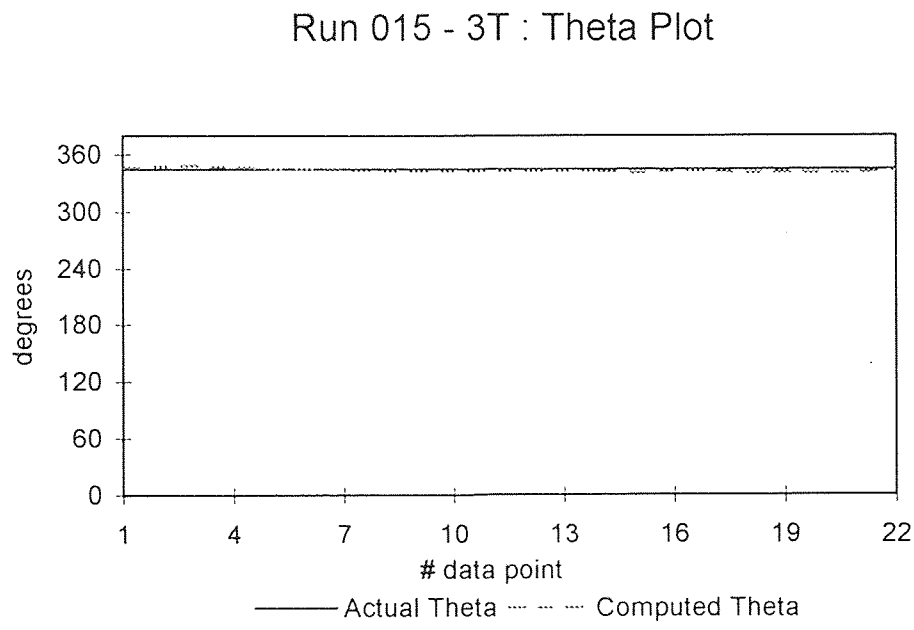

Figure B.11 Run015 : Theta Plot using 3 Transmitters

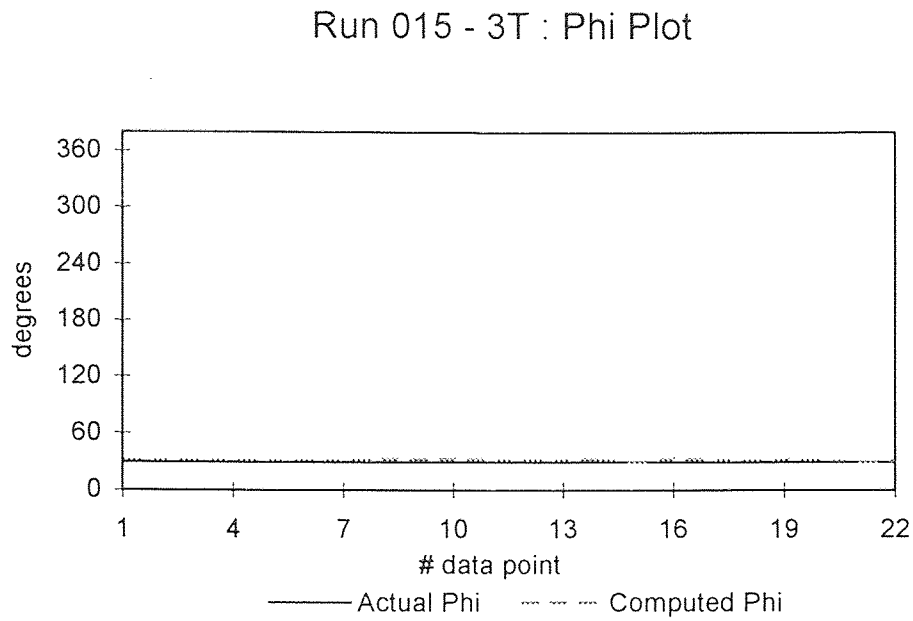

Figure B.12 Run015 : Phi Plot using 3 Transmitters

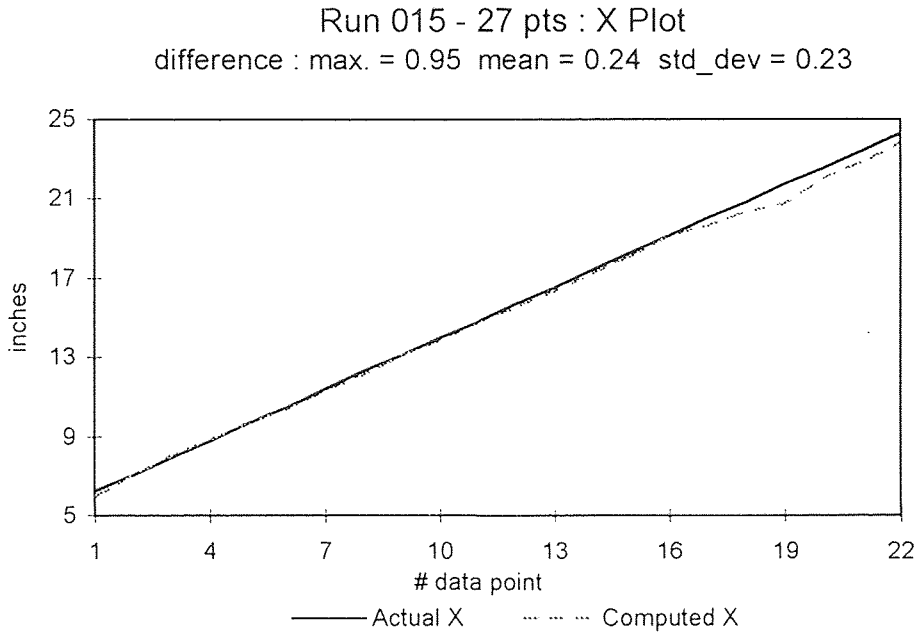

Figure B.13 Run015 : X Plot after 27 Point Correction

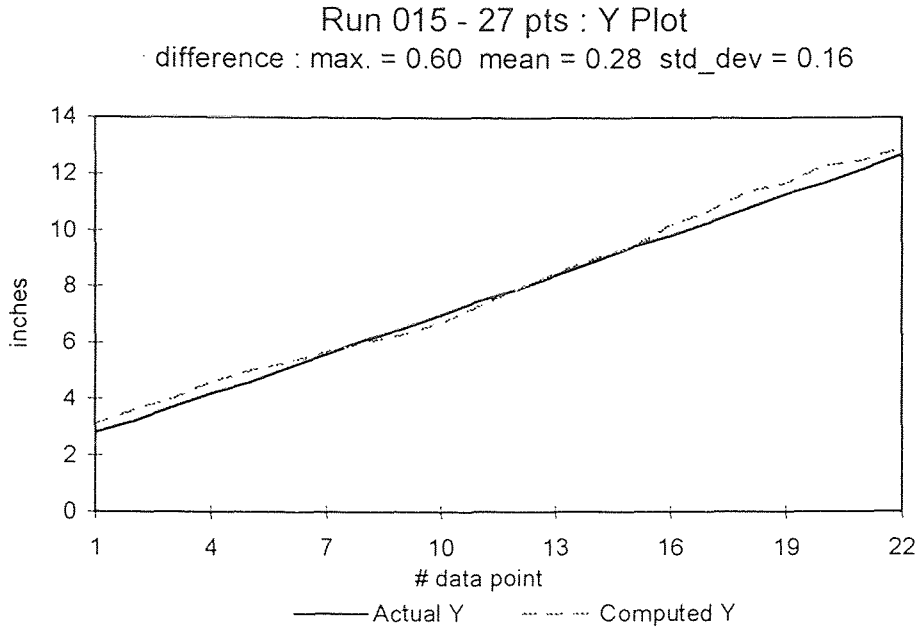

Figure B.14 Run015 : Y Plot after 27 Point Correction

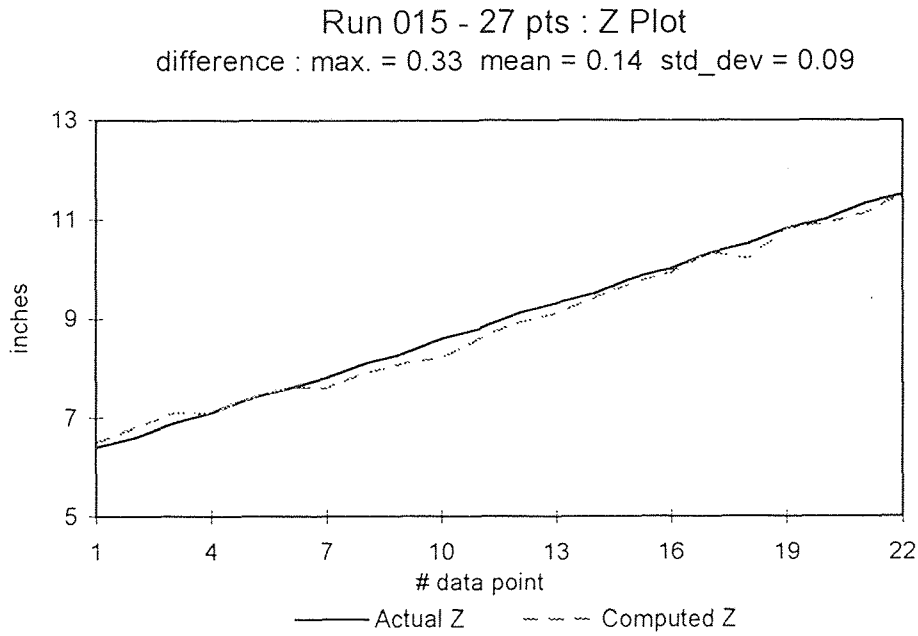

Figure B.15 Run015 : Z Plot after 27 Point Correction

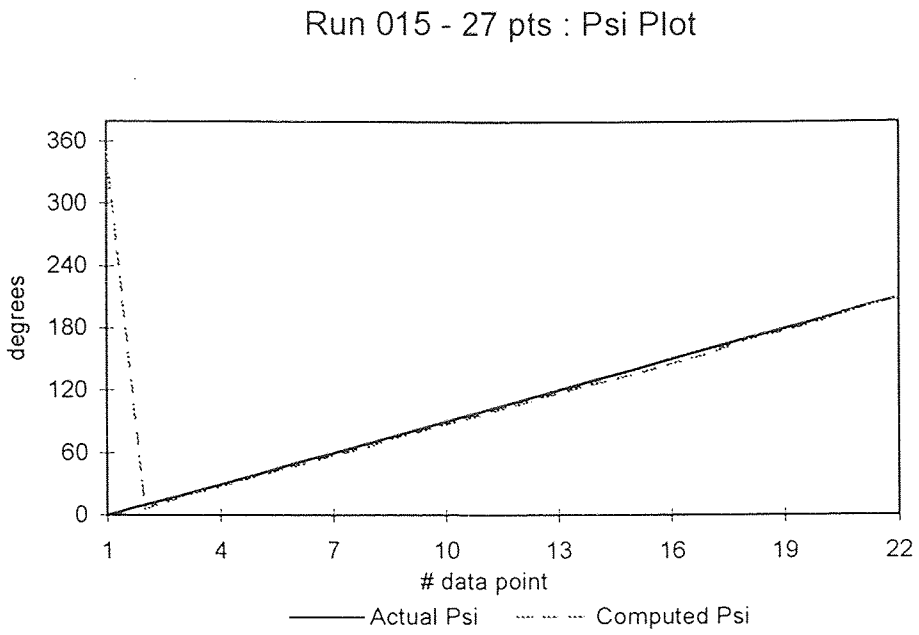

Figure B.16 Run015 : Psi Plot after 27 Point Correction

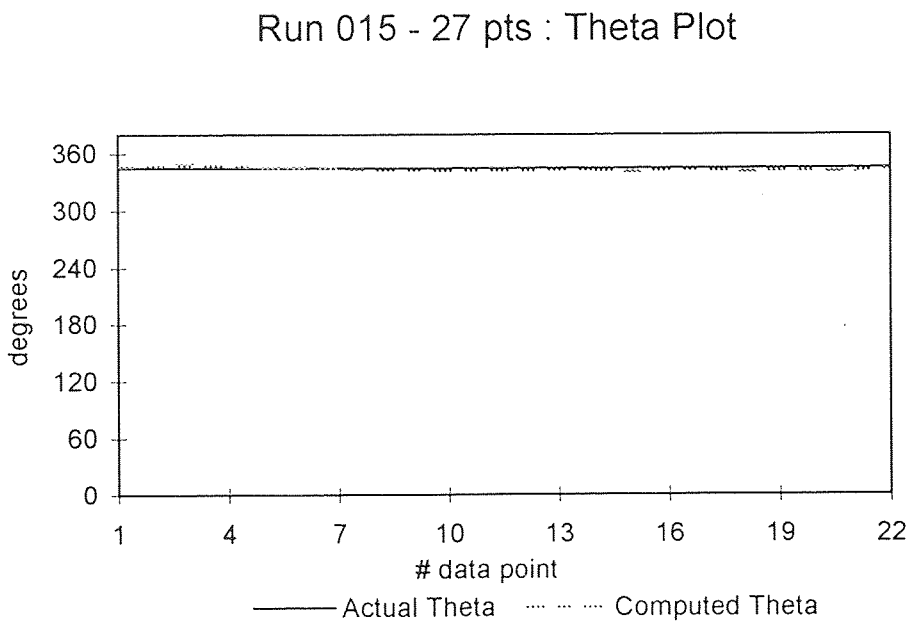

Figure B.17 Run015 : Theta Plot after 27 Point Correction

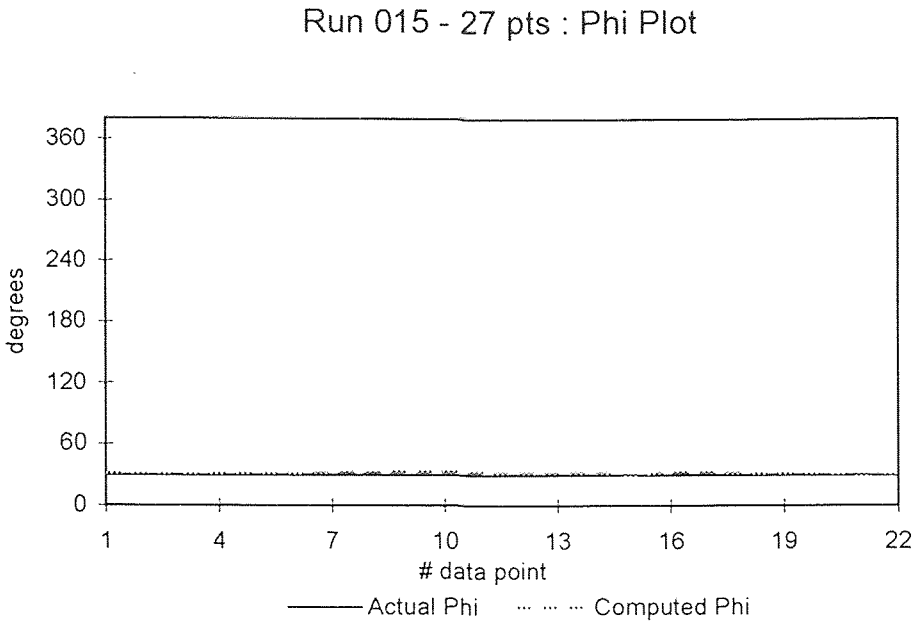

Figure B.18 Run015 : Phi Plot after 27 Point Correction

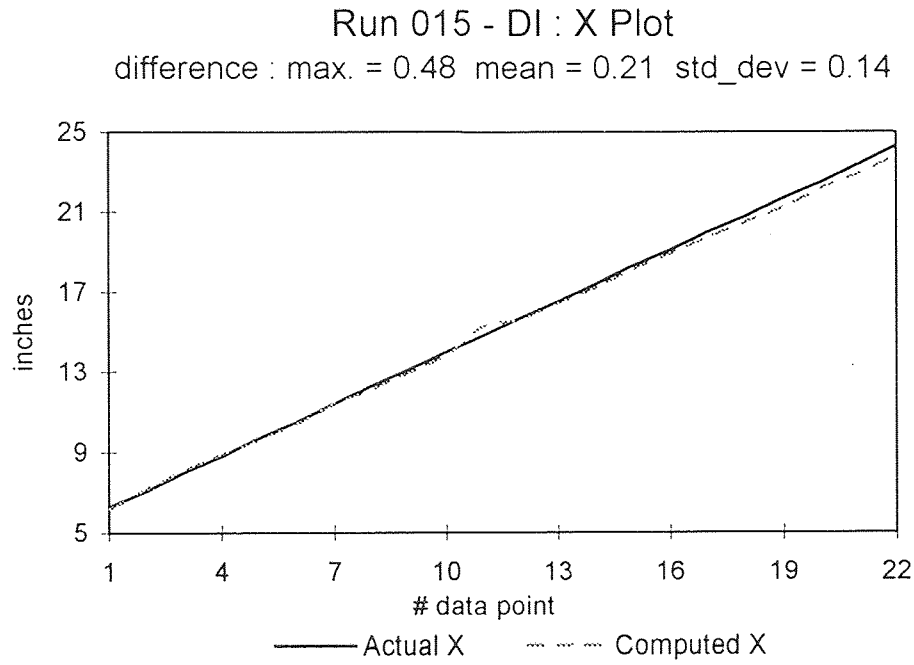

Figure B.19 Run015 : X Plot using Quality Information Selection

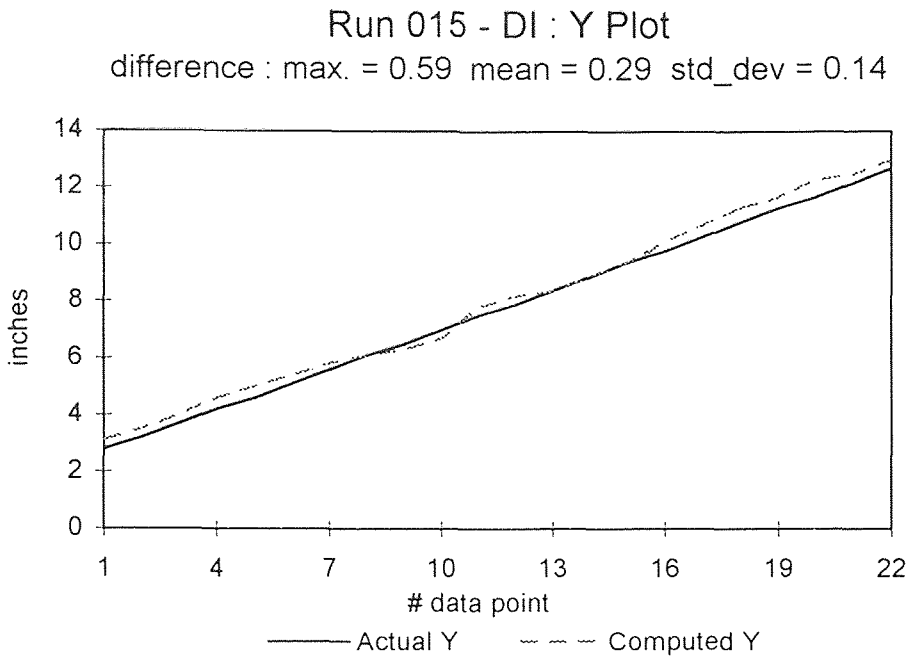

Figure B.20 Run015 : Y Plot using Quality Information Selection

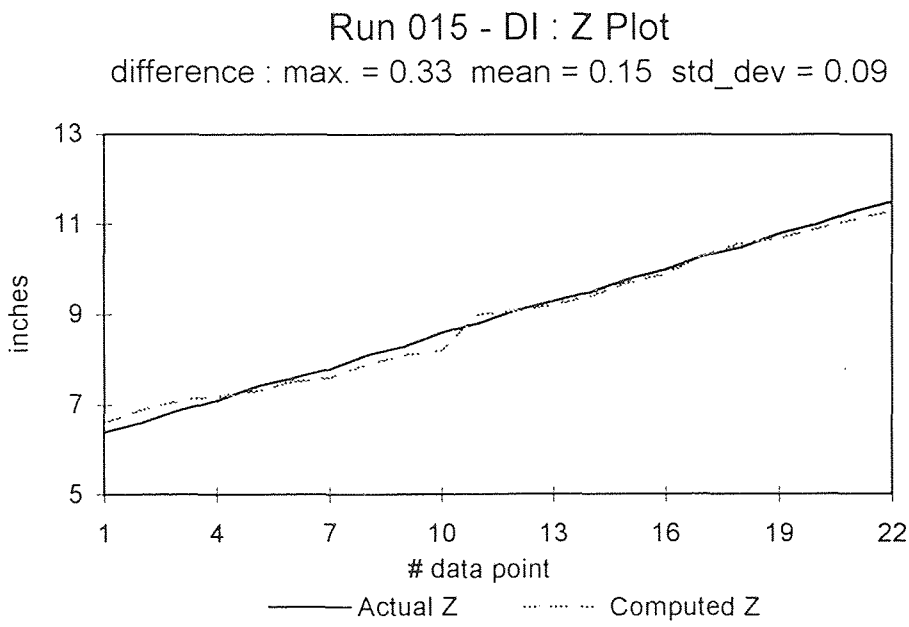

Figure B.21 Run015 : Z Plot using Quality Information Selection

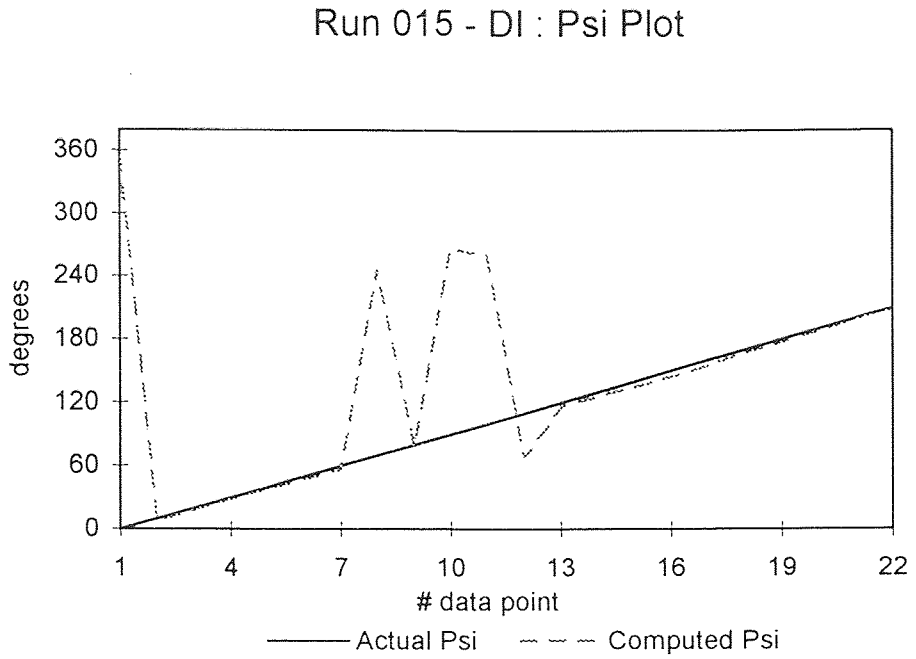

Figure B.22 Run015 : Psi Plot using Quality Information Selection

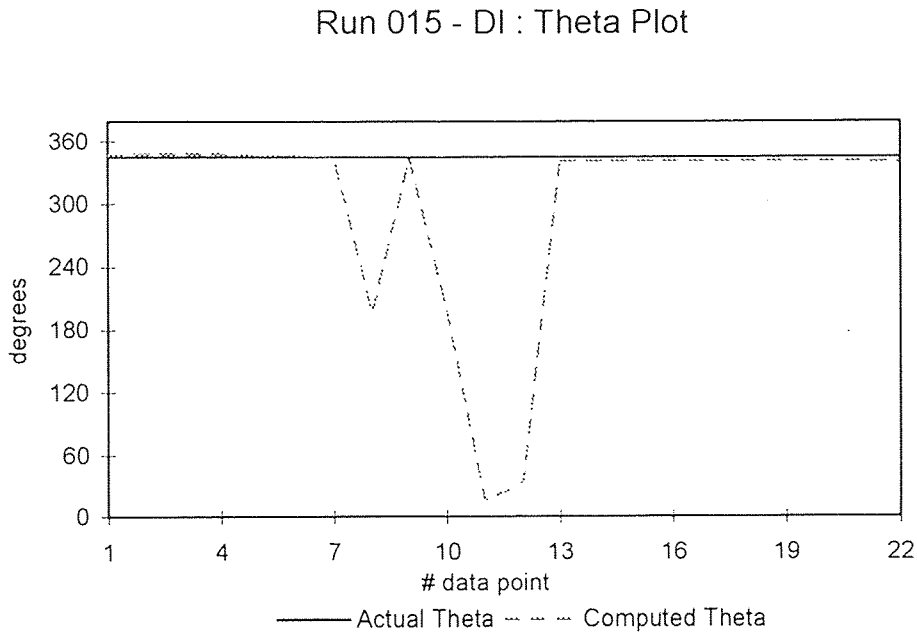

Figure B.23 Run015 : Theta Plot using Quality Information Selection

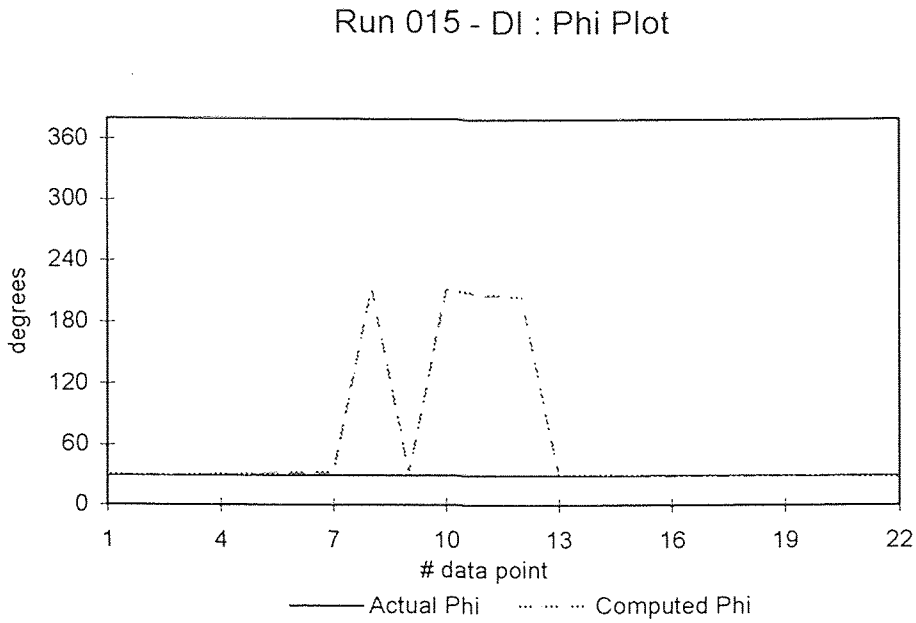

Figure B.24 Run015 : Phi Plot using Quality Information Selection

APPENDIX C

POSITION AND ORIENTATION PLOTS II

Trajectory for Figures C-1 through C-12 presented below as related to chute in Figure 2.3 is as follows:

Start Point : X = 10", Y = 5" and Z = 7"

End Point : X = 27", Y = 13" and Z = 7"

Increment : 1" between any two subsequent data points. The direction of trajectory for majority of points is along either X or Y axis. When X is at 21", trajectory comes back and goes forth to cross plane of antenna 2 (at X = 20") five times in all, by increasing X and Y alternatively. Solid lines in plots show the exact trajectory course.

Based on direction of trajectory and constant orientation, values of X[] become:

Start Point : X[] = [10, 5, 7, 20^{o}, 20^{o}, 20^{o}]

End Pont : X[] = [27, 13, 7, 20^{o}, 20^{o}, 20^{o}]

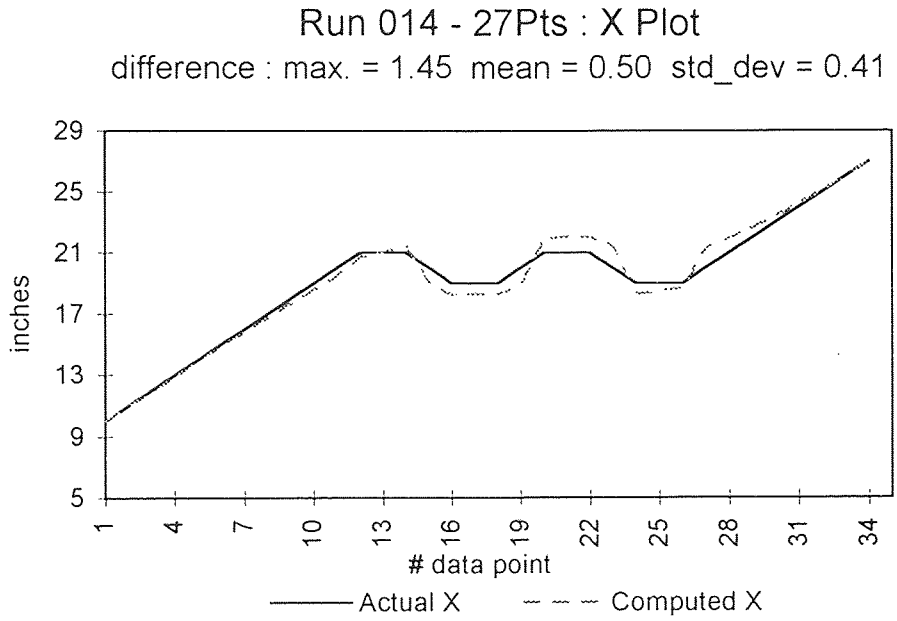

Figure C.1 Run014 : X Plot after 27 Point Correction

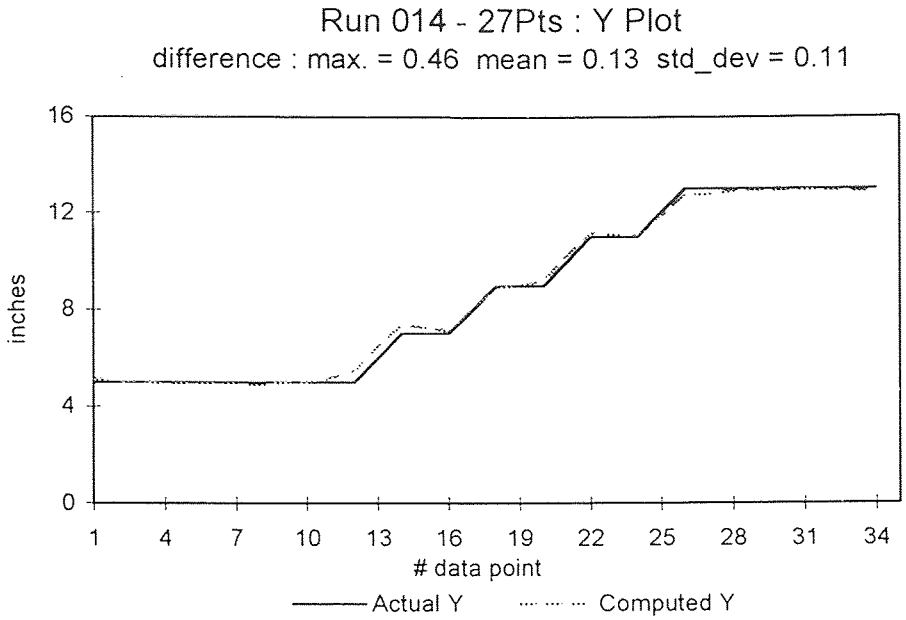

Figure C.2 Run014 : Y Plot after 27 Point Correction

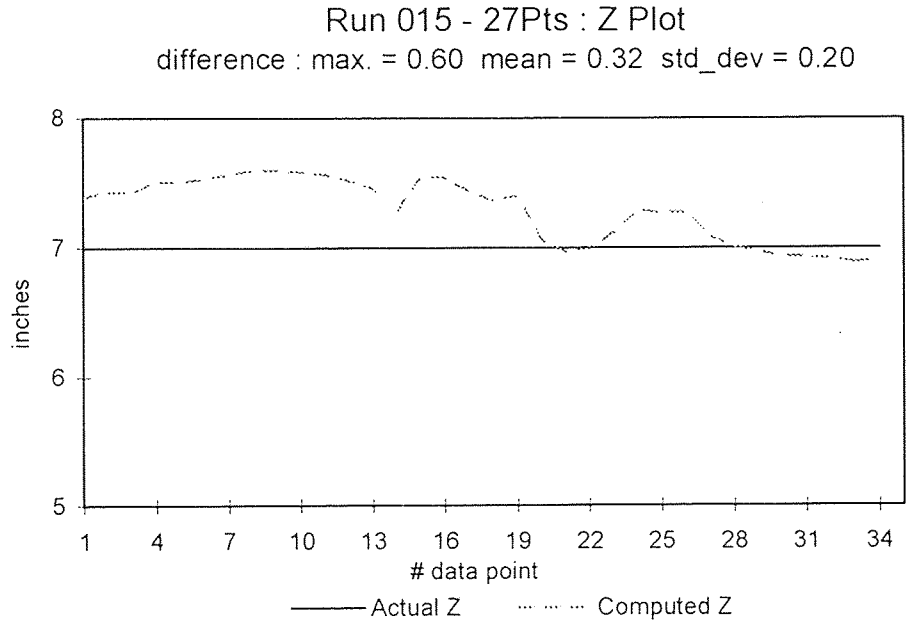

Figure C.3 Run014 : Z Plot after 27 Point Correction

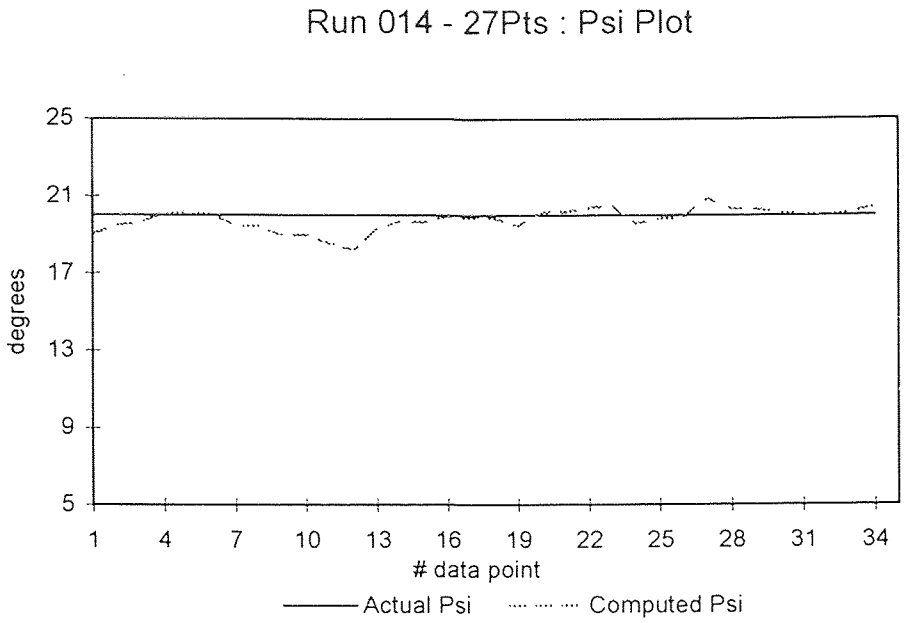

Figure C.4 Run014 : Psi Plot after 27 Point Correction

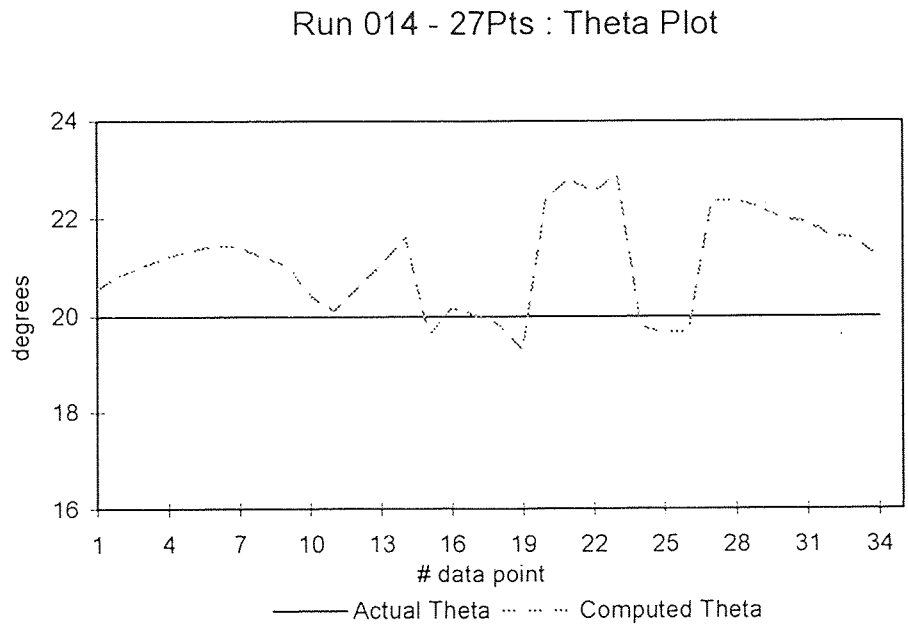

Figure C.5 Run014 : Theta Plot after 27 Point Correction

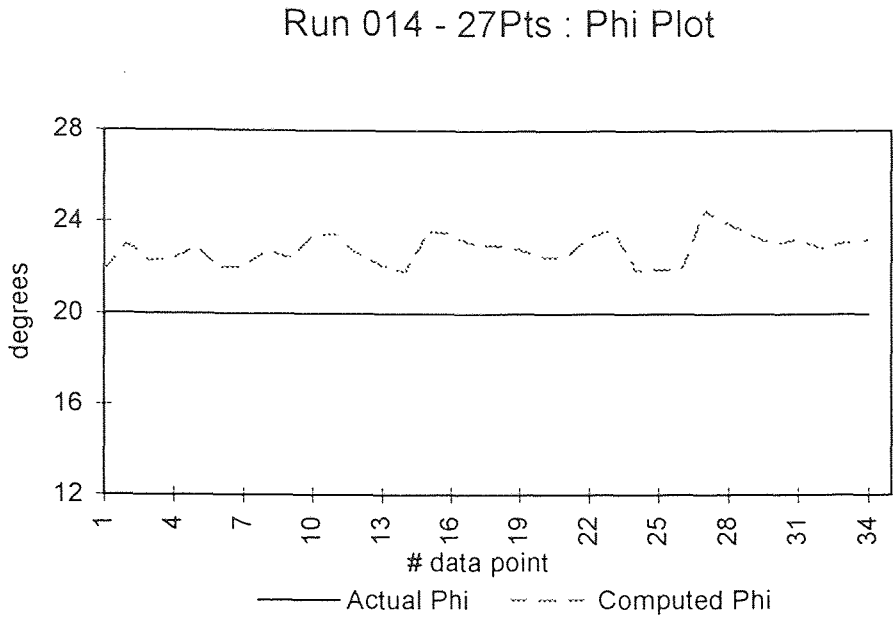

Figure C.6 Run014 : Phi Plot after 27 Point Correction

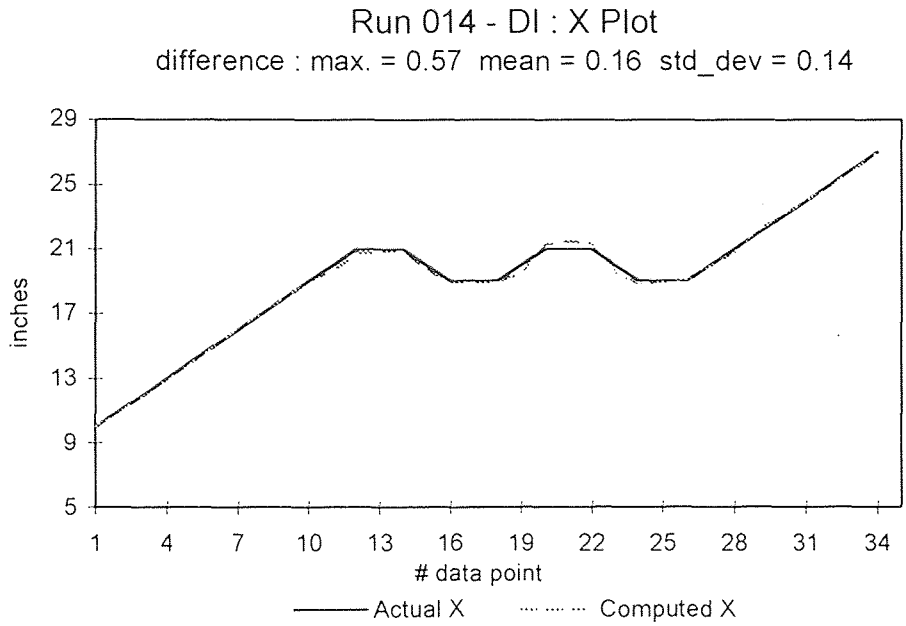

Figure C.7 Run014 : X Plot using Quality Information Selection

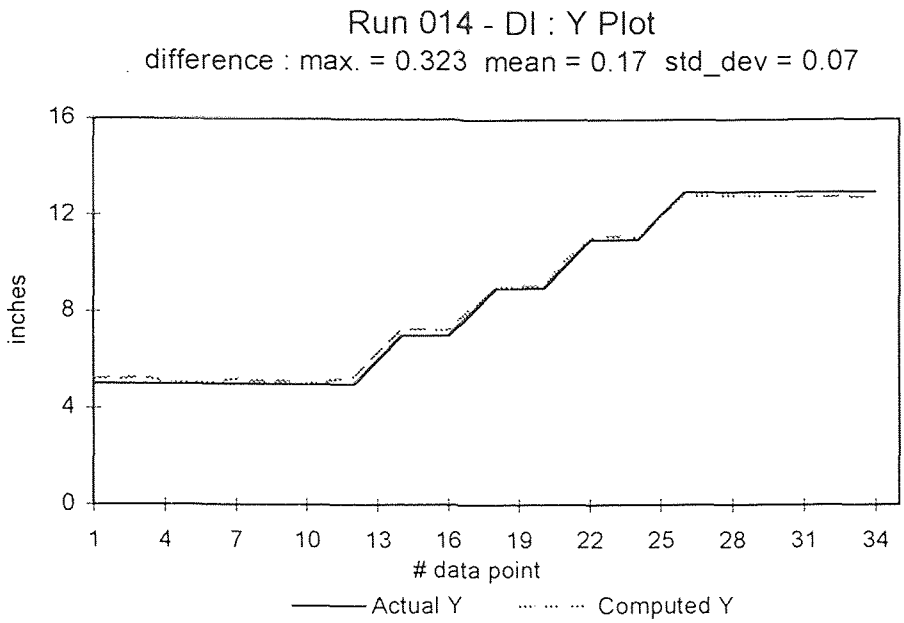

Figure C.8 Run014 : Y Plot using Quality Infomation Selection

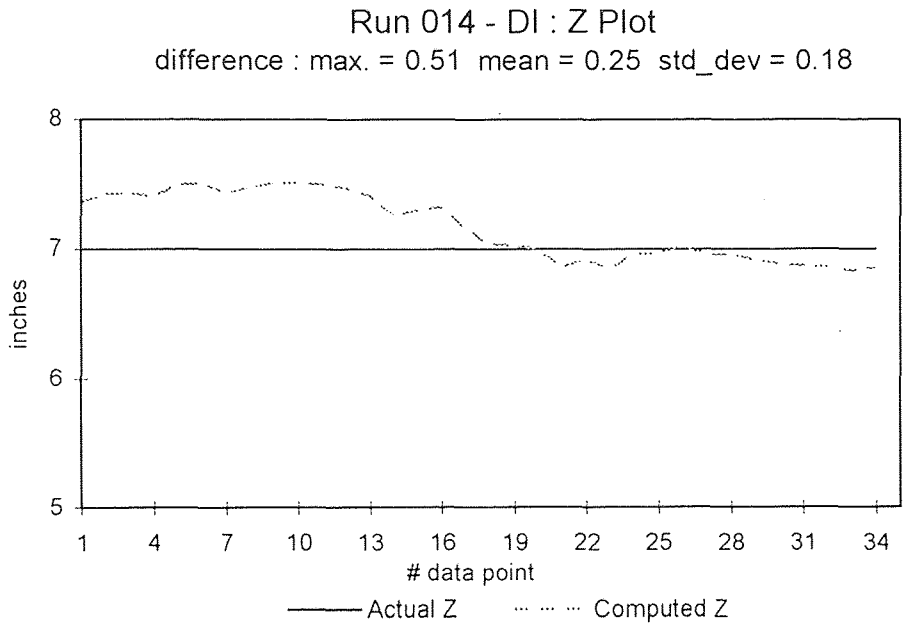

Figure C.9 Run014 : Z Plot using Quality Infomation Selection

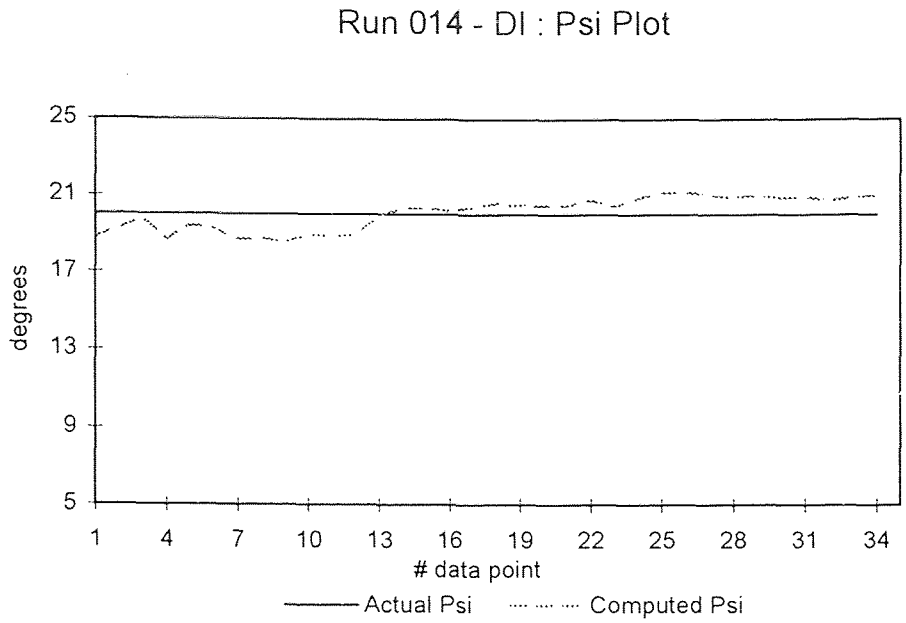

Figure C.10 Run014 : Psi Plot using Quality Infomation Selection

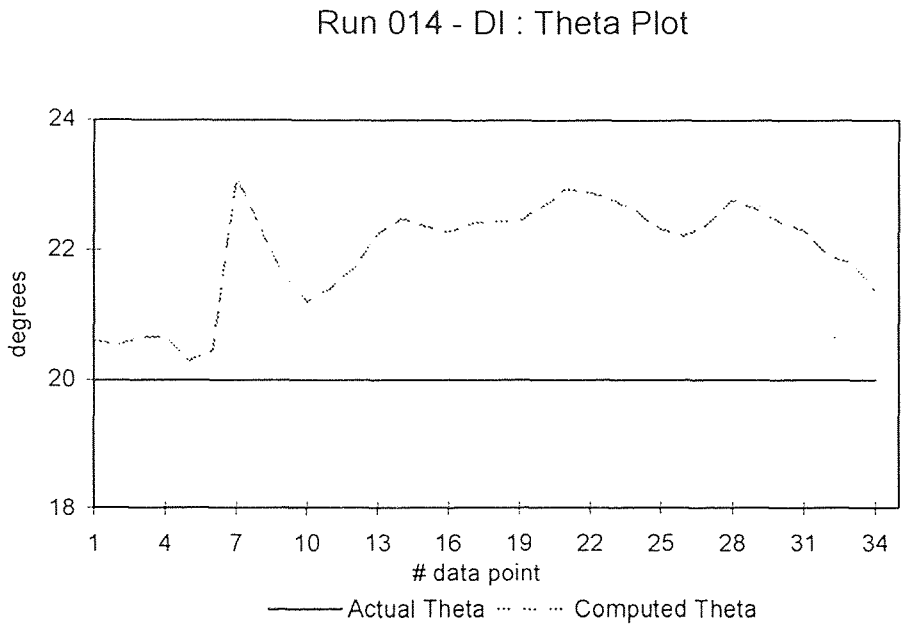

Figure C.11 Run014 : Theta Plot using Quality Infomation Selection

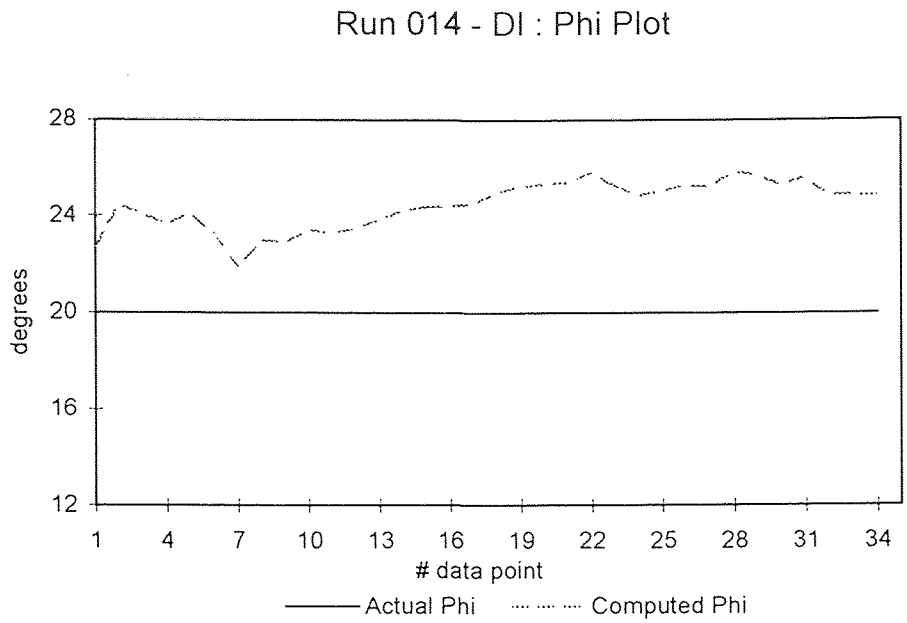

Figure C.12 Run014 : Phi Plot using Quality Infomation Selection

Double Sine Curve Trajectory :

Trajectory for Figures C-13 through C-19 presented below as related to chute in Figure 2.3 is as follows:

Start Point : X = 2", Y = 10" and Z = 10"

End Point : X = 38", Y = 10" and Z = 10"

Increment : 1" Along X axis.

Description : The trajectory is a double sine curve. It means that when the trajectory is projected onto XY plane Y is a sinsoidal function and when projected onto XZ plane, Z is a sinsoidal function. As Y amplitude is 7", it varies from Y_{min} = 3" to Y_{max} = 17". As Z amplitude is 5", it varies from Z_{min} = 5" to Z_{max} = 15". The orientation of trajectory is held constant at [ψ = 40, θ = 30 and ϕ = 20]. Actual values of X[] at each data point is in table following figure[C-19]

Based on direction of trajectory and constant orientation, values of X[] become:

Start Point : X[] = [2, 10, 10, 40^o, 30^o, 20^o]

End Pont : X[] = [38, 10, 10, 40^o, 30^o, 20^o]

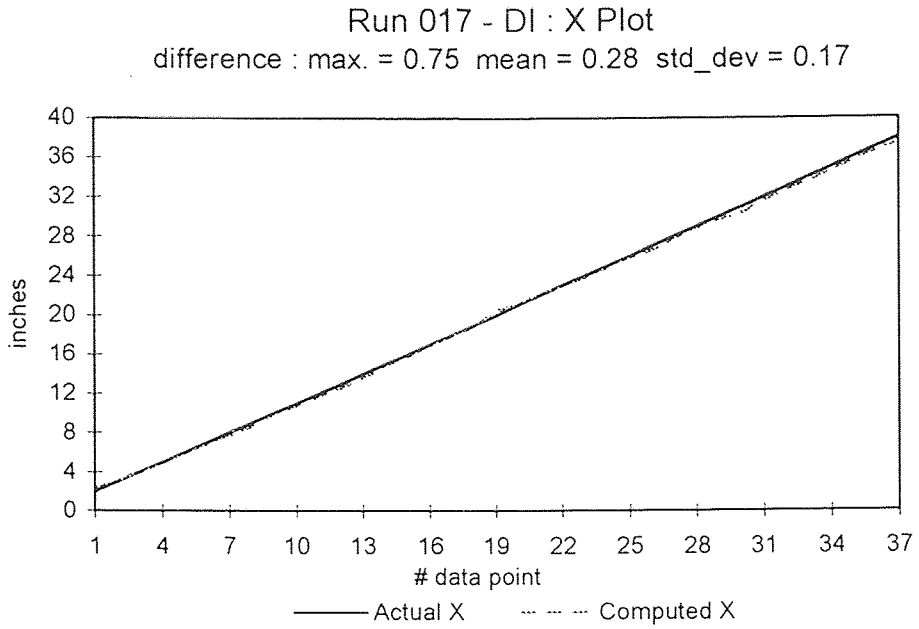

Figure C.13 Run017 : X Plot for Double Sine Curve Trajectory

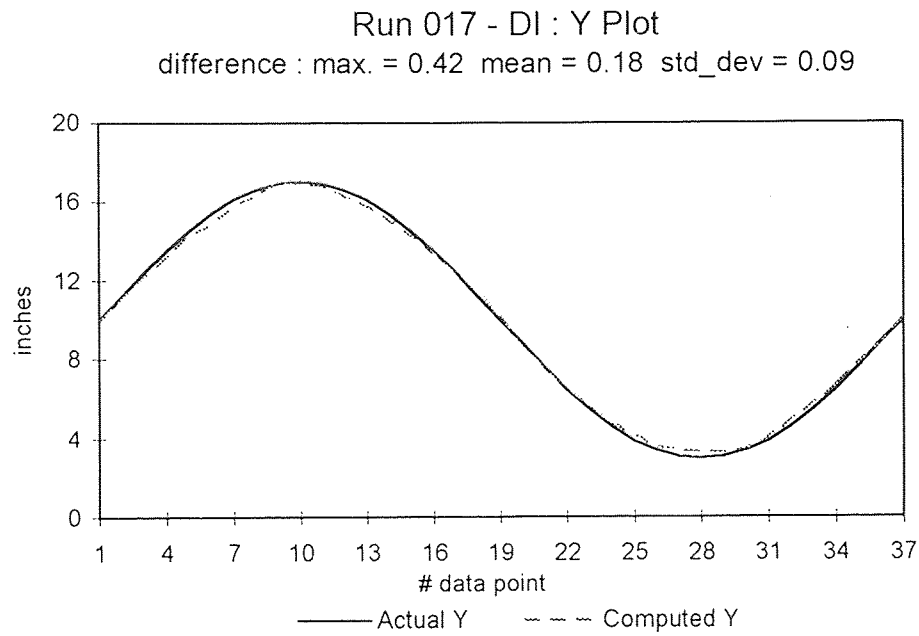

Figure C.14 Run017 : Y Plot for Double Sine Curve Trajectory

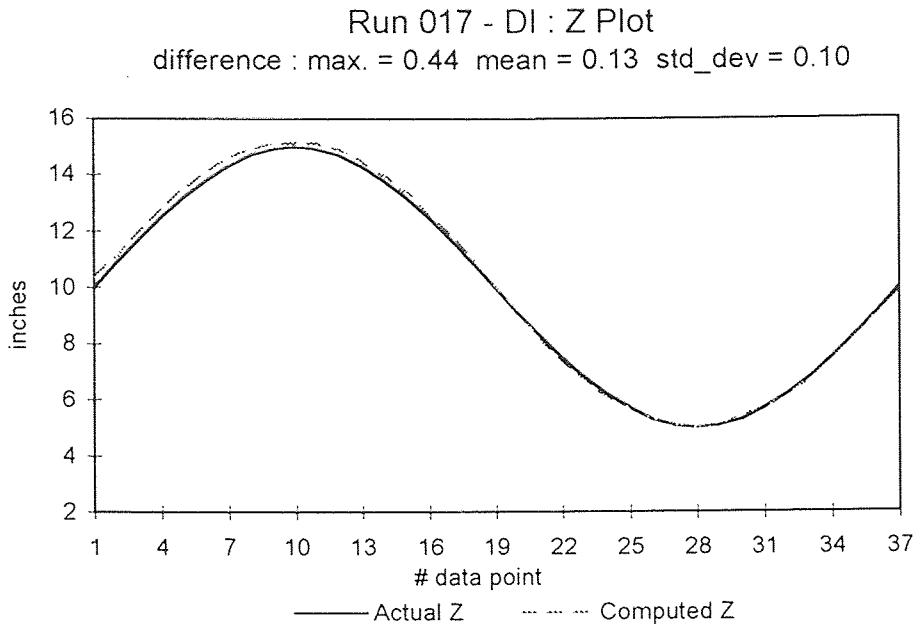

Figure C.15 Run017 : Z Plot for Double Sine Curve Trajectory

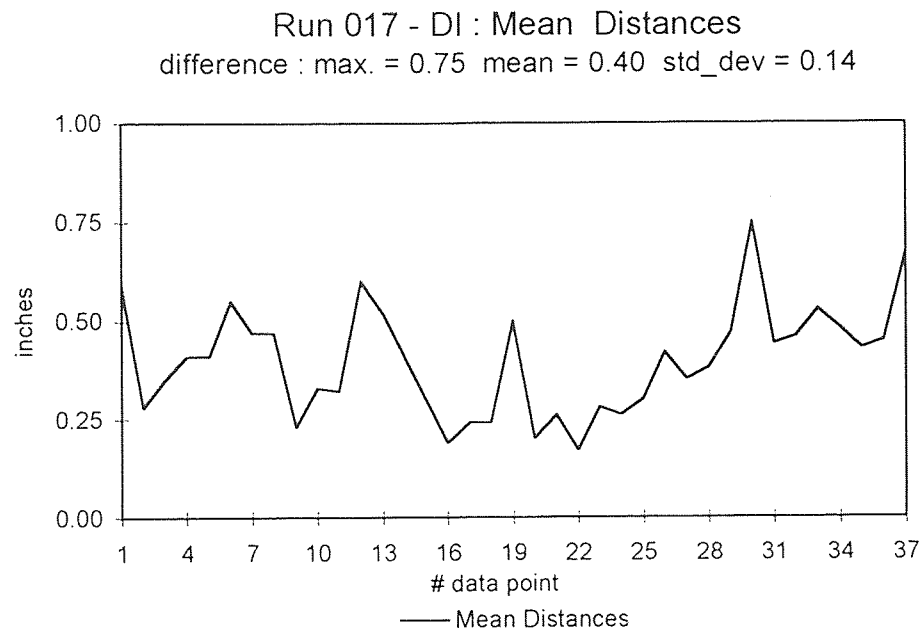

Figure C.16 Run016 : Distance Deviation Plot for Double Sine Curve Trajectory

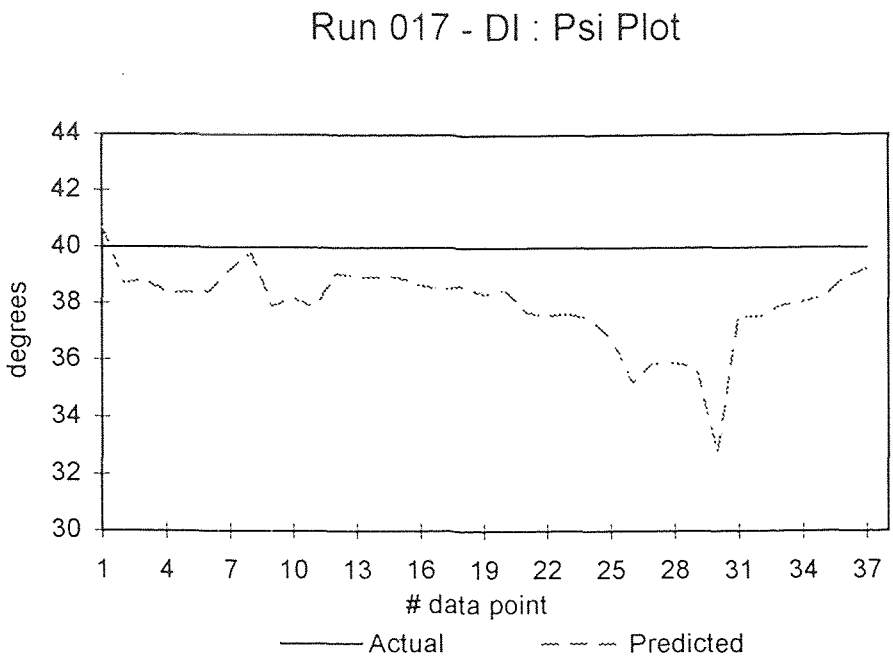

Figure C.17 Run017 : Psi Plot for Double Sine Curve Trajectory

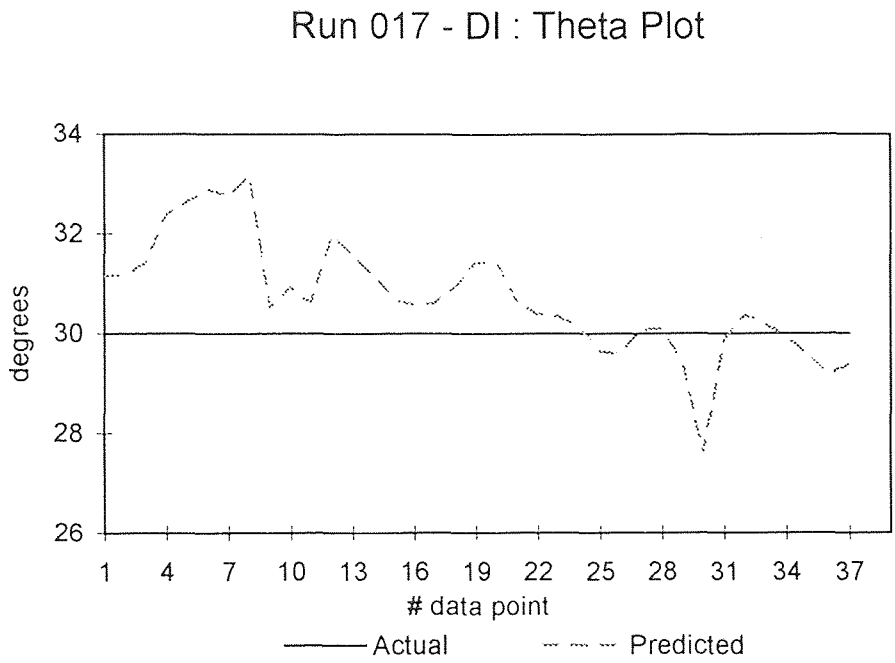

Figure C.18 Run017 : Theta Plot for Double Sine Curve Trajectory

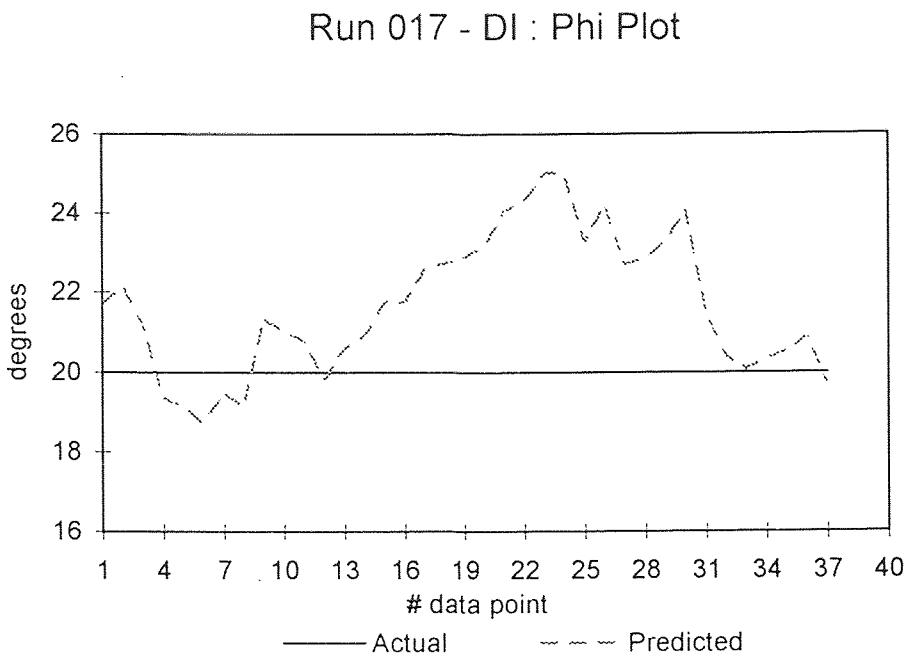

Figure C.19 Run017 : Phi Plot for Double Sine Curve Trajectory

Table C-1 : Listing of X[] for Double Sine Curve

X	Y	Z	Psi	Theta	Phi
2	10	10	40	30	20
3	11.22	10.87	40	30	20
4	12.39	11.71	40	30	20
5	13.5	12.5	40	30	20
6	14.5	13.21	40	30	20
7	15.36	13.83	40	30	20
8	16.06	14.33	40	30	20
9	16.58	14.7	40	30	20
10	16.89	14.92	40	30	20
11	17	15	40	30	20
12	16.89	14.92	40	30	20
13	16.58	14.7	40	30	20
14	16.06	14.33	40	30	20
15	15.36	13.83	40	30	20
16	14.5	13.21	40	30	20
17	13.5	12.5	40	30	20
18	12.39	11.71	40	30	20
19	11.22	10.87	40	30	20
20	10	10	40	30	20
21	8.78	9.13	40	30	20
22	7.61	8.29	40	30	20
23	6.5	7.5	40	30	20
24	5.5	6.79	40	30	20
25	4.64	6.17	40	30	20
26	3.94	5.67	40	30	20
27	3.42	5.3	40	30	20
28	3.11	5.08	40	30	20
29	3	5	40	30	20
30	3.11	5.08	40	30	20
31	3.42	5.3	40	30	20
32	3.94	5.67	40	30	20
33	4.64	6.17	40	30	20
34	5.5	6.79	40	30	20
35	6.5	7.5	40	30	20
36	7.61	8.29	40	30	20
37	8.78	9.13	40	30	20
38	10	10	40	30	20

REFERENCES

[1] Ashok, A. S., "Computational Aspects of a Three Dimensional Non-Intrusive Particle Motion Tracking System", M.S. Thesis, New Jersey Institute of Technology, Newark, New Jersey, 1992.

[2] Dave, R. N., A. S Ashok, and B. G. Bukiet, "On Development of a Three Dimensional Particle Motion Tracking System", *ASME Paper*, Winter Annual Meeting 1992.

[3] Dave R. N., and B. G. Bukiet, "Non-Intrusive Rigid Body Tracking Technique for Dry Particulate Flows, Part I: Theoretical Aspects," Submitted to *Review of Scientific Instruments*, 1994.

[4] Dave R. N., Private Communications, New Jersey Institute of Technology, Newark, New Jersey, 1994.

[5] Dennis, J. R., R. B. Schnabel, *Numerical Methods for Unconstrained Optimization and Nonlinear Equations*, Prentice-Hall, Engelwood Cliffs, New Jersey, 1983.

[6] Goldstein, H., *Classical Mechanics*, Addison Wesley Publishing Company, 1980.

[7] Moré, J. J., "The Levenberg-Marquardt Algorithm: Implementation and Theory", in *Numerical Analysis*, G. A. Watson, ed., Lecture Notes in Math. 630, Springer-Verlag, Berlin, 1977.

[8] Moré, J. J., B. S. Garbow and K. E. Hillstrom, "User Guide for MINPACK-1", Argonne National Lab Report, 1980.

[9] Parasar, A., Lab Notes, New Jersey Institute of Technology, Newark, New Jersey, 1992.

[10] Pual, R. P., *Robot Manipulators: Mathematics, Programming and Control*, MIT Press, Massachusettes, 1981.

[11] Savage, S. B., "Flow of Granular Materials with Applications to Geophysical Problems," *Continuum Mechanics in the Environmental Sciences and Geophysics*, IUTAM International Summer School on Mechanics, Udine, Italy, June 22-26, (1992).

[12] Troiano, A., Private Communications, New Jersey Institute of Technology, Newark, New Jersey, 1994.

[13] Troiano, A., Lab Notes, New Jersey Institute of Technology, Newark, New Jersey, 1994.

[14] Van Valkenburg, M. E., *Network Analysis*, Prentice-Hall, Engelwood Cliffs, New Jersey, 1974.

[15] Volcy, J. R., "Develpment of a Non-Intrusive Particle Motion Tracking Technique for Granular Flow Experiments", M.S. Thesis, New Jersey Institute of Technology, Newark, New Jersey, 1994.

[16] Volcy, J. R., Private Communications, New Jersey Institute of Technology, Newark, New Jersey, 1994.